INTER-CELL INTERFERENCE MANAGEMENT FOR CELLULAR SYSTEMS

A Thesis
Presented to
The Academic Faculty

by

Dae Won Lee

In Partial Fulfillment
of the Requirements for the Degree
Doctor of Philosophy in the
School of Electrical and Computer Engineering

Georgia Institute of Technology
August 2016

INTER-CELL INTERFERENCE MANAGEMENT FOR CELLULAR SYSTEMS

Approved by:

Professor Gordon L. Stüber,
Committee Chair
School of Electrical and Computer Engineering
Georgia Institute of Technology

Professor Geoffrey Y. Li, Advisor
School of Electrical and Computer Engineering
Georgia Institute of Technology

Professor Mary Ann Weitnauer
School of Electrical and Computer Engineering
Georgia Institute of Technology

Professor John R. Barry
School of Electrical and Computer Engineering
Georgia Institute of Technology

Professor Xingxing Yu
School of Mathematics
Georgia Institute of Technology

Date Approved: April 27, 2016

ACKNOWLEDGEMENTS

First of all, I would like to thank my advisor, Prof. Geoffrey Y. Li, who had the patience and understanding to help me through my graduate studies at Georgia Tech. Prof. Li's guidance were truly helpful in both technical and on a personal level.

I would also like to express thanks to my dissertation committee members, Prof. Gordon Stüber, and Prof. Mary Ann Weitnauer, on their help with the dissertation fulfilment process. Their valuable suggestions and comments were very helpful in shaping of this dissertation.

My gratitude extends to my fellow lab-mates, Lu Lu, and Cong Xong. My study at Georgia Tech would not been the same without them. Special thanks to Jinping Lu, Hao He, and Jiancun Fan for their wonderful efforts during our joint research.

Finally, I would like to thank my wife, Semi Koo, and my parents, who gave me the strength and will to pursue graduate studies. I dedicate this dissertation to them.

TABLE OF CONTENTS

LIST OF TABLES

LIST OF FIGURES

SUMMARY

The wide spread of mobile smart phones and ever-increasing demand for more throughput by the users has put a sever burden on cellular networks. Limited bandwidth availability and crowded base station deployments of the cellular system pushes network operators to improve existing network efficiency. This means reducing inter-cell interference such that each base station can maximize performance. In goal of this dissertation is to investigate techniques that mitigate inter-cell interference for modern cellular systems and focuses on development of practical scheduling algorithms for inter-cell interference coordination that can be applied to currently deployed LTE Release 8 networks and development of more advanced inter-cell interference mitigation techniques based on coordinated beamforming.

One of the classical methods of mitigating inter-cell interference is inter-cell interference coordination. Not only does it help improve cellular data coverage but also allow more efficient use of valuable wireless spectrum. This dissertation investigates soft frequency reuse for LTE systems. Systems employing soft frequency reuse is analyzed and it is found that classification of cell-edge users and cell-center users is critical. To improve performance, de-centralized scheduling algorithms that include optimal user classification and balances throughput and fairness among users is proposed. Additional sub-optimal methods to reduce the computational complexity is introduced. Simulation demonstrates that gains of the 5th percentile user throughput can be increased without loss to the overall cell average throughput compared to a non-cooperating system.

Next, coordinated beamforming which require faster and tighter coordination

among base stations is investigated. Multi-user and multi-stream coordinated beamforming based on maximization of the harmonic-sum of signal-to-interference-plus-noise ratio is proposed. Simulation results show that it improves cell-edge users compared with prior researched coordinated beamforming algorithms based on minimizing mean square error, maximizing uplink signal-to-interference-plus-noise ratio, and maximizing weighted sum-rate. Additionally, proposed coordinated beamforming is further extended to multi-carrier systems with per-antenna power constraints. Low complexity algorithm that can be applied to coordinated beamforming algorithms with whitened match filter structure is proposed and simulated. The key idea is to update a common antenna power regulating diagonal matrix, which determines the antenna power of a precoding matrix in each iteration. The algorithm can be scaled to any number of subcarriers because it only updates a common diagonal matrix for all subcarrier. Simulations show that proposed algorithm enables excellent antenna power efficiency with low number of iterations and converges quickly. Furthermore, it can significantly mitigate inter-cell interference and improve performance over non-coordinating system.

CHAPTER I

INTRODUCTION

1.1 Background and Motivation

The high data-rate demands of today requires wireless networks to be much more efficient than before, especially for the cell-edge users, where the data rates are far more challenging than cell-center users. The performance of dense cellular networks, deployed to meet the increasing throughput demands of users, is limited by *inter-cell interference* (ICI). Therefore, mitigating ICI is an important issue in modern cellular systems.

There have been different ways to improve the throughput of cell-edge users. For example, a *generalized proportional fairness* (GPF) scheduler [61] can weigh the cell-edge users more to increase their throughput at the cost of reducing the average cell throughput. *Multi-input multi-output* (MIMO) techniques can use spatial beamforming to increase *signal-to-interference-and-noise ratio* (SINR) for cell-edge users. Techniques confined to a single cell do not consider ICI and therefore, they have limitations on achievable improvement to cell-edge users. For the downlink systems, traditional methods on mitigating ICI are to optimize the transmit power of *base stations* (BSs) in time or frequency domain to improve performance of the cell-edge users [64, 51], which is known as inter-cell interference coordination (ICIC).

The two major categories of ICIC are *fractional frequency reuse* (FFR) [53] and *soft frequency reuse* (SFR) [36]. The main difference being that SFR allows full frequency reuse for wireless networks. In SFR, the bandwidth for a cell is divided into two parts: *cell-edge band* (CEB) and *cell-center band* (CCB). Users are also divided into two groups, with each group being scheduled in CEB or CCB, respectively.

The users with strong interference from the neighboring cells are classified as the *cell-edge users* (CEUs) and the rest are the *cell-center users* (CCUs). To avoid interference among the CEUs in adjacent cells, their CEB's should be non-overlapped. Furthermore, the downlink transmit power of the CEB should be boosted compared to that of the CCB. The power boosting of the CEB increases the signal strength whereas the coordinated CEB allocation among cells reduces inter-cell interference. This leads to increase in the received SINR for the CEUs.

Nowadays, improvements in backhaul connection has allowed a large amount of information to be shared among BSs quickly. As a result, faster and tighter coordination among cells and advanced ICI mitigation techniques, such as *coordinated multi-point* (CoMP) transmission, can be deployed. CoMP can be classified into two large categories, *coordinated scheduling/coordinated beamforming* (CS/CB) and *joint processing* (JP) [50]. CB reduces the ICI experienced by the users by beamforming the transmit signal of interfering BS to steer the interference towards the null space of the interfered users. JP allows one or more neighboring BS to transmit the same desired signal rather than interference signals from the point-of-view of a selected user. This not only reduces ICI but increases signal strength as well. Although JP has higher throughput, it also has higher implementation challenges, such as accurate time-synchronization requirement and huge information exchange among cells.

The goal of this research is to investigate techniques that mitigate ICI for modern cellular systems. Chapter 2 focuses on practical scheduling algorithms that can be applied to currently deployed LTE Release 8 networks, while Chapter 3 and 4 focuses on more advanced ICI mitigation techniques based on coordinated beamforming.

1.2 Literature Survey

Included in the following sections of the literature survey include a discussion of CB in *multi-input single-output* (MISO) and MIMO systems and beamforming techniques

that take PAPC into account.

1.2.1 CB in MISO and MIMO Systems

The idea of CB comes from mid-nineties, mainly targeting a so-called SINR-leveling problem [24], i.e. the power levels and the beamforming vectors are calculated to achieve some common SINRs in the system or to maximize the minimum SINR. Sine then there has been various CB algorithms that target different system aspects, such as minimizing total transmit power, maximizing sum rate, minimizing *mean-square error* (MSE), and minimizing interference leakage power.

A straight-forward method for CB is to extended the *zero-forcing* (ZF) beamforming for MU-MIMO. Since ZF beamforming nulls the interference to the selected users, ZF-based CB can null out interference for users in the other cells. However, complete-interference nulling generally requires greater number of transmit antennas than the number of users in the system, and direct extension is not practical. Therefore, ZF CB that omits nulling of interference to users with large pathloss is proposed in [38]. This algorithm computes the ZF beams that matter the most, which is a heuristic cell/user prioritization approach.

One of the classical CB objectives is to *minimize total transmit power* (Min-TTP), while satisfying a minimum SINR among users [21]. The Min-TTP optimization problem is expressed as

$$\text{minimize} \sum_{k=1}^{K_j} \|\mathbf{P}_j^{(k)}\|_F^2, \tag{1}$$

subject to

$$\text{SINR}_j^{(k,r)} \geq \gamma_j^{(k)}, \tag{2a}$$

where $\|\cdot\|_F$ is the Frobenius norm of the matrix, $\gamma_j^{(k)}$ is the minimum SINR constraint for User k in Cell j.

It can be shown that total transmit power objective is a quadratic function of the precoding vector and the SINR inequalities can be also made into a quadratic

function inequality in MISO systems. Therefore, the optimization problem is a convex problem and optimum precoding vectors can be found in polynomial time using convex optimization methods [13]. Other variation of the Min-TTP problem is adding a leakage interference price to the problem objective [60]. It was shown that even with the interference pricing, the problem is also solvable using convex optimization methods and solution is unique.

As the BSs have access to stable electrical grids, minimizing the transmit power may not be so critical. Instead optimizing the sum rate of all users under transmit power constraints may be more attractive for cellular operators. Maximizing *weighted sum-rate* (WSR) is expressed as

$$\text{maximize} \sum_{j=1}^{J} \sum_{k=1}^{K_j} \sum_{r=1}^{L_j^{(k)}} \log_2(1 + \text{SINR}_j^{(k,r)}), \tag{3}$$

subject to

$$\sum_{k=1}^{K_j} \|\mathbf{P}_j^{(k)}\|_F^2 \leq P_j \tag{4a}$$

where P_j is the total power constraint for cell j.

Precoding matrices that maximize WSR directly is complex because the precoding matrices of cells are all coupled in the sum-rate equation. In MISO systems, it is possible to find Rank 1 precoding vectors using a iterative estimation algorithm [43]. In each iteration, eigenvectors of a matrix derived from the *Karush-Kuhn-Tucker* (KKT) condition of the WSR objective is found and the computed eigenvectors are used to subsequently update the KKT condition matrix.

Alternatively, it can be shown that finding the precoding vectors that maximize the WSR is equivalent to a weighted *minimum mean-square error* (MMSE) precoding vector derived from the uplink virtual SINR [66]. The weights of the MMSE precoding vector are chosen such that it maximizes the sum rate and can be found using the KKT conditions. For MIMO systems, the maximizing the WSR is a non-convex problem

and therefore a suboptimal solution can be found by solving the WSR problem with a fixed receiver filter, which effectively makes the problem into a MISO system [18, 76, 47]. The receive filter is updated using the computed precoding matrices and new precoding matrices that achieve maximum WSR is iteratively computed. The algorithm will find better precoding matrices that maximize WSR and is guaranteed to converge.

The concept of iteratively computing CB precoding matrices and receiver filters such that it improves overall system performance can be found in several other literatures [44, 41, 92]. This will be denoted as the alternating optimization algorithm. How the precoding matrix and the receiver filter is computed defines the maximizing or minimizing objective. It was shown that differently weighted MMSE precoding in a iterative algorithm can result in maximizing the virtual uplink SINR, maximizing the weighted sum rate, or minimizing the total MSE [73], where the weighted MMSE precoding can be expressed in the following form.

$$\mathbf{P}_j^{(k)} = \left(\sum_{i=1}^{J} \sum_{l=1}^{K_i} \alpha_i^{(l)} \mathbf{H}_{ji}^{(l)\dagger} \mathbf{W}_i^{(l)} \mathbf{W}_i^{(l)\dagger} \mathbf{H}_{ji}^{(l)} + \beta_j \mathbf{I} \right)^{-1} \mathbf{H}_{jj}^{(k)\dagger} \mathbf{W}_j^{(k)} \mathbf{D}_j^{(k)}, \tag{5}$$

where $\mathbf{P}_j^{(k)}$ is the precoding matrix for user k in cell j, $\mathbf{W}_i^{(l)}$ is the receive filter for user l in cell i, $\alpha_i^{(l)}$ and β_j are the weight coefficients, and $\mathbf{D}_j^{(k)}$ is a diagonal matrix that normalizes the column vectors of the precoding matrix. It is also interesting to note that CB that maximizes the received signal power with interference limiting constraints can be also represented into a weighted MMSE precoding matrix form [65].

Although, maximizing the sum rate and the overall system performance is important, modern cellular networks also need to consider fairness among users as the data rate demands for each user is growing. CB that maximize the *minimum SINR* (Min-SINR) of users is one example of such fairness. Maximizing Min-SINR optimization

problem is expressed as

$$\text{maximize} \min_{\forall j,k,r} \text{SINR}_j^{(k,r)}, \tag{6}$$

subject to

$$\sum_{k=1}^{K_j} \|\mathbf{P}_j^{(k)}\|_F^2 \leq P_j \tag{7a}$$

In [14], it was shown that CB precoding matrices can be computed such that minimum SINR of users can be maximized through iterative computation of optimal transmit powers and precoding matrices with the help of Perron-Frobenius theorems. Alternatively, CB that maximize the lower bound of the SINR of users has been proposed in [30], which can be also represented in a weighted MMSE precoding matrix form.

Other CB algorithms worth mentioning are interference pricing algorithms, where the objective is to maximize the sum rate [23, 73] or minimize the transmit power [60] with some interference pricing. The interference pricing algorithms compute the CB precoding matrices such that it either maximizes or minimizes the objective while keeping the overall interference to a minimum.

1.2.2 Beamforming with Power Constraints

The capacity of the system is always of interest, since it gives some hints on the performance of new techniques. The capacity region of a MIMO Gaussian broadcast channel with PAPC was shown to be the same as the capacity region of a dual multiple-access channel with uncertain noise [48]. A capacity study of a single-user system with and without beamforming, where PAPC is met with equality, was conducted in [67] and [87], respectively. In all of these studies, it was shown that the capacity of single-cell system with PAPC can be quite close to the capacity of system with *total power constraint* (TPC).

One of the earliest study of beamforming with PAPC was for a single cell system with ZF beamforming for multiple users [10]. It focused on finding the total power

scaling factor that would satisfy the PAPC and maximize sum rate for given ZF precoding vectors. Therefore, the beamforming did not met PAPC with equality and some of the transmit power was not used. To fully utilize all the transmit power, beamforming for single cell, single user, single spatial stream beamforming that only matches the phase of the channel was proposed in [34], and constant envelop precoding, where all the elements of the precoding matrix have identical power was proposed in [58]. While both beamforming algorithms met PAPC with equality, it imposes significant restrictions on the beamforming coefficients.

PAPC was first applied to ZF beamforming in MISO systems and the precoding vectors were computed using convex optimization [39]. Later, multi-stream ZF beamforming for MIMO systems was investigated in [40]. Although, studies presented a close form formulation of the precoding matrix, the proposed algorithm in [40] could not be applied for single stream beamforming and required maximal likelihood (ML) receiver for all users.

PAPC applied to one of the classical beamforming objectives, Min-TTP, in a MISO system was investigated in [93, 91, 94, 74]. It was identified that the problem can be formulated into a convex problem with an unknown covariance parameter and therefore solvable using convex optimization methods [13]. Same beamforming objective for MIMO systems was investigated in [54], where it utilized the alternating optimization algorithm used in other various literature to tackle MIMO systems.

Beamforming that maximizes WSR with PAPC was investigated in [84, 11, 22]. Similar to Min-TTP with PAPC problem, convex optimization method can be used [22]. In [84], the beamforming problem was approximated such that geometric programming (GP) can be utilized to compute the precoding matrices. In [11], precoding matrices that maximize WSR was computed indirectly by use of weighted MMSE precoding, similar to CB studies in [66, 18, 76, 47, 73].

Convex optimization methods were also utilized to compute beamforming with

PAPC that maximize Min-SINR [26] and minimize MSE [88, ?], respectively. However, convex optimization methods can be computationally complex and low-complexity beamforming with PAPC has been proposed in [80]. The algorithm simply scales each row of the MMSE precoding matrix such that it mets PAPC in an alternating optimization algorithm. Although, the algorithm is simple it does not guarantee convergence and in some cases may diverge and result in poor performance. Another attempt at low-complexity beamforming algorithms with PAPC was presented in [70, 46]. It proposed algorithms that iteratively computes the a single row vectors of the precoding matrix in each iteration step. It was shown that the proposed algorithms are guaranteed to converge.

1.3 Dissertation Outline

Outline of this dissertation is as follows. In Chapter 2, SFR inter-cell interference coordination is investigated. Effect of user classification and transmit power configuration to performance of SFR is analyzed. Distributed scheduling algorithm that can be applied to current LTE system is proposed and simulated. In Chapter 3, multi-stream multi-user coordinated transmit beamforming for wireless networks with multiple transmit and receive antennas is investigated. Low-complex iterative algorithms to compute coordinated beamforming matrices is proposed and simulated. Additionally, applicability of the proposed algorithm to TDD systems with partial and imperfect CSI knowledge is analyzed. In Chapter 4, coordinated beamforming discussed in Chapter 3 is further extended to multi-carrier systems with per-antenna power constraints. Low complexity algorithm that can be applied to coordinated beamforming algorithms with whitened match filter structure is proposed and simulated. The contents of Chapter 2 and 3 are based on previous publication by the author [20, 49].

CHAPTER II

SCHEDULING AND POWER-ALLOCATION ALGORITHM FOR SFR

2.1 Introduction

There are different ways to improve the throughput of cell-edge users. For example, *generalized proportional fairness* (GPF) scheduler [61] can weigh the cell edge users more to increase their throughput at the cost of reducing the average cell throughput. *Multi-input multi-output* (MIMO) techniques can utilize spatial beamforming to increase *signal-to-interference-and-noise ratio* (SINR) for cell edge users. A group of cells can cooperate to reduce inter-cell interference via regulating scheduling and transmit power, which is also known as *inter-cell interference coordination* (ICIC). ICIC techniques do not necessarily require any modification to existing *user equipment* (UE) and can be implemented with some minimal changes in the base station. Therefore, this chapter focuses on *orthogonal frequency division multiple access* (OFDMA) based ICIC throughput improvement that can be implemented with the Release 8 downlink LTE.

There are two major categories of ICIC, called *fractional frequency reuse* (FFR) [53] and *soft frequency reuse* (SFR) [36]. Since SFR allows full frequency reuse for wireless networks, this chapter will focus on low-complexity SFR scheduling that takes both throughput and fairness into consideration. In SFR, the bandwidth for a cell is divided into two parts: *cell-edge band* (CEB) and *cell-center band* (CCB). Users are also divided into two groups, scheduled in CEB and CCB, respectively. The users with strong interference from the neighboring cells are classified as the *cell-edge users* (CEUs) and the rest are the *cell-center users* (CCUs). To avoid interference among

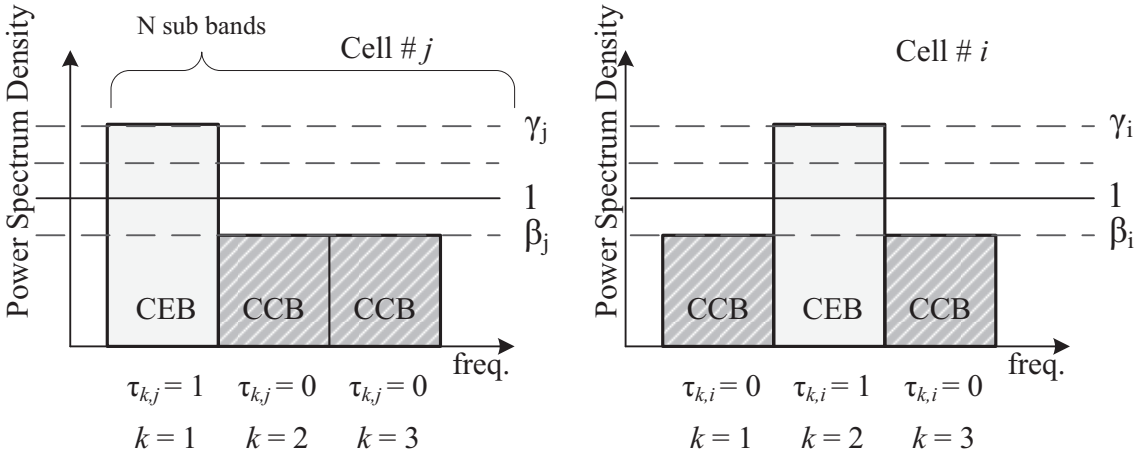

Figure 1. An example of relationship between frequency and power spectrum density for soft frequency reuse deployed systems

the CEUs in adjacent cells, their CEB's should be non-overlapped. Furthermore, the downlink transmit power of the CEB should be boosted compared to that of the CCB. For example, a 3-way SFR divides the whole bandwidth into 3 sub-bands, one for CEB and two for CCB. If CCB is attenuated by -1.77dB, then CEB will be boosted by 2dB so that total downlink transmit power of the SFR system maintains the same as that of the non-ICIC system. The power boosting of the CEB increases the signal strength whereas the coordinated CEB allocation among cells reduces inter-cell interference. This leads to increase in the received SINR for the CEUs. The example in Figure 1 shows the relationship between frequency and power spectrum density for two neighboring cells, where $\tau_{k,i}$ is the CEB/CCB indicator for cell i for sub-band k, and is configured to 1 for CEB and 0 for CCB, and γ and β represent the power gains applied to CEB and CCB, respectively.

In order to deploy ICIC techniques to downlink LTE systems, additional restrictions imposed by the LTE standard needs to be considered. One of the restrictions is the transmit power of the data channel. The LTE standard allows transmit power of the data channel to an UE to be either power boosted or attenuated by $\{-6\text{dB}, -4.77\text{dB}, -3\text{dB}, -1.77\text{dB}, 0\text{dB}, 1\text{dB}, 2\text{dB}, 3\text{dB}\}$ compared to the *Common*

Reference Signal (CRS) power [2]. In order to correctly demodulate data signals, the UE must know the power gap between the transmission power density of the CRS and data signal in advance, especially to demodulate *Quadrature Amplitude Modulation* (QAM) signals. This information is conveyed through *Radio Resource Control* (RRC) configuration messaging, which may take up to 64 ms configuration delay [2]. So for all practical purposes, the transmit power density of the data channel is configured in a semi-static manner.

In order to operate SFR in a system, the scheduling process must derive the resource allocation information for each user and the transmit power of CEB and CCB for each cell. In addition, scheduler should also consider fairness among users. Previous research in [12] investigates transmit power optimization for the CEB and the CCB along with dynamic resource allocation. Fairness and *quality-of-service* (QoS) for the ICIC system have been considered in [96]. The above approaches can improve the performance of wireless networks. However, their computational complexity grows exponentially with the number of users and the number of cells. Furthermore, the computation must be performed in every *transmit time interval* (TTI), which is 1 ms in LTE systems. Additionally, joint optimization across all coordinating cells means that the scheduling decisions and information in each TTI must be conveyed to all coordinating cells with a very low delay. Even with all the breakthrough in wired communications, synchronizing information across the whole network with delay smaller than 1 ms is extremely challenging. Therefore, low-complexity de-centralized SFR is desired in LTE systems, which is a focus of this chapter. Even though some literature, such as [16, 62], has investigated SFR based ICIC techniques and have shown interesting analytical results, there is no direct analytical comparison between SFR and traditional non-ICIC systems.

The rest of this chapter is organized as following. In Section 2.2, comparison of SFR and traditional non-ICIC systems are discussed and important properties of

SFR throughput performance are identified. In Section 2.3, a novel low-complexity SFR algorithm taking fairness and throughput into consideration is discussed. In Section 2.4, the throughput improvement of the proposed algorithm is demonstrated through computer simulation based on the realistic deployment scenario endorsed by the *International Telecommunication Union* (ITU) Radiocommunication Group. Conclusions are drawn in Section 2.5.

Here are some symbols that will be used in this chapter.

- $P_{j,i}^{(l)}$: received downlink signal power for cell i from UE j in cell l.
- γ_i, β_i : relative power (boost or attenuation) gains for CCB and CEB at cell i, respectively.
- $\tau_{k,i}$: CEB indicator on whether sub-band k of the cell i is CEB or CCB, 1 for CEB and 0 for CCB.
- $\mathcal{S}_i$: set of UEs in cell i.
- $|\mathcal{S}|$: cardinality of the set $\mathcal{S}$.
- $\mathcal{S}_i^{\text{CEU}}$, $\mathcal{S}_i^{\text{CCU}}$: sets of UEs classified as CEUs and CCUs in cell i, respectively, $\mathcal{S}_i^{\text{CCU}} \cup \mathcal{S}_i^{\text{CEU}} = \mathcal{S}_i$ and $\mathcal{S}_i^{\text{CCU}} \cap \mathcal{S}_i^{\text{CEU}} = \emptyset$.
- $\delta_j^{(i)}$: UE classification indicator on whether UE j in cell i is classified as CEU or CCU, 1 for CEU and 0 for CCU.
- κ_i : CCU population ratio defined as $\kappa_i = |\mathcal{S}_i^{\text{CCU}}|/|\mathcal{S}_i|$, $(1-\kappa_i) = |\mathcal{S}_i^{\text{CEU}}|/|\mathcal{S}_i|$.
- N : number of sub-bands in the system.
- $\mathcal{F}$: set of cells in the network.

2.2 Comparison of Non-ICIC and SFR System

In this section, SINR and throughput for the users in non-ICIC systems and in SFR systems are derived and compared. It is assumed that the cells are fully loaded, where ICIC schemes are most desired due to strong interference from neighboring cells. Additionally, it is assumed that number of SFR bands is fixed and same for all cells.

2.2.1 Throughput of a non-ICIC System

For a non-ICIC system, the *general proportional fairness* (GPF) scheduler [61] is assumed. The GPF scheduler allocates any resource at time t to the user with the maximum PF metric, which is defined as

$$PF_t = \frac{R_t^{\text{est}}}{(T_t^{\text{avg}})^{\alpha}}, \tag{8}$$

where R_t^{est} is the estimated throughput for each user at time t, α determines the fairness-throughput trade-off, and T_t^{avg} is the average data rate of the user. The average data rate can be obtained by

$$T_t^{\text{avg}} = \epsilon \cdot T_{t-1}^{\text{avg}} + (1-\epsilon) \cdot T_{t-1}^{\text{suc}}, \tag{9}$$

where T_{t-1}^{suc} is the actual throughput of the system for the user at time $t-1$, and ϵ in the above equation is a forgetting factor and is typically chosen be very close to 1. When $\alpha = 1$, the GPF scheduler turns into a *proportional fairness* (PF) scheduler. It becomes a greedy scheduler when $\alpha = 0$, and an absolute fair scheduler when $\alpha = \infty$.

First, evaluation of the throughput of a non-ICIC system is shown. The average SINR of user j in cell l in a non-ICIC system can be expressed as

$$\text{SINR}_j^{(l)} = \frac{P_{j,l}^{(l)}}{\sum_{i \in \mathcal{F}, i \neq l} P_{j,i}^{(l)} + \sigma_n^2}, \tag{10}$$

where σ_n^2 is the power of additive white Gaussian noise, $P_{j,i}^{(l)}$ is the received downlink signal power of cell i from UE j in cell l and is called the *Reference Signal Received*

Power (RSRP) [3] in LTE. If the system is interference limited, which is typical for an urban cellular deployment, the SINR in (10) can be approximated as

$$\widehat{\mathrm{SINR}}_j^{(l)} = \frac{P_{j,l}^{(l)}}{\sum_{i\in\mathcal{F}, i\neq l} P_{j,i}^{(l)}}. \tag{11}$$

If the PF scheduler is used, in a long run, the PF scheduler will allocate to each user equal amounts of bandwidth on the average [7, 33], thus the average bandwidth allocated for a user in cell l will be $B/|\mathcal{S}_l|$, where B is the whole bandwidth for a cell. From the SINR derivation results, the approximation of user throughput can be expressed as

$$R_j^{(l)} = \frac{B}{|\mathcal{S}_l|}\log_2(1+\widehat{\mathrm{SINR}}_j^{(l)}). \tag{12}$$

2.2.2 Throughput of an SFR System

It is assumed that only one of sub-band is allocated for the CEB in an SFR system as described in [36], and each sub-band consists of multiple subcarriers. For example, for SFR with $N = 3$ in a 10 MHz LTE system, the CEB consists of 17 resource blocks out of total 50 ones, where the resource block is the minimum unit of resource. This is about $1/N$ of the whole system bandwidth. In SFR systems, the CEB is power boosted by γ_i (> 1). Because the total transmit power of a given cell cannot exceed the regulatory constraint in LTE systems, the power for the CCB needs to be attenuated by β_i (< 1) so that $\gamma_i + (N-1)\beta_i = N$.

For SFR systems, the SINR for sub-band k for user j in cell l can be expressed as

$$\mathrm{SINR}_{k,j}^{\text{SFR-}(l)} = \frac{\left(\delta_j^{(l)}\gamma_l + (1-\delta_j^{(l)})\beta_l\right) P_{j,l}^{(l)}}{\sum_{i\in\mathcal{F}, i\neq l}\left(\tau_{k,i}\gamma_i + (1-\tau_{k,i})\beta_i\right) P_{j,i}^{(l)} + \frac{\sigma_n^2}{N}}. \tag{13}$$

The SINR in (13) is a non-trivial form to analyze because the CEB indicator, $\tau_{k,i}$, for other cells is its integral part. Instead, an approximation of the lower bound, the upper bound, and the average SINR will be used to get more insights. The detailed

derivation is shown in Appendix A.1. The average SINR approximation is computed by taking the expectation of the interference term and treating the CEB indicator as a random binary variable with a probability of $1/N$ to be 1 and expressed as

$$\widehat{\mathrm{SINR}}_j^{\text{SFR-}(l)} = \frac{\left(\delta_j^{(l)}\gamma_l + (1-\delta_j^{(l)})\beta_l\right) P_{j,l}^{(l)}}{\sum_{i\in\mathcal{F}, i\neq l} P_{j,i}^{(l)}}. \tag{14}$$

The lower and upper SINR bounds can be represented in terms of the average SINR approximation computed in (14) and they are given as

$$\frac{1}{\gamma^{\max}}\widehat{\mathrm{SINR}}_j^{\text{SFR-}(l)} \leq \widehat{\mathrm{SINR}}_j^{\text{SFR-}(l)} \leq \frac{1}{\beta^{\min}}\widehat{\mathrm{SINR}}_j^{\text{SFR-}(l)}, \tag{15}$$

where $\gamma^{\max}$ and $\beta^{\min}$ are the maximum power boost of CCB and minimum power attenuation of CEB of all cooperating cells, respectively, and defined as

$$\begin{aligned} \gamma^{\max} &= \max_{i\in\mathcal{F}} \gamma_i, \\ \beta^{\min} &= \min_{i\in\mathcal{F}} \beta_i. \end{aligned} \tag{16}$$

From the average SINR, the throughput for the CEUs and the CCUs can be expressed as

$$\tilde{R}_{j\in\mathcal{S}_i^{\text{CEU}}}^{(l)} = \frac{B}{N}\frac{1}{|\mathcal{S}_i^{\text{CEU}}|}\log_2(1+\widehat{\mathrm{SINR}}_j^{\text{SFR-}(l)}), \tag{17}$$

and

$$\tilde{R}_{j\in\mathcal{S}_i^{\text{CCU}}}^{(l)} = \frac{(N-1)B}{N}\frac{1}{|\mathcal{S}_i^{\text{CCU}}|}\log_2(1+\widehat{\mathrm{SINR}}_j^{\text{SFR-}(l)}), \tag{18}$$

respectively. The lower and upper bounds of the throughput for the CEUs and CCUs are found by replacing the average SINR with the lower and upper bounds of SINR.

2.2.3 Throughput Comparison

When the SINR is low, which is likely the scenario for the CEU, capacity is linear with respect to SINR and the throughput in (17) can be approximated as

$$\begin{aligned}\tilde{R}^{(l)}_{j\in\mathcal{S}_l^{\mathrm{CEU}}} &\approx \frac{B}{N}\frac{1}{|\mathcal{S}_l^{\mathrm{CEU}}|}\widehat{\mathrm{SINR}}_j^{\text{SFR-}(l)} \\ &= \frac{|\mathcal{S}_l|}{N|\mathcal{S}_l^{\mathrm{CEU}}|}\frac{B}{|\mathcal{S}_l|}\gamma_l\widehat{\mathrm{SINR}}_j^{(l)} \\ &= \frac{\gamma_l}{N(1-\kappa_l)}\frac{B}{|\mathcal{S}_l|}\widehat{\mathrm{SINR}}_j^{(l)} \\ &\approx \frac{\gamma_l}{N(1-\kappa_l)}R_j^{(l)}.\end{aligned} \tag{19}$$

The lower and upper approximate throughput bounds can be found as

$$\tilde{R}^{\text{min-}(l)}_{j\in\mathcal{S}_l^{\mathrm{CEU}}} \approx \frac{\gamma_l}{\gamma^{\max}N(1-\kappa_l)}R_j^{(l)}, \tag{20}$$

and

$$\tilde{R}^{\text{max-}(l)}_{j\in\mathcal{S}_l^{\mathrm{CEU}}} \approx \frac{\gamma_l}{\beta^{\min}N(1-\kappa_l)}R_j^{(l)}, \tag{21}$$

respectively. The detailed derivation for the lower and upper bounds are given in Appendix A.1.

Throughput approximation in (19), (20), and (21) allows us to directly compare the throughput of CEU in SFR and non-ICIC systems. From (19), in order for the CEU to have any throughput gain on the average, the inequality, $\gamma_l/(N(1-\kappa_l)) > 1$, must be satisfied. In the worst case scenario, performance of the cell-edge users cannot be improved if $\gamma_l/(\gamma^{\max}N(1-\kappa_l)) \leq 1$ from (20). Therefore, it is important to configure the ICIC parameters properly to get performance improvement.

For typical CCUs, the SINR is much larger than one. Consequently, the throughput of a CCU can be approximated by

$$\begin{aligned}\tilde{R}^{(l)}_{j\in\mathcal{S}_l^{\mathrm{CCU}}} &\approx \frac{(N-1)B}{N}\frac{1}{|\mathcal{S}_i^{\mathrm{CCU}}|}\log_2\left(\widehat{\mathrm{SINR}}_j^{\text{SFR-}(l)}\right) \\ &= \frac{(N-1)B}{N}\frac{1}{|\mathcal{S}_i^{\mathrm{CCU}}|}\log_2\left(\beta_l\widehat{\mathrm{SINR}}_j^{(l)}\right) \\ &= \frac{(N-1)|\mathcal{S}_l|}{N|\mathcal{S}_i^{\mathrm{CCU}}|}\frac{B}{|\mathcal{S}_l|}\left(\log_2\beta_l + \log_2\widehat{\mathrm{SINR}}_j^{(l)}\right) \\ &\approx \frac{N-1}{N\kappa_l}\frac{B}{|\mathcal{S}_l|}\log_2\beta_l + \frac{N-1}{N\kappa_l}R_j^{(l)}.\end{aligned} \tag{22}$$

Similar to throughput approximation of CEUs, the lower and upper throughput bounds can be expressed as

$$\tilde{R}^{\text{min-}(l)}_{j\in\mathcal{S}_l^{\mathrm{CCU}}} \approx \frac{N-1}{N\kappa_l}\frac{B}{|\mathcal{S}_l|}\log_2\frac{\beta_l}{\gamma^{\max}} + \frac{N-1}{N\kappa_l}R_j^{(l)}, \tag{23}$$

and

$$\tilde{R}^{\text{max-}(l)}_{j\in\mathcal{S}_l^{\mathrm{CCU}}} \approx \frac{N-1}{N\kappa_l}\frac{B}{|\mathcal{S}_l|}\log_2\frac{\beta_l}{\beta^{\min}} + \frac{N-1}{N\kappa_l}R_j^{(l)}, \tag{24}$$

respectively.

Since $\beta_l < 1$ and $\gamma_i > 1$ in (22) and (23), the first term in (22) and (23) is non-positive. Because of this, if $(N-1/(N\kappa_l)) < 1$ then $\tilde{R}^{(l)}_{j\in\mathcal{S}_l^{\mathrm{CCU}}} < R_j^{(l)}$. The same statement is true for the upper bound throughput if $\beta_l \leq \beta^{\min}$ in (24). From these equations, throughput for the CCUs with ICIC is typically lower than that with traditional non-ICIC if $N-1 < N\kappa_l$. In fact, this shows us that for CCUs, κ_l is the most dominant term to throughput improvement. So in order for the CCUs to have any throughput improvement, the ratio $(N-1)/(N\kappa_l)$ needs to be large enough to compensate for the loss incurred by β_l in (22).

From the above analysis, the power gains, β_i and γ_i, and the numbers of the CEUs and the CCUs play critical roles in the throughput of the SFR system. One of the most dominant factors is the population ratio of CEUs and CCUs. In order for the CEUs to get high throughput, the number of the CEUs in the cell needs to

be small. For CCUs to have minimal throughput loss or even to have some gain, the number of the CCUs must be small. The population ratio between the CEUs and the CCUs will guide their throughput tradeoff. Similar tradeoff exists for the power gains, where increasing the power of the CEB will increase throughput for the CEUs but it will also decrease the power of the CCB and result in throughput loss for the CCUs. Because of the trade-off relationship, it is difficult to improve the performance of both the CEUs and the CCUs at the same time.

2.3 Proposed SFR algorithms

To overcome computational complexity and scheduling information exchange latency for the dynamic resource allocation while obtaining fairness as well as optimal transmit power for CEB and CCB, the SFR scheduling operations are seperated into two parts. The first part, denoted as the parameter update, will compute the power gains of CEB and CCB and classify UEs (CCU or CEU) taking fairness into account. The parameter update requires coordinated information among the cells and will be only computed in a long term basis. The second part, denoted as the resource allocation, will perform dynamic resource allocation for each cell independently based on GPF. Note that during the update of the power gains and the UE classification, before new parameter configuration is available, the dynamic resource allocation can be still performed based on the previous (i.e. latest) one. Therefore, this architecture allows high latency information exchange among cells in the first part while keeping low-complexity scheduling for the resource allocation for each TTI in the second part.

Figure 2 shows the flowchart of the proposed SFR algorithm. It is a de-centralized multi-cell cooperation algorithm. Each cell first updates power gains for CEB and CCB as well as UE classification. The computation of the optimal power gains and UE classification is based on RSRP reporting from the UEs. Because RSRP measurement depicts the long term average signal strength of the cells, the computed results for

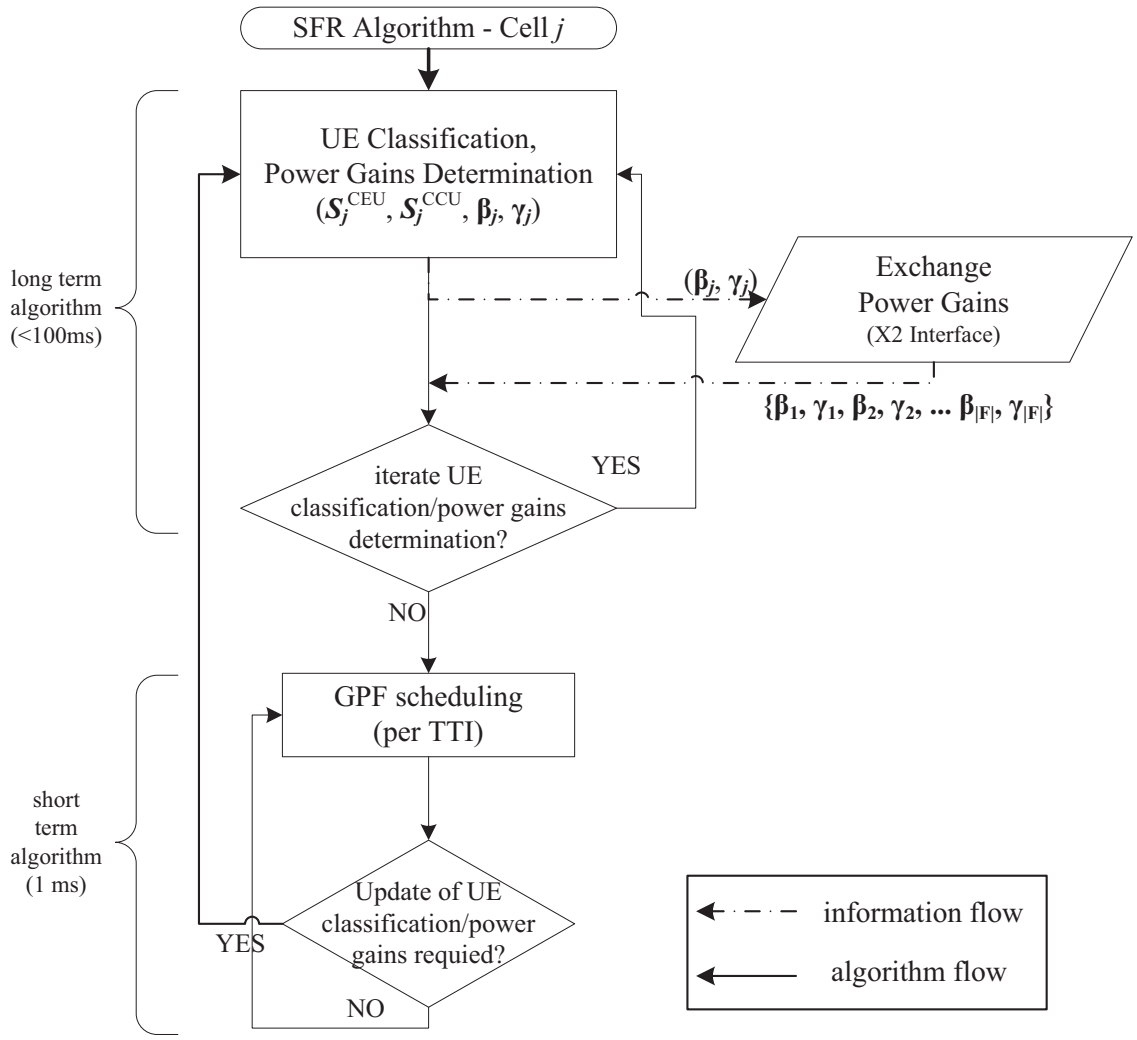

Figure 2. An example of the parameter configuration in an SFR system

power gains and UE classification can be used in a long term basis. The minimum reporting interval of RSRP information by the UEs used to compute power gains and UE classification is 120 ms [2]. If the mobility of the UEs is low, the RSRP information will not change frequently and larger reporting interval can be used.

The power gains of other cells are received through base-station-to-base-station link called the X2 interface [12]. If no information of power gain of cell i is available, then set $\beta_i = \gamma_i = 1$. The updated power gains are exchanged among base stations. In LTE systems, the *relative narrow-band transmit power* (RNTP) [4] message can represent the power gains as well as the CEB and CCB locations for each cell. From

the updated power gains, $\{\beta_1, \gamma_1, ..., \beta_{|\mathcal{F}|}, \gamma_{|\mathcal{F}|}\}$, the UE classification can be updated. An iteration is defined as an exchange of RNTP message among cells. After some iterations of power gain computation and UE classification, the scheduler configures UEs with the updated parameters. Each cell performs resource scheduling separately and in parallel for each TTI. If a cell detects significant changes in the SINR of UEs in the cell (e.g. new reporting of RSRP measurements), then it can perform power gain computation and UE classification again. Note that resource scheduling for each TTI can be still made during the power gain computation and UE classification based on the previous parameters.

The power gain exchanges among cells are not expected to be the bottleneck of the algorithm as most modern X2 interface implementations are able to meet 10 ms round trip latency requirements [59] set by many of the LTE operators in the world. The expected time interval of the update of power gains and UE classification is a magnitude longer than the time needed for exchanging information among cells.

In general, the RNTP message should be exchanged among all SFR participating cells in the network. But, in practice, the power gain information of a cell only needs to be conveyed to its surrounding cells that are significantly affected by its power gain change.

2.3.1 Prior Research on UE Classification and Power Allocation

Distance based UE classification has been developed for FFR systems [81, 29]. Since distance information is not accurate enough and does not always reflect received signal or interference strength, the distance metric may not truly represent whether a UE is under severe interference or not.

To overcome this issue, UE classification should be based on UE's wideband SINR directly [63, 64, 32, 83]. The *SINR threshold* (STH) based UE classification can be

expressed as,

$$\begin{aligned}\mathcal{S}_l^{\text{CEU}} &= \{j|\forall j \in \mathcal{S}_l,\ \text{SINR}_j^{(l)} \geq \text{SINR}_{\text{thresh}}\},\\ \mathcal{S}_l^{\text{CCU}} &= \{j|\forall j \in \mathcal{S}_l,\ \text{SINR}_j^{(l)} < \text{SINR}_{\text{thresh}}\}.\end{aligned} \tag{25}$$

where $\text{SINR}_{\text{thresh}}$ is the SINR threshold.

Alternatively, UEs are classified and its power gains are allocated for CCB and CEB by maximizing sum of user's throughputs in the system [5, 12, 6, 71, 95, 15]. The *max-sum throughput* (MST) algorithm can be expressed as

$$\{\hat{\mathcal{S}}_l^{\text{CCU}}, \hat{\beta}_l\} = \underset{\mathcal{S}_l^{\text{CCU}}, \beta_l}{\text{argmax}} \sum_{j \in \mathcal{S}_l} \sum_{k=1}^{N} \frac{B}{N M_j^{(l)}} r_{j,k}^{(l)}, \tag{26}$$

subject to

$$r_{j,k}^{(l)} = \log_2\left(1 + \text{SINR}_{k,j}^{\text{SFR-}(l)}\right), \tag{27a}$$

$$\beta_l \in \{10^{-0.6}, 10^{-0.477}, 10^{-0.3}, 10^{-0.177}, 1\}, \tag{27b}$$

$$N = \gamma_l + (N-1)\beta_l, \tag{27c}$$

$$\mathcal{S}_l^{\text{CCU}}, \mathcal{S}_l^{\text{CEU}} \subset \mathcal{S}_l, \tag{27d}$$

$$\mathcal{S}_l^{\text{CCU}} \cap \mathcal{S}_l^{\text{CEU}} = \emptyset, \mathcal{S}_l^{\text{CCU}} \cup \mathcal{S}_l^{\text{CEU}} = \mathcal{S}_l, \tag{27e}$$

where $M_j^{(l)} = \delta_j^{(l)}|\mathcal{S}_i^{\text{CEU}}| + (1-\delta_j^{(l)})|\mathcal{S}_i^{\text{CCU}}|$ and $\text{SINR}_{k,j}^{\text{SFR-}(l)}$ is from (13). The CEU set and CEB power gain for cell l is obtained from $\hat{\mathcal{S}}_l^{\text{CEU}} = \mathcal{S}_l \setminus \hat{\mathcal{S}}_l^{\text{CCU}}$ and $\hat{\gamma}_l = N - (N-1)\hat{\beta}_l$.

Once the UE is classified and power gains are determined, GPF scheduling can be performed for each TTI in the resource allocation part of the SFR algorithm.

2.3.2 Proposed UE Classification and Power Allocation Algorithm

The MST algorithm is greedy and may result in unfairness among users. In order to prioritize the most coverage limited user, the optimization problem is formulated to maximize the minimum of all user's throughput. However, max-min problem is usually hard to tackle. Furthermore, the overall throughput of the cell is ignored

in the max-min problem. Thus, to enhance throughput for coverage limited users while having sufficiently good cell average throughput, the harmonic sum of the user throughput is maximized. This approach achieves a good tradeoff between fairness and throughput. The *max-harmonic-sum throughput* (MHT) algorithm can be expressed as,

$$\{\hat{\mathcal{S}}_l^{\mathrm{CCU}}, \hat{\beta}_l\} = \underset{\mathcal{S}_l^{\mathrm{CCU}}, \beta_l}{\operatorname{argmax}} \frac{1}{\displaystyle\sum_{j \in \mathcal{S}_l} \frac{1}{\sum_{k=1}^{N} \frac{B}{NM_j^{(l)}} r_{j,k}^{(l)}}}, \tag{28}$$

subject to the same constraints as (27).

It can be easily shown that for any set of positive numbers, $\{x_1, x_2, ..., x_N\}$,

$$\min\{x_1, x_2, \cdots, x_N\} \geq \frac{1}{\sum_{i=1}^{N} \frac{1}{x_i}}. \tag{29}$$

Therefore maximizing the harmonic sum will indirectly maximize the minimum value.

In addition, different from just maximizing the minimum value, maximizing the harmonic sum also takes the overall throughput into account since

$$\frac{1}{N} \sum_{i=1}^{N} x_i \geq \frac{N}{\sum_{i=1}^{N} \frac{1}{x_i}}. \tag{30}$$

In summary, harmonic sum maximization results in UE classification and power allocation in favor of the users with a low SINR while considering the overall average throughput as well, which achieves a good trade-off between fairness and throughput.

The geometric sum of user's throughputs, which is denoted as the *max-geometric-sum throughput* (MGT) algorithm, is considered. Since the geometric mean is upper bounded by arithmetic mean and lower bounded by the harmonic mean, it takes a less priority to the coverage limited users and slightly more priority to cell average throughput. It is interesting to note that maximizing the geometric sum is equivalent to the definition of proportionally fair optimization metric [42] for maximizing $\prod_{i=1}^{N} x_i$ is equivalent to maximizing $\sum_{i=1}^{N} \log x_i$.

The MST, MGT, and MHT UE classification algorithms allows us to prioritize the users in various ways, where the arithmetic sum is used to prioritize cell center

Table 1. UE classification and power gain determination algorithm

Algorithm UE classification and power gain determination algorithm

Initialization : $\mathcal{B} = \{10^{-0.6}, 10^{-0.477}, 10^{-0.3}, 10^{-0.177}, 1\}$, $H_{\text{best}} = 0$, $\mathcal{U} = \{j | j \in \mathcal{S}_l\}$.
for $m = 1, \cdots, |\mathcal{B}|$ **do**
    set $\beta_l = \mathcal{B}_m$ and $\gamma_l = N - (N-1) \cdot \mathcal{B}_m$.
    for $n = 1, \cdots, 2^{|\mathcal{U}|}$ **do**
        set $\delta_j^{(l)} = \lfloor \frac{n}{2^{v-1}} \rfloor \bmod 2$ for $j = \mathcal{U}_v$ for $1 \leq v \leq |\mathcal{U}|$.
        compute SINR for each sub-band for each user, $\text{SINR}_{k,j}^{(l)}$, as in (13) for $\forall j \in \mathcal{S}_l$.
        compute estimated throughput, $\tilde{R}_j^{(l)}$, as in (17) and (18) for $\forall j \in \mathcal{S}_l$.
        compute harmonic mean of estimate throughput $H = 1/(\sum_{j \in \mathcal{S}_l} 1/\tilde{R}_j^{(l)})$
        if $H_{\text{best}} < H$ **then**
            set $H_{\text{best}} = H$, $\hat{\beta}_l = \beta_l$, $\hat{\gamma}_l = \gamma_l$.
            set $\hat{\mathcal{S}}_l^{\text{CEU}} = \{j | \delta_j^{(l)} = 1, j \in \mathcal{S}_l\}$ and $\hat{\mathcal{S}}_l^{\text{CCU}} = \{j | \delta_j^{(l)} = 0, j \in \mathcal{S}_l\}$.
        end if
    end for
end for

users, whom contribute the most to cell average throughput, the harmonic sum is the prioritize coverage limited users (e.g. the users with low throughput), and finally geometric sum is used to be prioritize the coverage limited users and cell center users in a proportionally fair manner.

Pseudo code of the MHT SFR algorithm for UE classification and power gain determination is shown in Table 1. Note that $\mathcal{B}_m$ and $\mathcal{U}_v$ denote the m-th and v-th element of the set $\mathcal{B}$ and $\mathcal{U}$, respectively. The computed power gains from the algorithm will be shared among cells that can be used to update β_i and γ_i in the next iteration of the algorithm.

2.3.3 Computational Complexity Reduction for Harmonic Sum Maximization

The UE classification and power gain determination for the MHT algorithm is integer and combinatorial optimization problem and solved by exhaustively search for all

possible parameter space of β and $\mathcal{S}_l^{\text{CCU}}$. The computational complexity of the MHT algorithm can be further reduced by restricting the searching space of UE classification. Since UEs with low and high SINR will typically be chosen as the CEU and the CCU, respectively, the $\lfloor |\mathcal{S}_i|/N \rfloor$ of the lowest and highest SINR UEs to CEUs and CCUs, which are denoted as $\mathcal{S}_i^{\text{fix-CEU}}$ and $\mathcal{S}_i^{\text{fix-CCU}}$, respectively, are fixed to a specific value. Note that number, $\lfloor |\mathcal{S}_i|/N \rfloor$, was chosen heuristically based on observations from simulations of various deployment scenarios. The algorithm searches for optimal solution only within the UEs belonging to neither $\mathcal{S}_i^{\text{fix-CEU}}$ nor $\mathcal{S}_i^{\text{fix-CCU}}$, that is

$$\mathcal{U} = \mathcal{S}_i \setminus \mathcal{S}_i^{\text{fix-CEU}} \setminus \mathcal{S}_i^{\text{fix-CCU}}. \tag{31}$$

The above change will add one more restriction in the optimization objective function constraint (27), which can be expressed as

$$\mathcal{S}_i^{\text{fix-CEU}} \subset \mathcal{S}_i^{\text{CEU}}, \mathcal{S}_i^{\text{fix-CCU}} \subset \mathcal{S}_i^{\text{CCU}}. \tag{32}$$

This will allow us to reduce the UE classification search space from $|\mathcal{B}|2^{|\mathcal{S}_i|}$ to $|\mathcal{B}|2^{\lceil |\mathcal{S}_i|/N \rceil}$. Note that this type of computationally complexity reduction technique may be only applicable for the MHT algorithm, which prioritizes coverage limited UEs.

The computational complexity can be further reduced by relaxing the optimization binary UE classification variable, $\delta_j^{(l)}$, and using convex program methods. First, the expected throughputs for an UE is computed assuming that the UE is classified as CCU and CEU. Next, the softly classified UE throughput is expressed as a convex combination of the throughputs of CCU and CEU. The soft classification is solved to maximize the objective function and then finally the relaxed variable, $\delta_j^{(l)}$, is quantized into binary.

Note that the MHT optimization objective function (28) is not a convex nor concave function. Thus the objective function itself cannot be optimized by means of convex program. However, (28) can be transformed into a convex one by fixing the power gains, β_l and γ_l, as well as the total number of CEUs and CCUs. Once $\delta_j^{(l)}$ is

solved as an continuous variable between 0 and 1, it can be quantized into binary by finding j which correspond to the highest values of $\delta_j^{(l)}$ and set to 1, while rest of $\delta_j^{(l)}$ is set to 0. The processes repeats for all possible values of power gains, $\{\beta_l, \gamma_l\}$, and number CEUs and CCUs, $|\mathcal{S}_l^{\text{CEU}}|$, and $|\mathcal{S}_l^{\text{CCU}}|$, and find the set of parameters which maximize the objective function.

The convex relaxation of the objection function in (13) can be expressed as

$$\text{maximize} \quad \frac{1}{\displaystyle\sum_{j\in\mathcal{S}_l} \frac{1}{A_j^{(l)}\delta_j^{(l)} + B_j^{(l)}(1-\delta_j^{(l)})}}, \tag{33}$$

subject to

$$0 \le \delta_j^{(l)} \le 1, \quad \forall j \in \mathcal{S}_l \tag{34a}$$

$$\sum_{j\in\mathcal{S}_l} \delta_j^{(l)} = \Delta_l, \tag{34b}$$

where $A_j^{(l)}$ and $B_j^{(l)}$ are estimated user throughputs for CEB and CCB, respectively, and defined as

$$\begin{aligned} A_j^{(l)} &= \frac{B}{N\Delta_l} \log_2\left(1 + \gamma_l \cdot \widetilde{\text{SINR}}_j^{(l)}\right), \\ B_j^{(l)} &= \frac{B(N-1)}{N(|\mathcal{S}_l| - \Delta_l)} \log_2\left(1 + \beta_l \cdot \widetilde{\text{SINR}}_j^{(l)}\right), \end{aligned} \tag{35}$$

and $\widetilde{\text{SINR}}_j^{(l)}$ is the reference SINR and defined as

$$\widetilde{\text{SINR}}_{k,j}^{(l)} = \frac{P_{j,l}^{(l)}}{\displaystyle\sum_{i\in\mathcal{F}, if\neq l} \left(\tau_{k,i}\gamma_i + (1-\tau_{k,i})\beta_i\right) P_{j,i}^{(l)} + \frac{\sigma_n^2}{N}}. \tag{36}$$

Since the harmonic sum in (33) itself is not convex and cannot be solved directly, (33) is transformed into an equivalent convex program that can be efficiently solved using *Second Order Conic Programming* (SOCP) [13]. The equivalent optimization problem for (33) can be expressed as

$$\text{minimize} \quad \sum_{j\in\mathcal{S}_l} t_j^{(l)}, \tag{37}$$

subject to constraints in (34) and

$$z_j^{(l)} = A_j^{(l)}\delta_j^{(l)} + B_j^{(l)}(1-\delta_j^{(l)}), \tag{38a}$$

$$\left\| \begin{bmatrix} 2 \\ z_j^{(l)} - t_j^{(l)} \end{bmatrix} \right\|_2 \leq z_j^{(l)} + t_j^{(l)}, \quad \forall j \in \mathcal{S}_l, \tag{38b}$$

$$-t_j^{(l)} \leq 0. \tag{38c}$$

The derivation of equivalent transformation of optimization problem is shown in Appendix A.2. The SOCP can be casted as a *semi-definite programming* (SDP) and the state of the art method for solving SDP is with running time of $O(n^{3.5}\log\epsilon^{-1})$ [13], where n is the number of UEs per cell and ϵ is a small constant. This allows us to reduce the UE classification computational complexity from an exponential to a polynomial running time.

Table 2 shows the pseudo code of the MHT SFR algorithm with convex relaxation. Note that in Table 2, $\delta_j^{(l)*}$ denotes the optimal solution to the SOCP in (37).

2.3.4 Resource Allocation Algorithm for SFR

After UE is classified and power gains are determined, a cell performs resource allocation based on GPF [89, 61]. In SFR systems, CEUs and CCUs will be restricted to scheduling on CEB and CCB, respectively.

Let $x_v^{(i)}$, for $v = 1, ..., V$, be the scheduling outcome of resource allocation of V resource blocks of cell i. If a resource block v is allocated to user j in cell i, then $x_v^{(i)} = j$. The resource allocation vector $\bar{\mathbf{x}}_i = (x_1^{(i)}, x_2^{(i)}, ..., x_V^{(i)})^T$ will determine overall resource block allocation. Additionally, let $\mathcal{X}_i^{\text{CEB}}$ and $\mathcal{X}_i^{\text{CCB}}$ be the resource blocks assigned as CEB and CCB for cell i, respectively. The CEB and CCB set can be

Table 2. Reduced complexity UE classification and power gain determination algorithm

Algorithm Reduced complexity UE classification and power gain determination algorithm

Initialization : $\mathcal{B} = \{10^{-0.6}, 10^{-0.477}, 10^{-0.3}, 10^{-0.177}, 1\}$, $H_{\text{best}} = 0$.
for $m = 1, \cdots |\mathcal{B}|$ **do**
  set $\beta_l = \mathcal{B}_m$ and $\gamma_l = N - (N-1) \cdot \mathcal{B}_m$.
  for $n = 1, \cdots |\mathcal{S}_l|$ **do**
    Set $\Delta_l = n$.
    Compute user throughput estimate $A_j^{(l)}$ and $B_j^{(l)}$ in (35).
    Solve the SOCP in (37).
    Find j's corresponding to highest Δ_l values of the solution to SOCP, $\delta_j^{(l)*}$.
    Set to $\delta_j^{(l)} = 1$ for those j's and $\delta_j^{(l)} = 0$ otherwise.
    Compute harmonic mean of estimate throughput $H = \frac{1}{\sum_{j \in \mathcal{S}_l} 1/\tilde{R}_j^{(l)}}$
    if $H_{\text{best}} < H$ **then**
      set $H_{\text{best}} = H$, $\hat{\beta}_l = \beta_l$, $\hat{\gamma}_l = \gamma_l$.
      set $\hat{\mathcal{S}}_l^{\text{CEU}} = \{j | \delta_j^{(l)} = 1, j \in \mathcal{S}_l\}$ and $\hat{\mathcal{S}}_l^{\text{CCU}} = \{j | \delta_j^{(l)} = 0, j \in \mathcal{S}_l\}$.
    end if
  end for
end for

determined by

$$\mathcal{X}_i^{\text{CEU}} = \left\{ v \;\middle|\; \begin{array}{r} \tau_{k,i} = 1, \\ v = U \cdot (k-1) + u, \\ u = 1, 2, \cdots, U \end{array} \right\}, \tag{39}$$

and

$$\mathcal{X}_i^{\text{CCU}} = \left\{ v \;\middle|\; \begin{array}{r} \tau_{k,i} = 0, \\ v = U \cdot (k-1) + u, \\ u = 1, 2, \cdots, U \end{array} \right\}, \tag{40}$$

where $U = \left\lfloor \frac{V}{N} + 0.5 \right\rfloor$ and sub-band index, k, can take a value from 1 to N.

The resource allocation for CEU can be expressed as

$$x_v^{(i)} = \underset{j \in \mathcal{S}_i^{\text{CEU}}}{\text{argmax}} \frac{f_R(C_{j,v,t}^{(i)})}{T_{j,i,t}^{\text{avg}}}, \quad \forall v \in \mathcal{X}_i^{\text{CEU}} \tag{41}$$

where $C_{j,v,t}^{(i)}$ denotes the reported *channel quality indicator* (CQI) of user j in cell i

for resource block v at TTI t, the function $f_R(\cdot)$ maps the CQI to the estimated data rate and can be obtained using the method in [25], and $T_{j,i,t}^{\text{avg}}$ is the actual average throughput for user j in cell i at time t defined as in (9). The resource allocation for the CCUs can be similarly expressed by changing $\mathcal{S}_i^{\text{CEU}}$ to $\mathcal{S}_i^{\text{CCU}}$ and $\mathcal{X}_i^{\text{CEU}}$ to $\mathcal{X}_i^{\text{CCU}}$.

2.3.5 Computation Complexity Analysis

This secition discusses the computational complexity of the proposed algorithms and they are compared with that of the centralized ICIC scheduling algorithm in [12]. The SINR and throughput estimation described in [12] is similar to that of (13) and (12). Therefore, the comparison of the computational complexity is performed in terms of the numbers of throughput estimate calculations.

The centralized scheduling method requires that the processing entity computes all the scheduling information together. The centralized algorithm in [12] can be expressed as

$$\max \sum_{i \in \mathcal{F}} \sum_{j \in \mathcal{S}_i} \sum_{v=1}^{V} b_{j,v}^{(i)} \breve{R}_{j,v}^{(i)}, \tag{42}$$

where $b_{j,v}^{(i)}$ is the binary user/resource block assignment variable that is 1 if UE j in cell i is assigned to resource block v and 0 otherwise, and $\breve{R}_{j,v}^{(i)}$ is the estimated throughput for resource block v if UE j in cell i is assigned to resource block v. The optimization also needs to consider certain constraints which does not effect the total computational complexity too much.

Assuming that number of values the transmission power can have is $|\mathcal{B}|$. In LTE, $\mathcal{B} = \{$ -6dB, -4.77dB, -3dB, -1.77dB, 0dB $\}$ and $|\mathcal{B}| = 5$. Then the algorithm needs to estimate the user throughput $\sum_{i \in \mathcal{F}} (|\mathcal{S}_i| V^2 |\mathcal{B}|^{|\mathcal{F}|})$ times. If the more than one resource block is allowed to be assigned to a single UE in [12], then it needs to compute the user throughput $\sum_{i \in \mathcal{F}} (|\mathcal{S}_i| V 2^V |\mathcal{B}|^{|\mathcal{F}|})$ times.

The computational complexity for the proposed SFR algorithms is slightly different for different UE classification and power gain determination approaches. The

proposed MHT SFR algorithm distributes the computation to each cell, and from (28) and (41), each cell only computes the user throughput $V|\mathcal{S}_i| + |\mathcal{B}| \cdot 2^{\lceil |\mathcal{S}_i|/N \rceil}$ times. For example, if there are 20 UEs per cell with 12 cells cooperating in 3 way SFR (i.e. $N = 3$), 4 possible values for β_i and γ_i, and 50 resource blocks (i.e. 10 MHz LTE system), the centralized scheduling algorithm requires approximately 2.2×10^{26} times of throughput calculations and the proposed algorithm only requires 1.5×10^3 times of throughput calculations. The MHT SFR algorithm with convex relaxation further reduces computational complexity. The convex program is an iterative algorithm only with polynomial complexity. Therefore, our algorithms are much simplified.

2.3.6 Convergence of Power Gains Among Cells

In general, if each cell updates its power gains, β_i and γ_i, based on its previously received power gain information from other cells then there is a possibility that some of the cells will oscillate between sets of values for the power gains and do not converge. Because there is only 4 states available for β_i for LTE downlink data transmissions, the algorithm actually converges quickly. Even though convergence of the algorithm can be guaranteed analytically, it always converges from the simulation results.

There have been solutions to ensure the convergence of the transmission power among cells for coordinated scheduling [95]. The basic idea is to assign a probability to the update of the power gains for each cell. The same principles can be adopted here to ensure the power gain convergence among cells for our algorithms. Proof of convergence is described in [95].

2.4 Simulation Evaluation

The simulations are based on ITU-R sector recommendations for the IMT-Advanced technology evaluation guidelines [37]. It is based on urban macro deployment scenario of ITU evaluation methodology, which is widely accepted model in 3GPP and ITU. Some key parameters are shown in Table 3.

Table 3. Simulation Configuration and Parameters

Simulation Parameter	Value
Total number of UE in the network	570 UEs randomly distributed in the entire network (average of 10 UEs per cell)
Channel Model (Scenario)	ITU Urban Macro [37]
System Bandwidth	10MHz
UE Speed	3km/hr
Antenna Configuration	2 Tx, 2 Rx
Tx Antenna Vertical Down Tilt	12°
UE location	100% outdoor, non-vehicular
Service Profile	Full Buffer Simulation
Handover Margin	1 dB
HARQ Model	IR Combining [79]
OLLA step size	0.25 dB
UE receiver algorithm	MMSE receiver with average interference covariance estimation
CQI processing delay	5ms
CQI feedback period	every 2ms
CQI quantization	4 bits (LTE) [4]
CQI mode	PUSCH CQI feedback mode 3-1 (CQI per sub-band, 1 PMI for all sub-band) [4]
Transmission Mode	LTE Transmission Mode 4 (Closed Loop Spatial Multiplexing) [4]

The specification of LTE systems were followed in the simulations, which includes *hybrid ARQ* (HARQ) retransmission, *channel quality indicator* (CQI) feedback, processing delay, and feedback quantization error. In order to fairly compare various configurations and algorithms, *Outer Loop Link Adaptation* (OLLA) on top of the CQI based link adaptation is applied to make sure that all UEs are controlled to have 10% *block-error rate* (BLER) for the initial transmission (i.e. non-retransmission) packets. In addition, *minimum mean square-error interference rejection combining* (MMSE-IRC) receivers are implemented in UEs, where each UE performs an estimate of interference covariance for the MMSE receive filter. This is much more realistic compared to the MMSE-IRC receivers using ideal interference covariance (i.e. exact channel coefficients of all interfering signals) is assumed in each subcarrier at the UE. The simulation is based on a 3 way SFR, with 1/3 bandwidth allocated for CEB. The CEB frequency allocation is based on the modular sectorized cell layout, where the CEB indicator for sub-band k in cell i is configured as

$$\tau_{k,i} = \begin{cases} 1, & \text{if } i \equiv k \bmod 3, \\ 0, & \text{otherwise.} \end{cases} \tag{43}$$

The sectorized cell's antenna orientation and the exact cellular layout is shown in Figure 3, where the numbers represent cell indices. The three triangular pointers are the directions of the antenna array's for each individual cell. Wrap around of the cells is implemented to remove the cellular boundary issues. Finally, the SFR algorithms in the simulations assumed that the power gains and UE classification are updated once every 1000 ms.

2.4.1 Comparison between Non-ICIC and Proposed SFR System

Table 4 shows throughput comparison between the non-ICIC system and various SFR algorithms configured with $\beta_i = 0.5$ and $\gamma = 2.0$.

Throughput for the STH algorithm in Table 4 shows that performance is sensitive

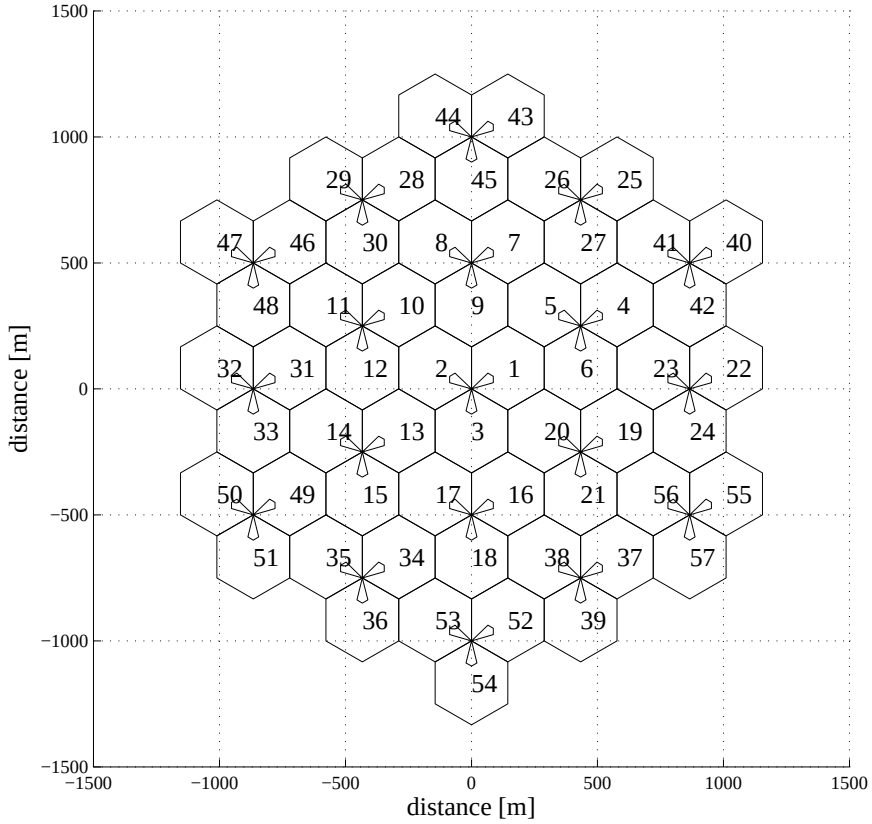

Figure 3. Cellular layout, antenna orientation, and cell number configuration for simulations

to SINR threshold and a 2dB change in the SINR threshold results in a large change in user throughput. When the SINR threshold is 4dB, it can increase the 5th percentile user throughput by 3.2%. As expected, the MST algorithm significantly improves the cell average performance by 40.3% but at the expense of -34.9% throughput loss for the 5th percentile throughput. The MHT algorithm improves the 5th percentile throughput by 20.9% while having similar cell average throughput as the non-ICIC system. The performance of the MGT algorithm is between that of the MST and MHT algorithms and it shows 14.3% and 11.7% gains for 5th percentile throughput and cell average throughput, respectively.

The simulation results for the MST, MGT, and MHT algorithm are well aligned with the analysis in Section 2.2. The network operator is able to control fairness among users by changing the UE classification algorithm. The STH algorithm will

Table 4. Throughput comparison for non-ICIC system and different SFR system

UE Classification Algorithm	Throughput		
	5th percentile Tput [Mbps]	10th percentile Tput [Mbps]	Cell Avg. Tput [Mbps]
Non-ICIC system (**Ref.**) $\alpha = 1$	0.40455	0.51303	13.9477
	0%	0%	0%
STH ($\text{SINR}_{\text{thresh}} = -2\text{dB}$)	0.26362	0.33508	10.6236
	-34.8%	-34.7%	-23.8%
STH ($\text{SINR}_{\text{thresh}} = 0\text{dB}$)	0.32532	0.40742	11.436
	-19.6%	-20.6%	-18.0%
STH ($\text{SINR}_{\text{thresh}} = 2\text{dB}$)	0.40892	0.50904	12.9989
	+1.1%	-0.8%	-6.8%
STH ($\text{SINR}_{\text{thresh}} = 4\text{dB}$)	0.41765	0.51091	14.5089
	+3.2%	-0.4%	+4.0%
STH ($\text{SINR}_{\text{thresh}} = 6\text{dB}$)	0.35839	0.45114	16.0415
	-11.4%	-12.0%	+15.0%
MST ($\beta = 0.5$, $\gamma = 2.0$)	0.26348	0.32508	19.5701
	-34.9%	-36.6%	+40.3%
MGT ($\beta = 0.5$, $\gamma = 2.0$)	0.46257	0.57484	15.5811
	+14.3%	+12.0%	+11.7%
MHT ($\beta = 0.5$, $\gamma = 2.0$)	0.48893	0.61258	14.4705
	+20.9%	+19.4%	+3.7%

be difficult to be implemented as it is difficult to pre-determine the optimal SINR threshold that optimizes performance as the optimal SINR threshold may be different for different deployment scenarios.

By adjusting the fairness-throughput trade-off exponent, α, in GPF scheduling in (8), the average throughput and 5th and 10th percentile throughput will vary. Figure 4 and Figure 5 show the 5th and 10th percentile throughput versus cell average throughput, respectively, for the non-ICIC system with different α's and the proposed SFR algorithms. Each point in the figures correspond to a 2-dimensional throughput

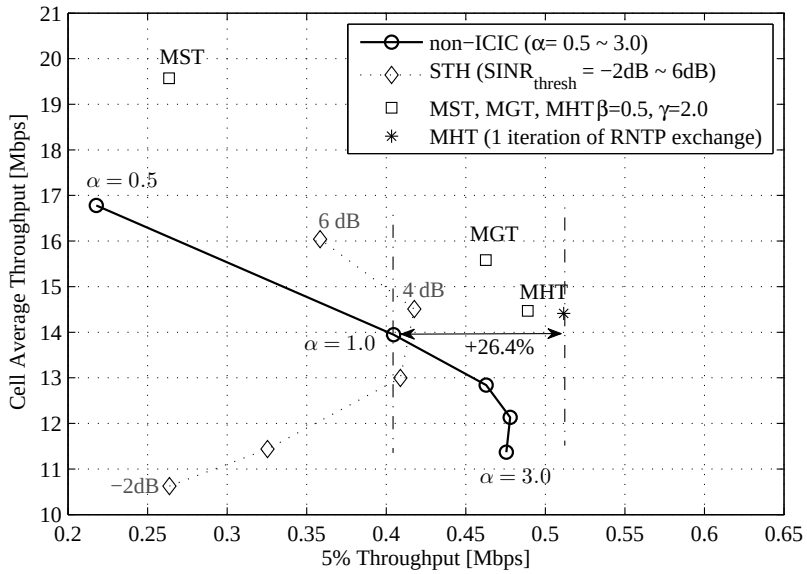

Figure 4. 5th percentile throughput and cell average throughput tradeoff comparison between non-ICIC and proposed SFR algorithms

coordinate. The reference curve for non-ICIC system has been plotted by interpolating the throughput coordinates with various PF exponents. In Figure 4, the 5th percentile throughput of the non-ICIC system saturates at 0.48 Mbps. However, the proposed MHT algorithm with one iteration of power gain among cells can achieve up to 0.51 Mbps and 0.63 Mbps for 5th and 10th percentile user throughput, respectively, improved by 22% and 26% throughput gains for 5th and 10th percentile throughput, respectively, compared to the non-ICIC system with GPF exponent $\alpha = 1$ without loss of cell average throughput.

Figure 6 compares the relative throughput of the search space restricting method and convex relaxation method against the full exhaustive search method for the MHT algorithm. From the figure, there are 3.9% and 9.1% loss for the 5th percentile user throughput for search space restriction and convex relaxation methods, respectively, compared to the exhaustive search method. The complexity reduction methods do show modest cell average gains of 3.4% and 4.8% for each method. This is because there exist a trade-off between 5th percentile throughput and cell average throughput.

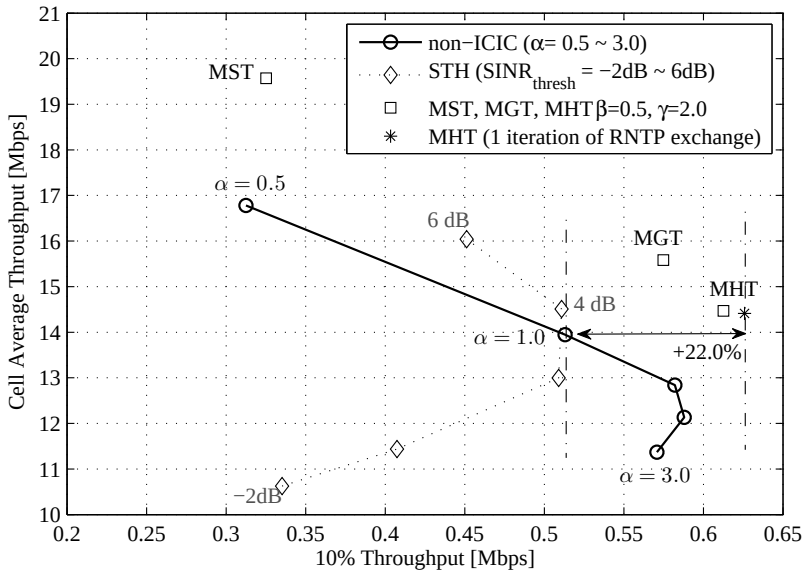

Figure 5. 10th percentile throughput and cell average throughput tradeoff comparison between non-ICIC and proposed SFR algorithms

Although the objective of the MHT algorithm is to prioritize the cell edge users, the reduced computational complexity methods are unable to compute solutions that enable to prioritize the cell edge users as much as the exhaustive one.

2.4.2 SFR System Performance and Number of Power Gain Information Exchanges

Table 5 shows the simulation results of the MHT SFR algorithm with 0, 1, 3, and 7 power gain information exchanges among cells prior to resource allocation scheduling. From Table 5, the simulation results quickly converge and three power gain information exchanges are enough. Note that performance improvement for the coverage limited (e.g. 5th and 10th percentile throughput) users can be seen even with one iteration where not all cells have fully converged.

In general, when the cells adjust their power gains independently based on information from the previous power gain exchange iteration, it is possible for cells to oscillate the power gains adjustment and never converge to a value. The quick convergence of the power gain among cells is observed to be possible due to the heavy

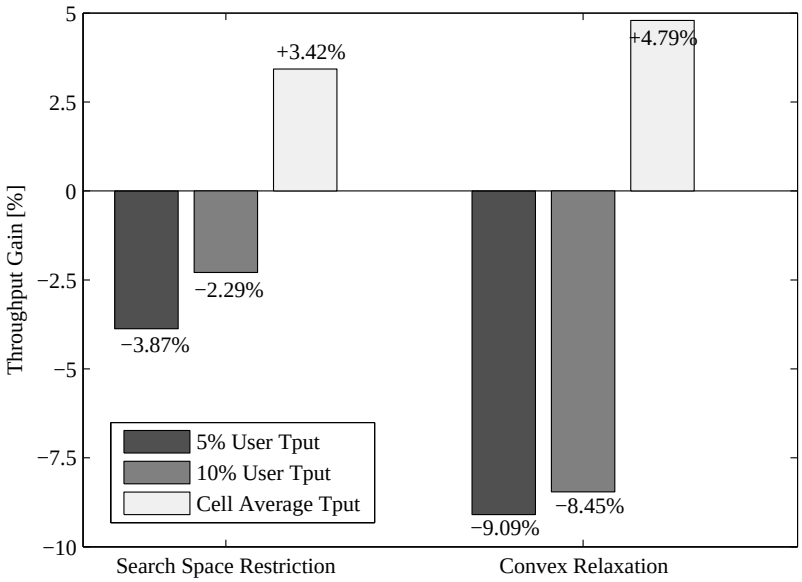

Figure 6. Relative throughput comparison of computational complexity reduction methods of MHT algorithm

quantization of the power gains for LTE. The large gap between different power gain states enable certain cells to fixate its power gain to a certain state regardless of some of the changes in power gain in other cells. This enables other cells to also converge to a power gain state as power gains of more cells converge. Note that the LTE specification only allows { -6, -4.77, -3, -1.77, 0 }dB to be configured for β_i for data transmission which rely on CRS to demodulate the received signals.

Table 5. Throughput comparison of MHT algorithm for various numbers of power gain exchange iterations

Number of iteration for MHT	Throughput		
	5th percentile User Tput [Mbps]	10th percentile User Tput [Mbps]	Cell Avg. Tput [Mbps]
0 iteration (**Ref.**)	0.46795	0.60164	13.6741
	0%	0%	0%
1 iteration	0.5115	0.62583	14.4122
	+9.3%	+4.0%	+5.4%
3 iteration	0.48786	0.61248	14.3188
	+4.3%	+1.8%	+4.7%
7 iteration	0.4904	0.6144	14.4066
	+4.8%	+2.1%	+5.3%

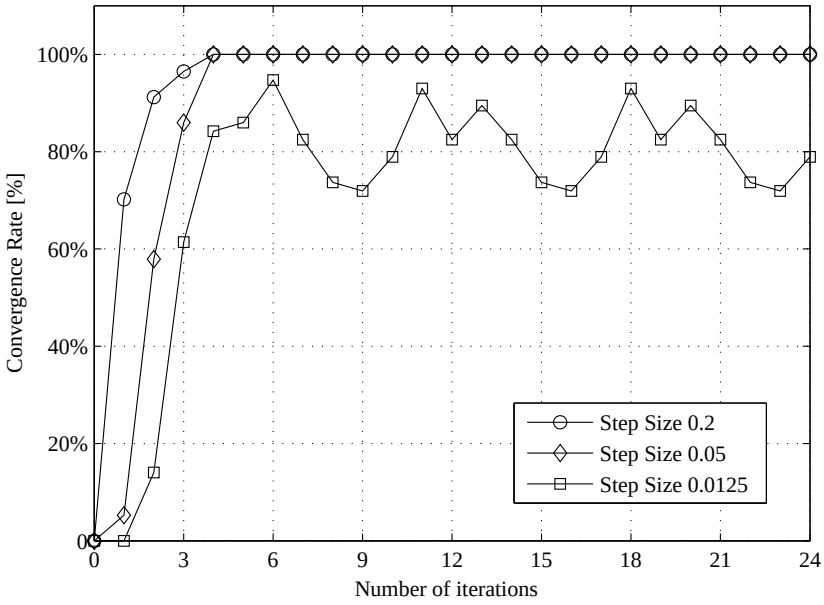

Figure 7. Comparison of convergence for various quantization of CEB power gain β_i

Figure 7 shows the effects of the power gain step size and convergence of power gain values among cells, where the convergence rate is defined as percentage of the number of cells that have not changed its power gains, β_i and γ_i, from its previous

power gain exchange iteration. If convergence rate is 100%, then no cells have adjusted the power gain compared to the previous iteration and all cells have fully converged. Simulation results show that convergence is tightly correlated with the step size of the power gain. If the step size is too small, the power gains among cells do not converge. Because of the natural of distribution of the UE distribution, some cells may be less affected by changes in power gain of its neighbor cells. These cells are affected more by its own power gain values and its UE classification. If the quantization step size of the power gain is large, these cells are forced to converge its own power gain value to quantized states. This helps other cells to converge as well in the next iteration as there are less changes to the interference level. This is essentially the same concept as the technique introduced in [95] that guarantees convergence. If certain cells do not change its power gain value, other cells will converge quickly and the whole convergence will be expedited. Probabilistic change condition on the power gains as proposed in [95] can be emulated by having fewer available choices of the power gain states. The LTE Release 8 only allows 4 power gain states for CCB of the SFR operations and 1 power gain state for normal (i.e. non-SFR) operations, $\{-6, -4.77, -3, -1.77, 0\}$ dB [4]. The convergence is not an issue for the proposed algorithm at all. For systems potentially with more flexibility in configuration of the power gains, he proposed methods as mentioned in [95] may be adopted.

2.5 Summary and Conclusion

In this chapter, soft frequency reuse SFR inter-cell interference coordination is investigated. The performance for SFR is sensitive to user classification and power gains. The proposed de-centralized SFR algorithms are robust and can significantly improve cell-edge and cell average throughput simultaneously. The computational complexity compared is significantly reduced compared to the centralized ICIC algorithm. The proposed algorithm quickly converges. Since all assumptions and constraints

are according to LTE specifications, the described algorithms can be readily used in practical systems.

CHAPTER III

CB ALGORITHM WITH PER BS POWER CONSTRAINT

3.1 Introduction

Coordinated beamforming (CB) for a system with multiple transmit antennas and single receive antenna, known as a *multi-input-single-output* (MISO) system, has been well studied. For example, CB that minimizes the total transmit power under minimum SINR constraint has been proposed using uplink-downlink duality [21]. Similarly, CB that maximizes the minimum of *signal-to-interference-plus-noise ratio* (SINR) of the scheduled users has been developed using *second-order conic programming* (SOCP) [31, 14, 55, 35]. For system with multiple receive antennas in addition to multiple transmit antennas, known as a *multi-input-multi-output* (MIMO) systems, a class of CB precoding algorithms that maximize *signal-to-leakage-plus-noise ratio* (SLNR) [72, 17, 27, 66] has been formulated as a generalized Rayleigh quotient problem and can be solved in polynomial time. However, finding optimal CB precoding matrices that *maximize virtual uplink SINR* (Max-VSINR) [73], *weighted sum rate* (Max-WSR) [76, 11, 47, **?**], *minimum of SINR* (Max-Min-SINR) [56, 84, 90], and *minimize mean-squared error* (Min-MSE) [82, 73, 45] is known to be a non-convex problem and no efficient algorithms for optimal solutions exist. As a result, suboptimal algorithms have been proposed to compute receive filters and transmit precoding matrices iteratively.

The focus of the research will be on low-complexity CB that can prioritize the performance of the 5% user throughput, denoted as cell-edge users. Single stream and single user CB has been investigated in [52]. It is possible to utilize existing

CB algorithms based on weighted utility, such as Max-WSR, to improve the cell-edge users. However, obtaining the right weights to improve and prioritize cell-edge users is difficult. This requires identification of the priority of users for scheduling and beamforming matrix computation, which is an chicken-and-egg problem. The difficulty stems from estimating which users will have the biggest issue coping with ICI in multi-stream, multi-user, and multi-cell environment. Changes in beamforming at the BS will drastically change ICI. Therefore, it is very hard to estimate the weights that will improve the throughput of users of cell-edge while not sacrifice the overall system performance too much. Alternatively, CB algorithms that maximize the minimum SINRs of users is the most straightforward approach for improving cell-edge performance. However, they require iterative search of SOCP feasibility test [56] and are in general quite complex and can be only implemented in a centralized algorithm (i.e. all CB matrices are computed at once without parallelism). Therefore, the challenge is to develop low-complex CB algorithms that prioritize cell-edge users and do no require additional parameters or weights to configure or optimize.

The harmonic sum of SINRs as the means to develop a low-complex CB algorithm is investigated. As implied in [20], maximizing the harmonic sum of user rates leads to higher prioritization of the cell-edge users and increases in 5% user throughput. Since the SINR of users have one-to-one relationship with the user rates, CB that maximizes the harmonic sum of SINRs should also improve the cell-edge user performance, which will be verified by simulations in Section 3.4. It should be noted that maximizing the harmonic sum of SINRs for multi-stream CB is non-convex. However, the objective can be manipulated to derive low-complexity algorithms that find local maxima of the harmonic sum of SINRs. Additionally, the proposed algorithms do not require the network to pre-determine the cell-edge users.

To best of author's knowledge, the harmonic sum of SINRs was used for a beamforming problem in early 2000 [8]. It has been shown that maximizing the harmonic

sum of the SINRs for MISO systems can be transformed into weighted Min-MSE for each user with power constraints, which is just a generalized eigenvalue problem. For multi-cell MIMO CB, the harmonic sum of SINRs cannot be decoupled such that beamforming for each user can be performed separately. Furthermore, direct formulation of the problem in the multi-stream, multi-cell, and MIMO system is non-convex and no efficient solutions exist. Therefore, the single-user single-stream CB in [52] is extended to multi-user multi-stream CB. Furthermore, low-complexity iterative CB algorithms that maximize the harmonic sum of SINRs of users in a MIMO system with *per BS power constraints* (PBPC) is invesitgated. The proposed algorithms iteratively compute the precoding matrices of the transmitter and the hypothetical receive matrices that may be used at the receiver, which has been utilized in many literatures to combat the MIMO system beamforming problems [82, 73, 45, 75, 76, **?**, 84, 90, 56].

The rest of this chapter is organized as follows. Section 3.2 describes the system model and justifies the assumptions used in this chapter. Section 3.3 develops algorithms to compute the CB matrices. Section 3.4 shows simulation results and concluding remarks are provided in Section 3.5.

3.2 System Model

Consider a network, as in Figure 8, with J BSs. Each link consists of a BS with N transmit antennas and users each with M receive antennas. They are all working at the same frequency and therefore may interfere with each other. Denote the $M \times N$ channel coefficient matrix from BS i to user k in BS j to be $\mathbf{H}_{ij}^{(k)}$. Since BS j serves user k, channel coefficient matrix, $\mathbf{H}_{ij}^{(k)}$, with $i \neq j$, is the interference channel. Let K_j be the number of scheduled users in BS j, and users are randomly distributed in the network.

In *multi-user MIMO* (MU-MIMO), several users are scheduled in the same frequency band simultaneously with the help of spatial division. Let $L_j^{(k)}$ be the number

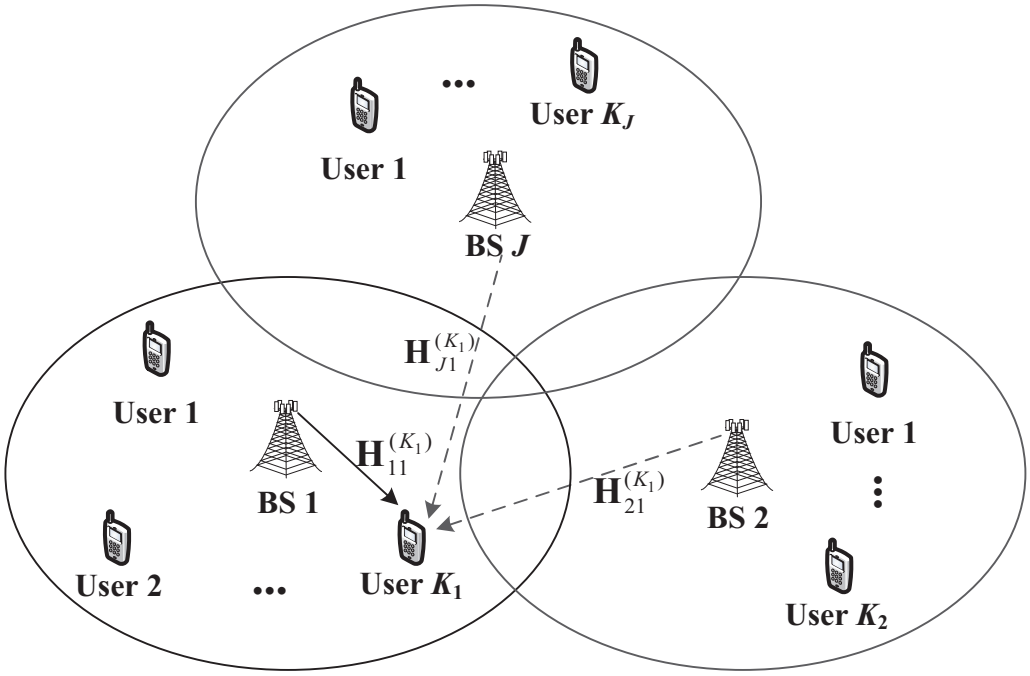

Figure 8. A cellular network with J cells

spatial streams for user k in BS j. The received signal for user k in BS j in a MU-MIMO system can be expressed as

$$\mathbf{y}_j^{(k)} = \mathbf{H}_{jj}^{(k)}\mathbf{P}_j^{(k)}\mathbf{x}_j^{(k)} + \sum_{l=1,l\neq k}^{K_j} \mathbf{H}_{jj}^{(k)}\mathbf{P}_j^{(l)}\mathbf{x}_j^{(l)} + \sum_{i=1,i\neq j}^{J}\sum_{l=1}^{K_i} \mathbf{H}_{ij}^{(k)}\mathbf{P}_i^{(l)}\mathbf{x}_i^{(l)} + \mathbf{n}_j^{(k)}, \tag{44}$$

where $\mathbf{P}_j^{(k)}$ and $\mathbf{x}_j^{(k)}$ are the $N \times L_j^{(k)}$ precoding matrix and the $L_j^{(k)} \times 1$ transmit-signal vector for user k from BS j, respectively, and $\mathbf{n}_j^{(k)}$ is the *additive white Gaussian noise* (AWGN) vector. The power of the transmitted signal is given by the diagonal entries of the transmit covariance matrix, $E[\mathbf{x}_j^{(k)}\mathbf{x}_j^{(k)\dagger}]$, where $(\cdot)^\dagger$ denotes the Hermitian of the matrix. The transmit covariance is assumed to be identity matrix, $\mathbf{I}$, that is, uniform power allocation is assumed. The power of AWGN is σ_n^2.

At each receiver, a $M \times L_j^{(k)}$ weight matrix, $\mathbf{W}_j^{(k)}$, is used to combine the received signals from different antennas of user k. As a result,

$$\hat{\mathbf{x}}_j^{(k)} = \mathbf{W}_j^{(k)\dagger}\mathbf{y}_j^{(k)}, \tag{45}$$

and $\hat{\mathbf{x}}_j^{(k)}$ is the estimated desired signal.

From (44), the SINR of the r-th spatial stream of user k in BS j can be expressed as

$$\mathrm{SINR}_j^{(k,r)} = \frac{S_j^{(k,r)}}{[\mathbf{W}_j^{(k)}]_r^\dagger \mathbf{Q}_j^{(k)} [\mathbf{W}_j^{(k)}]_r - S_j^{(k,r)}}, \tag{46}$$

where $[\cdot]_r$ is the r-th column vector of the matrix, $S_j^{(k,r)}$ is the signal power of r-th spatial stream and can be expressed as, $S_j^{(k,r)} = \left| [\mathbf{W}_j^{(k)}]_r^\dagger \mathbf{H}_{jj}^{(k)} [\mathbf{P}_j^{(k)}]_r \right|^2$, and $\mathbf{Q}_j^{(k)}$ is the total received signal covariance of user k in BS j and can be expressed as

$$\mathbf{Q}_j^{(k)} = \sum_{i=1}^{J} \sum_{l=1}^{K_i} \mathbf{H}_{ij}^{(k)} \mathbf{P}_i^{(l)} \mathbf{P}_i^{(l)\dagger} \mathbf{H}_{ij}^{(k)\dagger} + \sigma_n^2 \mathbf{I}. \tag{47}$$

The receive filter can be obtained by finding the column vectors of $\mathbf{W}_j^{(k)}$ that maximize SINR in (46), that is

$$\begin{aligned} [\hat{\mathbf{W}}_j^{(k)}]_r &= \arg \max_{[\mathbf{W}_j^{(k)}]_r} \mathrm{SINR}_j^{(k,r)} \\ &= \left(\mathbf{Q}_j^{(k)} \right)^{-1} \mathbf{H}_{jj}^{(k)} [\mathbf{P}_j^{(k)}]_r, \end{aligned} \tag{48}$$

which corresponds to *minimum mean-square error* (MMSE) receive filter.

When there is a single BS with only one user, there will be no interference. If the BS has no information on interference channels, then the best way is to treat it as white noise when designing beamforming matrices. In either case, optimal beamforming that maximizes user throughput for single user transmission will be the right sided singular vectors of the channel matrix corresponding to the largest singular values. Denote the *singular-value decomposition* (SVD) of channel matrix, $\mathbf{H}_{jj}^{(k)}$, as

$$\mathbf{H}_{jj}^{(k)} = \mathbf{U}_j^{(k)} \mathbf{\Sigma}_j^{(k)} \mathbf{V}_j^{(k)\dagger}, \tag{49}$$

where entries of the diagonal matrix $\mathbf{\Sigma}_j^{(k)}$ are ordered from the largest to the smallest. The optimal single user precoding matrix, $\mathbf{P}_j^{(k)}$, is the first $L_j^{(k)}$ column vectors of $\mathbf{V}_j^{(k)}$.

The proposed research is for coordinated beamforming in multi-cell networks when information on the desired signal and interference channels is provided at BSs. The

channel state information (CSI) is assumed to be known at the BSs, which can be done efficiently in TDD systems with uplink channel sounding.

3.3 Coordinated Beamforming for Multi-Stream Multi-User MIMO Systems

In this section, the problem of optimal CB that maximizes harmonic sum of SINRs of users is formulated and then a low complex algorithm is developed. With CSI, $\mathbf{H}_{ij}^{(k)}$, a centralized node can obtain precoding matrices for each cell based on the CB algorithm. It is assumed that number of transmit streams for each user is known and fixed. There has been some study on impact of number of streams transmitted to cell-center and cell-edge users [9], which shows that cell-edge users are likely to benefit more from a single stream transmission compared with cell-center users. Optimal configuration of the number of spatial streams is beyond the scope of this chapter. However, the proposed algorithm is formulated such that it will work with any number of transmit streams for each user.

3.3.1 Harmonic-Sum Objective Function

Optimization objective metrics, such as maximizing sum rate of the users [86] or maximizing the minimum of SINR of user [14, 31], are non-convex for multi-stream multi-user MIMO systems and no efficient method for the optimal solution exists. As a heuristic approach, the CB precoding matrices that maximize the harmonic-sum of SINRs is solved. Investigation of use of harmonic-sum of SINR for single-user single-stream CB case was performed in [52]. Simulation results in Section 3.4 show that the proposed CB algorithms based on maximizing harmonic-sum of SINRs can improve the cell-edge user throughput and require no prior knowledge of users.

It is well-known that for any N positive numbers, $x_1, x_2, ..., x_N$, the harmonic

mean is upper and lower bounded by $N \min x_n$ and $\min x_n$, respectively, that is

$$N \min x_n > \frac{N}{\sum_{n=1}^{N} \frac{1}{x_n}} \geq \min x_n. \tag{50}$$

Additionally, if SINRs of a certain stream of a user is much worst than rest of the streams of other users, $x_m(l)x_j, \forall j \neq m$, the harmonic sum of SINRs approximates the minimum SINR, that is

$$x_m = \min_n x_n = \frac{1}{\frac{1}{\min_n x_n}} \approx \frac{1}{\sum_{n=1}^{N} \frac{1}{x_n}}. \tag{51}$$

The harmonic sum is also upper bounded by the arithmetic mean through the arithmetic-harmonic inequality, that is

$$\frac{1}{N} \sum_{n=1}^{N} x_n \geq \frac{N}{\sum_{n=1}^{N} \frac{1}{x_n}}, \tag{52}$$

and the equality only holds when all the entries are identical. So if the SINRs of streams of users are very similar, the harmonic sum of SINRs approximates the arithmetic average of SINRs. These properties allow the maximization of harmonic sum to indirectly maximize the minimum SINR as well as the average SINR and can balance the overall throughput and cell-edge user performance. Some of these properties can be implied in studies of user scheduling for ICIC [20]. Furthermore, it also results in simpler CB algorithms than other metrics that prioritizes cell-edge users.

The harmonic-sum objective function for multi-cell multi-stream multi-user MIMO systems can be expressed as

$$\mathrm{SINR}_{\mathrm{H}} = \frac{1}{\sum_{j=1}^{J} \sum_{k=1}^{K_j} \sum_{r=1}^{L_j^{(k)}} \frac{1}{\mathrm{SINR}_j^{(k,r)}}}. \tag{53}$$

It should be noted that the multiple streams of each user have been treated as individual streams of multiple users with a single effective antenna at the receiver. This design principle is chosen to simplify the derivation of the CB algorithm. However, it should be further noted that the final beamforming matrix of a user may not be

optimized as a whole and may not diagonalize the effective channel at the receiver, which may cause some degradation for linear receivers. The performance degradation for linear receivers can be addressed by multiplying a conditioning matrix to the final matrix, which will be addressed in Section 3.3.5.

From (46) and (53), maximizing the harmonic-sum is equivalent to minimizing

$$\sum_{j=1}^{J}\sum_{k=1}^{K_j}\sum_{r=1}^{L_j^{(k)}}\frac{[\mathbf{W}_j^{(k)}]_r^{\dagger}\mathbf{Q}_j^{(k)}[\mathbf{W}_j^{(k)}]_r - S_j^{(k,r)}}{S_j^{(k,r)}}, \tag{54}$$

subject to (54) and

$$\sum_{k=1}^{K_j}\|\mathbf{P}_j^{(k)}\|_F^2 \leq P_0, \forall j, \tag{54a}$$

where $\|\cdot\|_F$ is the Frobenius norm of the matrix, and P_0 is the maximum allowable transmit power per BS. The precoding matrix constraint in (54a) is PBPC.

Scaling the receive filter, $\mathbf{W}_j^{(k)}$, by an arbitrary factor does not affect the received SINR in (46). Without loss of generality, the receive filter of each user can be scaled such that $S_j^{(k,r)} = |[\mathbf{W}_j^{(k)}]_r^{\dagger}\mathbf{H}_{jj}^{(k)}[\mathbf{P}_j^{(k)}]_r|^2 = 1$ is satisfied and the objective function can be expressed as minimizing

$$\sum_{j=1}^{J}\sum_{k=1}^{K_j}\sum_{r=1}^{L_j^{(k)}}([\mathbf{W}_j^{(k)}]_r^{\dagger}\mathbf{Q}_j^{(k)}[\mathbf{W}_j^{(k)}]_r - 1) \tag{55}$$

$$= \sum_{j=1}^{J}\sum_{k=1}^{K_j}\mathrm{Tr}\left(\mathbf{W}_j^{(k)\dagger}\mathbf{Q}_j^{(k)}\mathbf{W}_j^{(k)}\right) - \sum_{j=1}^{J}\sum_{k=1}^{K_j}L_j^{(k)}, \tag{56}$$

subject to

$$|[\mathbf{W}_j^{(k)}]_r^{\dagger}\mathbf{H}_{jj}^{(k)}[\mathbf{P}_j^{(k)}]_r| = 1, \forall r, k, j. \tag{56a}$$

Furthermore, phase rotation of the column vectors of the precoding matrices, $\mathbf{P}_j^{(k)}$, does not affect the total received signal covariance, $\mathbf{Q}_j^{(k)}$, in (47), nor the unit norm constraint, in (56a). Therefore, the constraint, $|[\mathbf{W}_j^{(k)}]_r^{\dagger}\mathbf{H}_{jj}^{(k)}[\mathbf{P}_j^{(k)}]_r| = 1$, is replaced by $[\mathbf{W}_j^{(k)}]_r^{\dagger}\mathbf{H}_{jj}^{(k)}[\mathbf{P}_j^{(k)}]_r = 1$ without loss of generality. In addition, constants do not affect the minimization problem and can be removed. Therefore, the objective function in

(55) can be simplified as minimizing

$$\sum_{j=1}^{J}\sum_{k=1}^{K_J}\mathrm{Tr}\left(\sum_{i=1}^{J}\sum_{l=1}^{K_i}\mathbf{W}_j^{(k)\dagger}\mathbf{H}_{ij}^{(k)}\mathbf{P}_i^{(l)}\mathbf{P}_i^{(l)\dagger}\mathbf{H}_{ij}^{(k)\dagger}\mathbf{W}_j^{(k)}\right) + \sum_{j=1}^{J}\sum_{k=1}^{K_J}\mathrm{Tr}\left(\mathbf{W}_j^{(k)\dagger}\mathbf{W}_j^{(k)}\sigma_n^2\right) \tag{57}$$

subject to (54a) and

$$\left(\mathbf{W}_j^{(k)\dagger}\mathbf{H}_{jj}^{(k)}\mathbf{P}_j^{(k)}\right)\circ\mathbf{I}=\mathbf{I},\forall j, \tag{57a}$$

where $\circ$ denotes entrywise multiplication, that is the Hadamard product.

It is interesting to note that the harmonic-sum maximization problem in (57) is similar to Min-MSE problem in [45, 73] with the exception of the additional affine constraint in (57a).

The objective function, (57), is partially convex and not jointly convex over $\mathbf{P}$ and $\mathbf{W}$. Because of it, conventional convex programming techniques [13] are not applicable here. Therefore, two suboptimal algorithms are developed subsequently. Unfortunately, the suboptimal algorithm only allows us to obtain local minima solutions and may result in a duality gap between the primal and dual solutions.

3.3.2 Alternating Optimization with Iterative Search

The solution to the optimization problem in (57) can derived using the Lagrange multiplier approach. The Lagrangian of the optimization problem is expressed as

$$\begin{aligned}
&L(\mathbf{P}, \mathbf{W}, \lambda, \Psi) \\
&= \sum_{j=1}^{J} \sum_{k=1}^{K_j} \sum_{i=1}^{J} \sum_{l=1}^{K_i} \mathrm{Tr}\left(\mathbf{W}_j^{(k)\dagger} \mathbf{H}_{ij}^{(k)} \mathbf{P}_i^{(l)} \mathbf{P}_i^{(l)\dagger} \mathbf{H}_{ij}^{(k)\dagger} \mathbf{W}_j^{(k)} \right) \\
&+ \sum_{j=1}^{J} \sum_{k=1}^{K_j} \mathrm{Tr}\left(\mathbf{W}_j^{(k)\dagger} \mathbf{W}_j^{(k)} \right) \sigma_n^2 \\
&+ \sum_{j=1}^{J} \left(\sum_{k=1}^{K_j} \mathrm{Tr}(\mathbf{P}_j^{(k)\dagger} \mathbf{P}_j^{(k)}) - P_0 \right) \lambda_j \\
&+ \sum_{j=1}^{J} \sum_{k=1}^{K_j} \mathrm{Tr}\left(\mathbf{\Psi}_j^{(k)} (\mathbf{I} - \mathbf{W}_j^{(k)\dagger} \mathbf{H}_{jj}^{(k)} \mathbf{P}_j^{(k)}) \right),
\end{aligned} \tag{58}$$

where λ_j is the non-negative dual variable for inequality constraint, (54a), and $\mathbf{\Psi}_j^{(k)}$ is the diagonal matrix with dual variables for equality constraint, (56a). Optimal solution lies on the critical values of the Lagrangian. As demonstrated in Appendix B.1, by setting $\frac{\partial L}{\partial \mathbf{P}} = 0$ and $\frac{\partial L}{\partial \mathbf{W}} = 0$, optimal $\mathbf{P}$ and $\mathbf{W}$ can be found, and they are expressed as

$$\hat{\mathbf{P}}_j^{(k)} = \frac{1}{2} \left(\mathbf{R}_j^{(k)} \right)^{-1} \mathbf{H}_{jj}^{(k)\dagger} \mathbf{W}_j^{(k)} \mathbf{\Psi}_j^{(k)}, \tag{59}$$

$$\hat{\mathbf{W}}_j^{(k)} = \frac{1}{2} \left(\mathbf{Q}_j^{(k)} \right)^{-1} \mathbf{H}_{jj}^{(k)} \mathbf{P}_j^{(k)} \tilde{\mathbf{\Psi}}_j^{(k)}, \tag{60}$$

where

$$\mathbf{R}_j^{(k)} = \sum_{i=1}^{J} \sum_{l=1}^{K_i} \mathbf{H}_{ji}^{(l)\dagger} \mathbf{W}_i^{(l)} \mathbf{W}_i^{(l)\dagger} \mathbf{H}_{ji}^{(l)} + \lambda_j \mathbf{I}, \tag{61}$$

and $\mathbf{\Psi}_j^{(k)}$ and $\tilde{\mathbf{\Psi}}_j^{(k)}$ are the diagonal matrices that scale the column vectors of the precoding matrix and the receive filter so that equality constraint, (56a), is met and given in Appendix B.1 (114) and (116), respectively.

From (59) and (60), the precoding matrix, $\mathbf{P}_j^{(k)}$, and the receive weight matrix, $\mathbf{W}_j^{(k)}$, can be computed iteratively. Furthermore, as proved in Appendix B.2, the

iteration converges and resulting precoding matrix for CB achieves equal or better performance than single cell beamforming if single cell beamforming is used as initial values. The proposed algorithm essentially transforms a multi-receive into a single-receive subspace CB problem. Next, CB precoding matrices are computed that minimize the objective. Finally, the receive filters are updates such that the original objective is further minimized and whole process repeats. This guarantees that the proposed CB algorithm will improve upon the single receive antenna case. Alternating optimization with iterative search algorithm is shown in Table 6. λ_j is searched in each iteration until PBPC is met within ϵ_λ tolerance or until $T_{\max}$ number of searches. The overall algorithm iterates at most $N_{\max}$ iterations or until the objective function is no further minimized than $\epsilon\%$ in each iteration.

The dual variable, λ_j, should be configured so that inequality constraint, (54a), is satisfied. As proved in Appendix B.3[1], $\|\mathbf{P}_j^{(k)}\|_F^2$ is a monotonically decreasing function of λ_j . Therefore, dual variable, λ_j, can be obtained via the bi-section method [52]. The optimal solution must satisfy complementary slackness conditions [13] and therefore λ_j should be configured such that $\sum_{k=1}^{K_j} \|\mathbf{P}_j^{(k)}\|_F^2 = P_0$ or $\lambda_j = 0$.

Alternatively, as $\|\mathbf{P}_j^{(k)}\|_F$ is a smooth monotonically decreasing function of λ_j, Newton's method to search for optimal λ_j instead of the bi-section method may be utilized. In general, the Newton's method converges faster than the bi-section method at the cost of higher computational complexity at each step. The bi-section and Newton's methods require $N^3 + LN^2 + 2NL^2 + N^2 + 2L$ and $2LN^3 + N^3 + N^2 + 9LN^2 + NL^2 + 10L$ complex additions/multiplications for each search for each user, respectively, where L is number of spatial streams per user. The results based on the simulation methodology described in Section 3.3 show that the bi-section and Newton's methods need an average of 11.3935 and 4.6905 searches, respectively, to

[1]It should be noted that proof of monotonicity of λ_j using eigenvalue decomposition as done in Min-MSE CB problem [76] is not applicable due to the additional dual variable, $\mathbf{\Psi}_j^{(k)}$, from the additional constraint (56a).

Table 6. alternating optimization with iterative search algorithm

Algorithm SINR harmonic-sum maximization (SHS-Max) CB algorithm

Initialization :
set a initial value for $\mathbf{P}_{j,(0)}^{(k)}$.
compute $\mathbf{W}_j^{(k)}$ based on $\mathbf{P}_{j,(0)}^{(k)}$ with (60).
compute objective function, f_0.
for $n = 1, \cdots N_{\max}$ **do**
  configure λ_j with an initial value.
  for $t = 1, \cdots T_{\max}$ **do**
    compute $\mathbf{P}_{j,(n)}^{(k)}$ for $\forall j, k$ using (59) and (114).
    if $|P_0 - \sum_{k=1}^{K_j} \|\mathbf{P}_{j,(n)}^{(k)}\|_F^2| > \epsilon_\lambda$ **then**
      update λ_j based on bi-section or Newton's method.
    else
      break for loop.
    end if
  end for
  update $\mathbf{W}_j^{(k)}$ for $\forall j, k$ using (60) and (116).
  compute objective function, f_n.
  if $(f_{n-1} - f_n)/f_n < \epsilon$ **then**
    break for loop.
  end if
end for
set optimal precoding matrix as $\hat{\mathbf{P}}_j^{(k)} = \mathbf{P}_{j,(n)}^k$
if $\sum_{k=1}^{K_j} \|\hat{\mathbf{P}}_j^{(k)}\|_F^2\| > P_0$ **then**
  scale back $\hat{\mathbf{P}}_j^{(k)}$ to met $\sum_{k=1}^{K_j} \|\hat{\mathbf{P}}_j^{(k)}\|_F^2\| \leq P_0$
end if

meet the error tolerance of $\epsilon_\lambda = 10^{-4}$.

Iterative update of λ_j at the n-th iteration for the Newton's method is given as

$$\lambda_j^{(n+1)} = \lambda_j^{(n)} - \frac{g(\lambda_j^{(n)})}{g'(\lambda_j^{(n)})}, \tag{62}$$

where $g(\lambda_j)$ can be expressed as

$$g(\lambda_j) = \sum_{k=1}^{K_j} \|\mathbf{P}_j^{(k)}\|_F^2 - P_0, \tag{63}$$

and $g'(\lambda_j)$, the derivative of $g(\lambda_j)$, can be expressed as

$$g'(\lambda_j) = \sum_{k=1}^{K_j} \sum_{r=1}^{L_j^{(k)}} \frac{2G_2^2(\lambda_j) - 2G_3(\lambda_j)G_1(\lambda_j)}{G_1^3(\lambda_j)}, \tag{64}$$

where

$$G_s(\lambda_j) = [\mathbf{W}_j^{(k)}]_r^\dagger \mathbf{H}_{jj}^{(k)} (\mathbf{R}_j^{(k)})^{-s} \mathbf{H}_{jj}^{(k)\dagger} [\mathbf{W}_j^{(k)}]_r$$

Note that some of the computations for $g'(\lambda_j)$ can be simplified by use of repeated matrix structure, $(\mathbf{R}_j^{(k)})^{-1}$, which is taken into account in the complexity analysis. Additionally, the updated $\lambda_j^{(n)}$ in certain conditions may result in a non-positive value. Since non-positive $\lambda_j^{(n)}$ may result in non-invertible covariance in (59), $\lambda_j^{(n)}$ is forced to be non-negative value in each update.

While the Newton's method has higher computational complexity per iteration, it is more attractive due to its quick convergence. Some of the computation for Newton's method can be computed in parallel using specialized hardware. However, the iterative aspects of the algorithm cannot be parallelized and must be implemented in a sequential fashion resulting in high processing latency. Therefore, algorithms that have faster convergence properties are favorable. In the next subsection, a heuristic algorithm that further reduces required number of iterations and with lower overall computational complexity is introduced.

3.3.3 Low-Complexity Method

The above method is with iterative search and is with high computational complexity due to the search of optimal λ_j for each step of computing the precoding matrices, $\mathbf{P}_j^{(k)}$. Therefore, a heuristic approach that incrementally updates λ_j once in each iteration of $\mathbf{P}_j^{(k)}$ and $\mathbf{W}_j^{(k)}$ (i.e. $T_{\max} = 1$) is considered. Comparison of the two proposed alternating optimization algorithms is shown in Figure 9.

Note that non-optimal value of λ_j may not meet the PBPC constraint (54a). Furthermore, the algorithm no longer guarantees maximization of the SINR harmonic-sum in each alternating iteration. However, simulations results have showed that

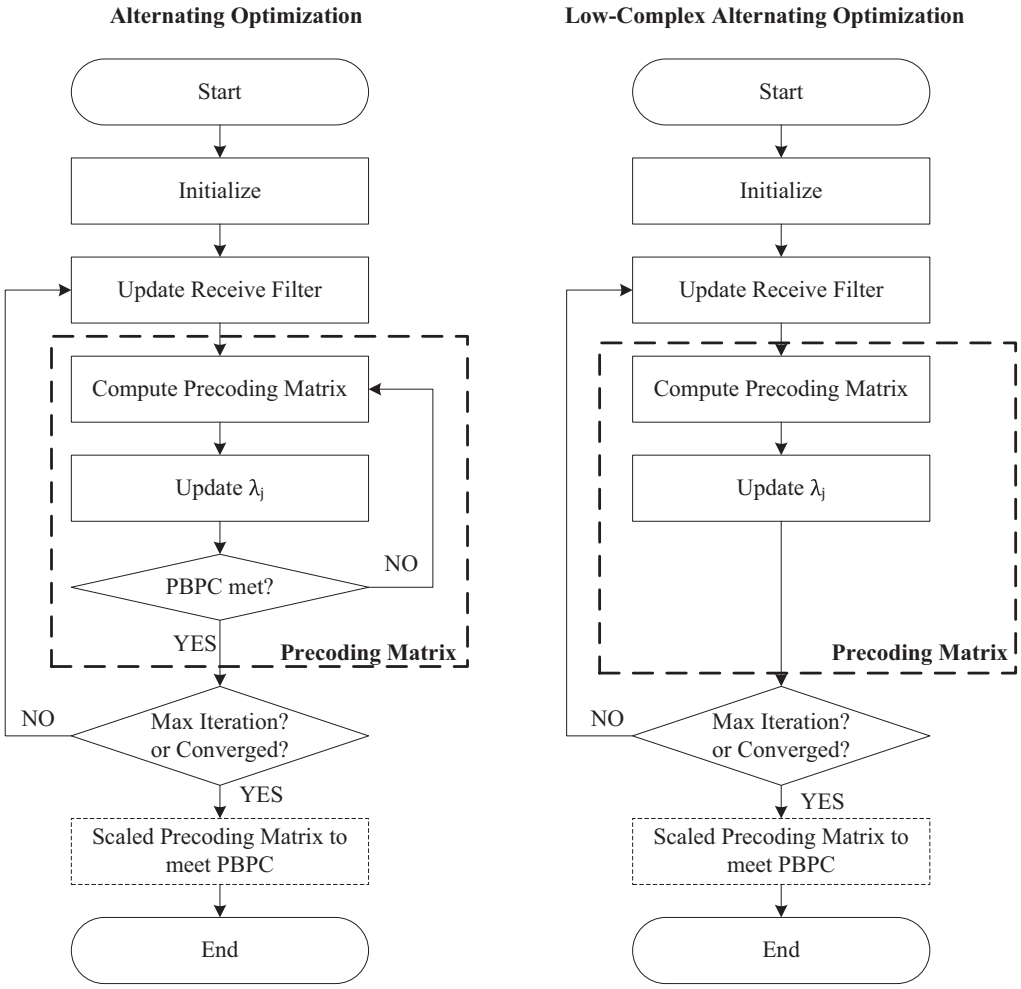

Figure 9. Algorithm flow comparison between alternating optimization and Low-Complexity alternating optimization

with the right update of the dual variable, λ_j, the proposed low-complexity algorithm does converge and cell-edge user performance can be improved. Our investigations showed that if λ_j is updated to aggressively, such as using Newton's method, the whole algorithm may not converge and lead to badly performing CB matrices. On the other hand, if λ_j is only incrementally updated, such as using bi-section method, the low-complexity algorithm requires many alternating iterations to converge.

The bi-section method essentially increases λ_j if $\sum_{k=1}^{K_j} \|\mathbf{P}_j^{(k)}\|_F^2/P_0$ is too large and decreases λ_j if $\sum_{k=1}^{K_j} \|\mathbf{P}_j^{(k)}\|_F^2/P_0$ is too small. Based on the principles of the bi-section

Table 7. low-complexity alternating optimization algorithm

Algorithm Low-complexity SINR harmonic-sum maximization CB algorithm

Initialization :
  set a initial value for $\mathbf{P}_{j,(0)}^{(k)}$.
  compute $\mathbf{W}_j^{(k)}$ based on $\mathbf{P}_{j,(0)}^{(k)}$ with (60).
  set $\lambda_{j,(0)} = 1$.
  compute objective function, f_0.
for $n = 1, \cdots N_{\max}$ **do**
    compute $\mathbf{P}_{j,(n)}^{(k)}$ for $\forall j, k$ using (59).
    update $\lambda_{j,(n)} = \lambda_{j,(n-1)} \cdot \sqrt{\sum_{k=1}^{K_j} \|\mathbf{P}_j^{(k)}\|_F^2 / P_0}$
    update $\mathbf{W}_j^{(k)}$ for $\forall j, k$ using (60).
    compute objective function, f_n.
    if $(f_{n-1} - f_n)/f_n < \epsilon$ **then**
        break for loop.
    end if
end for
set optimal precoding matrix as $\hat{\mathbf{P}}_j^{(k)} = \mathbf{P}_{j,(n)}^k$
if $\sum_{k=1}^{K_j} \|\hat{\mathbf{P}}_j^{(k)}\|_F^2\| > P_0$ **then**
    scale back $\hat{\mathbf{P}}_j^{(k)}$ to met $\sum_{k=1}^{K_j} \|\hat{\mathbf{P}}_j^{(k)}\|_F^2\| \leq P_0$
end if

method, the following heuristic update algorithm is proposed,

$$\lambda_{j,(n+1)} = \lambda_{j,(n)} \cdot \sqrt{\sum_{k=1}^{K_j} \|\mathbf{P}_j^{(k)}\|_F^2 / P_0}. \tag{65}$$

The idea is to scale λ_j such that it grows when $\sum_{k=1}^{K_j} \|\mathbf{P}_j^{(k)}\|_F^2/P_0$ is large, and to shrink λ_j when $\sum_{k=1}^{K_j} \|\mathbf{P}_j^{(k)}\|_F^2/P_0$ is small. Finally, if $\sum_{k=1}^{K_j} \|\mathbf{P}_j^{(k)}\|_F^2 = P_0$, λ_j is not updated further. The low-complexity alternating optimization algorithm is shown in Table 7. Although, the convergence of the low-complexity algorithm is not confirmed analytically, it has been demonstrated to converge numerically. More importantly, it provides better cell-edge user performance when the total number of iterations of the algorithm is very small, such as 4.

Table 8. Complex addition/multiplications in precoding matrix computation of various CB algorithms

WSR	Min-MSE	Max-VSINR	Max-SHS-SINR	Low-Complex Max-SHS-SINR
$K \cdot (L^3 + LMN + 2NL^2) + L^2 + NL^2 + LMN + T \cdot (3N^3 + 4N^2 + 5LN^2 + 2L)$	$K \cdot (LMN + 2NL^2) + T \cdot (3N^3 + 4N^2 + 5LN^2 + 2L)$	$K \cdot (LMN + 2NL^2) + N^3 + N^2 + LN^2$	$K \cdot (LMN + 2NL^2) + T \cdot (2LN^3 + N^3 + N^2 + 9LN^2 + NL^2 + 10L)$	$K \cdot (LMN + 2NL^2) + N^3 + 4N^2 + LN^2 + NL^2 + 2L$

3.3.4 Computational Complexity Comparison

CB algorithms, such as WSR, Min-MSE, Max-VSINR, Max-Min-SINR, and the proposed algorithms of this chapter, have in common that the solution is solved via alternating optimization. Therefore, the computation of the hypothetical receive filter can be identical and what is different is the how the precoding matrices are computed. Of course, depending on how the precoding matrices are computed, convergence as well as the performance change.

The complexity in computing the precoding matrices of mentioned algorithms is compared for each user in each alternating iteration. The required numbers of complex multiplication and addition for computing the precoding matrices for each user in each iteration are shown in Table 8. Max-SHS-SINR and Low-Complex Max-SHS-SINR refer to the proposed algorithms described in Table I and II, respectively. In the table, K is the total number of active users participating in CB, L is the number of transmitted streams per user, T is the number of iterations to find optimal λ_j using the Newton's method. From the analysis, the proposed low-complexity alternating optimization for solving Harmonic sum of SINRs is only slightly more complicated than the Max-VSINR, the least complex algorithm.

Table 9. Example of average simulation run time for various CB algorithms

WSR	Min-MSE	Max-VSINR	Max-SHS-SINR		Low-Complex Max-SHS-SINR	Min-Max-SINR
			Bi-section	Newton		
5.86 s	7.68 s	7.53 s	7.04 s	7.06 s	6.32 s	1565.22 s

The Max-Min-SINR CB algorithm requires iterative searches for the highest minimum SINR value using the bi-section algorithm, where each search requires to solve a SOCP problem [84]. A bi-section search is a SOCP problem with $K \times LN$ dimensioned solution and K second order cone inequalities with $L \times 1$ dimensions. This can be solved using an interior point method, an iterative algorithm, and requiring $\mathcal{O}(N^2L^3K^3)$ calculations per iteration of the interior point method [57]. Given that the number of users, K, is expected to be much greater than the number of transmit antennas per BS, N, or the number of streams per user per BS, L, it can be easily seen that overall computational complexity of Max-Min-SINR CB algorithm is much higher than other CB algorithms mentioned above.

To illustrate the difference in computational complexity of various CB algorithms, the average simulation run time of each CB algorithm using Matlab on a Intel i7 CPU is shown in Table 9. The comparison is the run time for computing CB matrices for 57 cells, each with 4 transmit antennas, and 228 users (i.e. 4 users per cell), each with 2 receive antennas. It should be noted that the Min-Max-SINR is implemented using a generalized *semi-definite programming* (SDP) tool, SDPT3 [85], and therefore further run time optimization is possible with specialized SOCP solver implementation. However, even taking into account that run time for Min-Max-SINR may be reduced by few factors, the difference between the Min-Max-SINR CB algorithm and the proposed algorithms is still substantial.

Furthermore, the mentioned CB algorithms, Max-WSR, Min-MSE, Max-VSINR,

and the proposed CB algorithms can be computed in a distributed manner. Because computation of a CB precoding matrix of one BS, (60), does not require any information about precoding matrix of another BS. Therefore, the precoding matrices can be computed for each BS in parallel as long as the hypothetical receive filters and CSI are shared among BSs. However, Max-Min-SINR CB algorithm requires computation of all CB precoding matrices of all BSs simultaneously.

3.3.5 Precoding Matrix Conditioning for Multi-Stream CB

It should be noted that for multi-stream CB (i.e. $L_j^{(k)} > 1$), the column vectors of $\hat{\mathbf{P}}_j^{(k)}$ for user k in BS j are not necessarily orthogonal at the receiver and can be further optimized. If the *maximum likelihood* (ML) receivers are used, the precoding conditioning matrix is not needed to obtain the capacity that can be achieved using the precoding matrix basis, $\hat{\mathbf{P}}_j^{(k)}$ [28]. However, if linear receivers are used, diagonalization of the effective channel matrix is needed in order to maximize performance.

To find a precoding matrix that diagonalizes the effective channel, the principle precoding matrix can be conditioned by a multiplication of an unitary matrix such that the final precoding matrix can be expressed as

$$\hat{\mathbf{P}}_j^{(k)} = \mathbf{P}_j^{(k)} \mathbf{V}_j^{(k)}, \tag{66}$$

where the conditioning matrix, $\mathbf{V}_j^{(k)}$, for user k in BS j is unitary. Note that introduction of the unitary conditioning matrix for user k in BS j does not change the interference covariance in (47) for any other users. Therefore it does not effect the reception of signals of other users and can be computed independently after the calculation of the precoding matrix basis, $\mathbf{P}_j^{(k)}$, of all users.

The effective channel after the linear receive filtering, $\hat{\mathbf{W}}_j^{(k)\dagger} \mathbf{H}_{jj}^{(k)} \mathbf{P}_j^{(k)} \mathbf{V}_j^{(k)}$, needs to be diagonal. If the MMSE receive filter is used, that is $\mathbf{W}_j^{(k)} = (\mathbf{Q}_j^{(k)})^{-1} \mathbf{H}_{jj}^{(k)} \mathbf{P}_j^{(k)} \mathbf{V}_j^{(k)}$, the effective channel after linear receive filtering, $\hat{\mathbf{X}}_j^{(k)}$, can be expressed as

$$\hat{\mathbf{X}}_j^{(k)} = \mathbf{V}_j^{(k)\dagger} \mathbf{P}_j^{(k)\dagger} \mathbf{H}_{jj}^{(k)\dagger} (\mathbf{Q}_j^{(k)})^{-1} \mathbf{H}_{jj}^{(k)} \mathbf{P}_j^{(k)} \mathbf{V}_j^{(k)}. \tag{67}$$

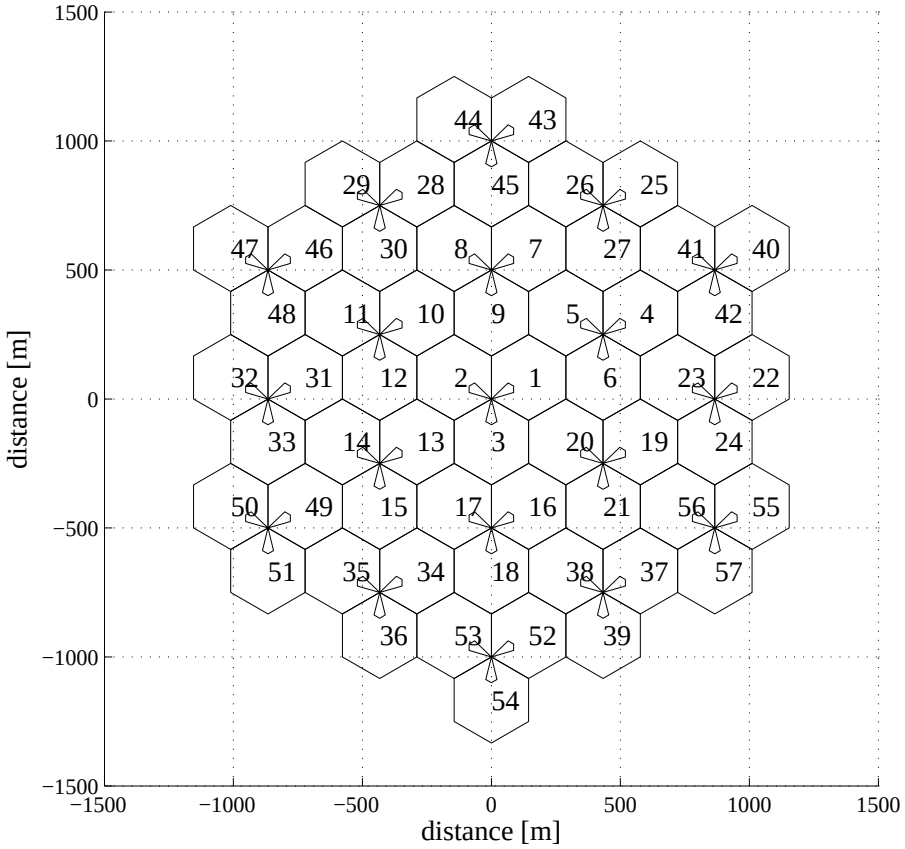

Figure 10. Cell layout for simulation evaluation

Therefore, the unitary conditioning matrix, $\mathbf{V}_j^{(k)}$, consist of the eigenvectors that satisfy

$$\mathbf{P}_j^{(k)\dagger}\mathbf{H}_{jj}^{(k)\dagger}(\hat{\mathbf{Q}}_j^{(k)})^{-1}\mathbf{H}_{jj}^{(k)}\mathbf{P}_j^{(k)} = \mathbf{V}_j^{(k)}\mathbf{S}_j^{(k)}\mathbf{V}_j^{(k)\dagger}, \tag{68}$$

where $\mathbf{S}_j^{(k)}$ is a diagonal matrix.

3.4 Simulation Evaluation

In this section, numerical results of the proposed algorithms are presented. The proposed algorithms are compared with *single cell SLNR beamforming* (SC-SLNR BF) [27], Max-VSINR CB [73], Max-WSR CB [**?**], Min-MSE CB [73], and Max-Min-SINR [84]. The proposed CB algorithms described in Sections 3.3.1 and 3.3.2, will be denoted as *SINR harmonic-sum maximizing CB* (SHS-CB) algorithm and *low-complexity SINR harmonic-sum maximizing CB* (LC-SHS-CB), respectively.

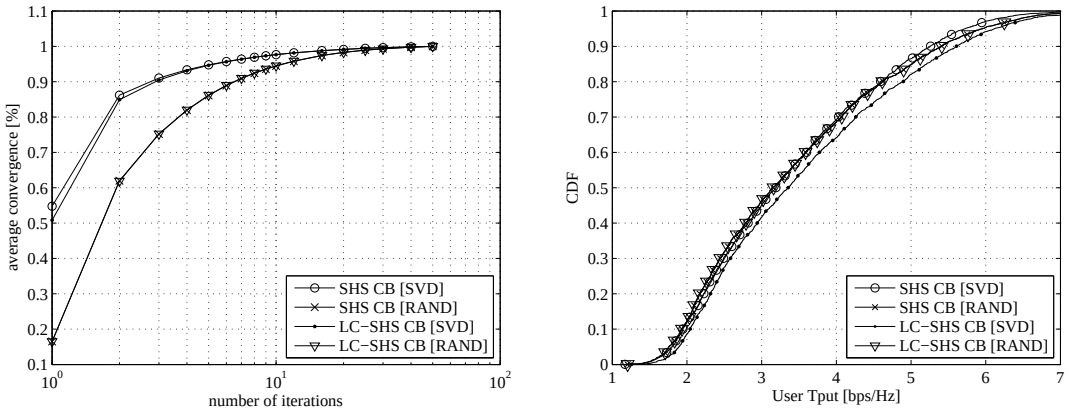

(a) Convergence **(b)** User throughput

Figure 11. Comparison between single cell SVD precoding (SVD) and random matrix (RAND) based initial value configurations

All simulation results are based on 3GPP simulation methodology [1]. The simulated network consists of 57 sectorized BSs with directional antennas as in Figure 10. Each BS site has 3 sectors and they are located in a hexagonal grid with geographical wrap around to mimic an infinitely large network. The distance between any two BS sites is 500 m. The maximum transmit power for a 10 MHz channel is 43 dBm, and the noise power density is -174 dBm/Hz. The directional antennas have a half-power beam-width of 70° and 17 dBi antenna gain with 20 dB front-to-back ratio. The channel is spatially uncorrelated and with flat fading, generated by complex Gaussian random variable. Pathloss model is $128.1 + 37.6 \log_{10}(d/1000)$, where d is the distance between the transmitter and the receiver. Users are uniformly and randomly distributed over the entire network. The received SINR has been mapped to throughput using $\log_2(1 + \text{SINR})$. Simulation is with 4 scheduled users per BS, 2 spatial streams per user, 8 transmit antennas at the BS, and 4 receive antennas at each user, unless specified. The network is assumed to have full CSI of links between users and BS, which is obtained through channel reciprocity in the TDD systems, and all 57 cells are cooperating in the CB.

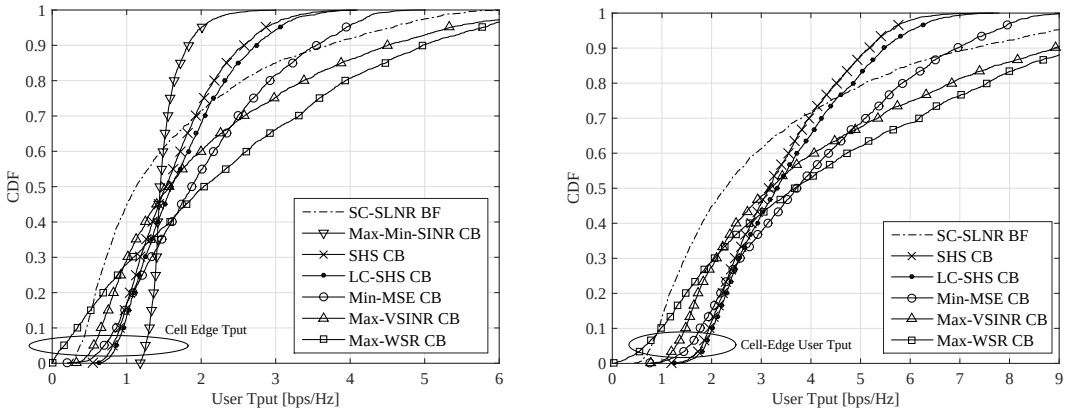

(a) User throughput in 4x2 MIMO System **(b)** User throughput in 8x4 MIMO System

Figure 12. Cumulative user throughput distribution

3.4.1 Initial Values and Convergence

As the proposed CB algorithms are sub-optimal and iterative, the initial value will affect performance and convergence. The proposed algorithms are evaluated with the following initial precoding matrices:

i) complex random matrices,

ii) single cell SVD based precoding.

Figure 11 compares the average convergence trajectories of the SVD based and the random matrix based initial precoding matrices for the proposed algorithms on 4,000 channel realizations. The proposed algorithms can reach 95% of the converged objective within the average of 5 alternating iterations using single cell SVD precoding as initial values. From the above figures, the SVD based initial precoding matrices have faster convergence with similar performance to that of the random initial precoding matrix. Therefore, single cell SVD precoding as initial values are utilized in the subsequent simulations.

3.4.2 Throughput Comparison

Figure 12a compares cumulative user throughput of different CB algorithms with 4 transmit antennas at BS, 2 receive antennas at each user, and 1 spatial stream per user. Other than Max-WSR CB algorithm, all CB algorithms improve the 5-th percentile user throughput (i.e. cell-edge user throughput). The proposed algorithms, SHS CB and LC-SHS CB, outperforms all other CB algorithms in improving cell-edge user throughput other than Max-Min-SINR CB. Table 10 shows the numerical results with 5 and 10 alternating iterations based on the same simulation setup.

Figure 12b compares cumulative user throughput of different CB algorithms with 8 transmit antennas at BS, 4 receive antennas at each user, and 2 spatial stream per user. It should be noted that the precoding conditioning matrix, as described in Section 3.3.5, has been applied to the proposed CB algorithms. Max-Min-SINR CB results has been omitted due to computational challenges. The performance trends of the algorithm between 1 spatial stream and 2 spatial streams per user are similar.

The percentage gains are referenced to the SC-SLNR BF algorithm, which is used as an informative reference for non-coordinating scheme. From the table, LC-SHS CB has 130% gain for 5-th percentile user throughput compared with SC-SLNR BF without any loss for average user throughput. It has the highest 5-th percentile user throughput gains while not degrading the average user throughput compared to SC-SLNR BF. The proposed CB algorithms, SHS CB and LC-SHS CB, has 16% and 23% higher cell-edge user throughput compared with Min-MSE CB, which has the second highest cell-edge user throughput if excluding Max-Min-SINR CB. Even if the Max-Min-SINR has the highest 5-th percentile user throughput, it is at the cost of significantly higher computation complexity and average user throughput degradation. In fact, Max-Min-SINR has computational complexity of $\mathcal{O}(TK^3N^2L^3)$ per alternating optimization iteration, where T is the number of bi-section iterations needed to estimate the maximum of the minimum SINR of users. The number of users, K,

Table 10. User throughput comparison

	5 iterations		10 iterations	
	5% User Tput [b/Hz/s]	User Avg. Tput [b/Hz/s]	5% User Tput [b/Hz/s]	User Avg. Tput [b/Hz/s]
SC-SLNR	0.3747	1.6206	0.3747	1.6206
	0.0%	0.0%	0.0%	0.0%
SHS CB	0.8083	1.6377	0.8114	1.6636
	+115.73%	+1.06%	+116.57%	+2.65%
LC-SHS CB	0.8620	1.7334	0.8685	1.7634
	+130.07%	+6.96%	+131.79%	+8.81%
Max-Min-SINR CB	1.2559	1.5191	1.2703	1.5449
	+235.19%	-6.26%	+239.04%	-4.67%
Min-MSE	0.6961	2.0315	0.7237	2.0632
	+85.77%	+25.35%	+93.15%	+27.31%
Max-VSINR	0.5613	2.1304	0.5644	2.1651
	+49.82%	+31.45%	+50.63%	+33.60%
Max-WSR	0.1604	2.3868	0.0026	2.5479
	-57.20%	+47.28%	-99.30%	57.22%

is the dominating factor of computation. This is in the order of magnitude more complex than LC-SHS CB, which only has computational complexity of $\mathcal{O}(KNML)$ per alternating optimization iteration.

Interestingly, the LC-SHS CB algorithm seems to outperform the SHS CB algorithm. This is possible since both LC-SHS and SHS CB are sub-optimal algorithms that search for local maxima of the SINR harmonic-sum objective and simulation is terminated before full convergence.

Additionally, harmonic sum of user SINRs are shown in Figure 13. The harmonic sum of all users in the network is computed for each user distribution drop and multiple drops are simulated. The proposed objective, harmonic sum of user SINRs, serves as a means to derive a low-complex algorithm rather than as a figure of merit.

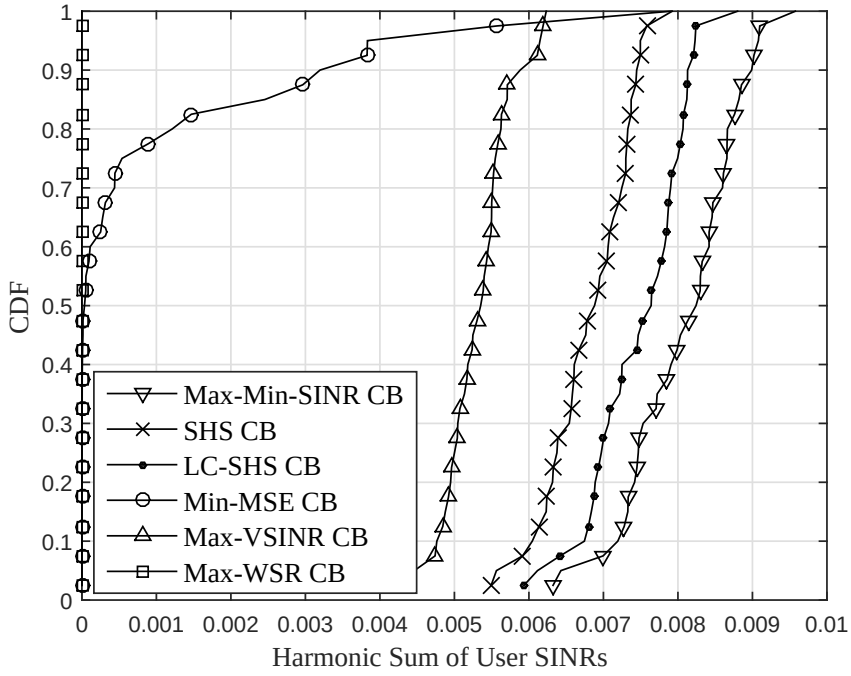

Figure 13. Cumulative distribution of harmonic sum of user SINRs

However, from the figure, the higher harmonic sum of SINRs results in improvement of the cell-edge users throughput as indicated in Section 3.3.

3.4.3 Multi-Stream Precoding Conditioning Comparison

In addition, the proposed CB algorithms with and without conditioning of the precoding matrices are compared in Table 11, where 5 iterations are used. From the table, it can be verify that the final conditioning of the precoding matrix always increases the throughput for linear receivers.

3.4.4 Performance Impact from Partial CSI Knowledge

For *time duplex division* (TDD) systems, BSs may utilize uplink pilots to estimate the channel and get CSI based on channel reciprocity. However, channel estimation based on uplink pilots has some limitations, which lead to having partial CSI knowledge at the network. To investigate the uplink pilot signal reception issues, LTE uplink power control is modeled for *sounding reference signal* (SRS) [4]. The number of

Table 11. Precoding conditioning comparison

		5% User Tput [b/Hz/s]	User Avg. Tput [b/Hz/s]
SHS CB	without conditioning	1.7853	3.2909
	with conditioning	1.8031	3.3636
LC-SHS CB	without conditioning	1.8618	3.4737
	with conditioning	1.8705	3.5509

links between a BS and a user that will have pilot *signal-to-noise ratio* (SNR) below a certain value are analyzed.

In the simulation, full-pathloss compensation and no accumulated power control, pilot transmission bandwidth of 9 MHz, and maximum transmit power of 23 dBm, which corresponds to $\alpha = 1$, $f_c(i) = 0$, and $M_{\text{SRS}} = 50$ in the power control formula in Section 5.1.3 of [4] is assumed. Two different power control configurations, P_0 = -125 dBm and -115 dBm in Section 5.1.3 of [4], have been evaluated, which correspond to serving BS target SNR of 7 dB and 17 dB, respectively, in the simulated scenario.

Figure 14 shows the probability distribution of number of links from BSs to a user that has higher than 0 dB or -5 dB for two different power control configurations. Simulation results show that with P_0 = -125 dBm power control configuration, less than 3 and 9 BSs out of 57 are able to received pilots from a users with higher than SNR of 0 dB and -5 dB, respectively. The number of BSs that are able to receive pilots from a user with higher than SNR of 0 dB and -5 dB with P_0 = -115 dBm increases to 9 and 16, respectively.

Figure 15 shows the user throughput of SHS CB and LC-SHS CB with P_0 = -125 dBm and -115 dBm power control configurations. It has been assumed the CSI is not available for links lower than received SNR of 0 dB and -5 dB and perfect CSI is available for link otherwise. The ideal case in the figure represents CB with full CSI

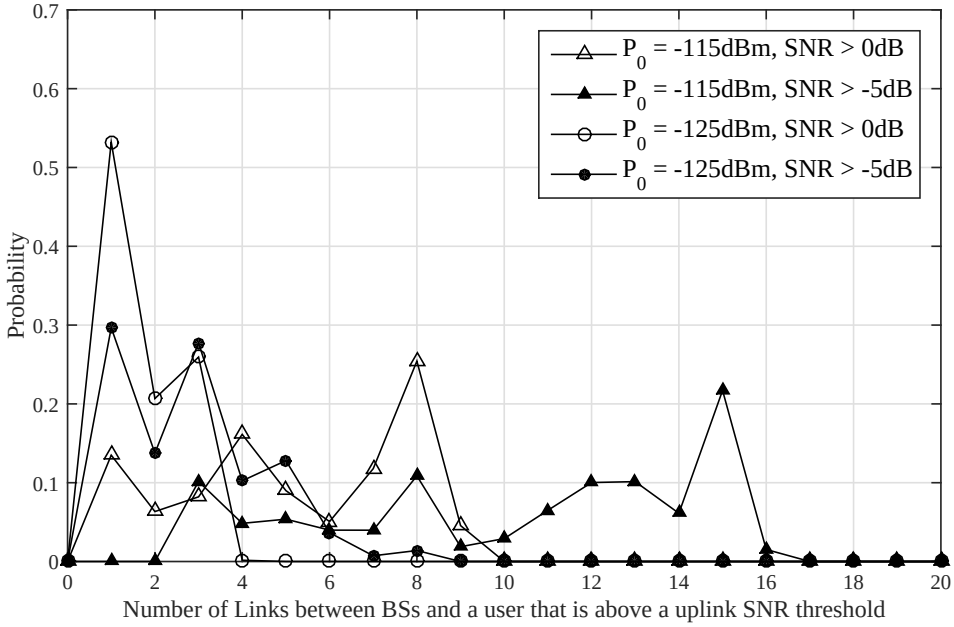

Figure 14. Probability distribution of number of links from a user to BSs with various receive SNRs

knowledge. Even though the CSI knowledge is limited, simulation results show that the proposed CB algorithms performance does not degrade much. ICI from interfering links are dominant, which is similar to serving BS signal strength. Therefore, as long as appropriate power control parameters are configured and CSI is made available for the strongest interfering links, the proposed CB algorithm is robust to partial CSI available at the transmitter.

CSI estimation error can affect the performance of the proposed algorithms. Table 12 shows user throughput results with *channel estimation*(CE) processing gains of 4, 8, 12 dB and uplink power control configuration of P_0 = -115 dBm and -125dBm. When the overall uplink transmit power is low, i.e. P_0 = -125 dBm, and CE processing gain is low, i.e. 4 dB, the proposed CB algorithm may have up to 11% cell-edge user throughput loss compared to perfect CSI cases for the LC-SHS CB algorithm. Increasing the overall uplink transmission power into P_0 = -115 dBm significantly reduces user throughput loss to less than 1%. Therefore, right configuration of uplink

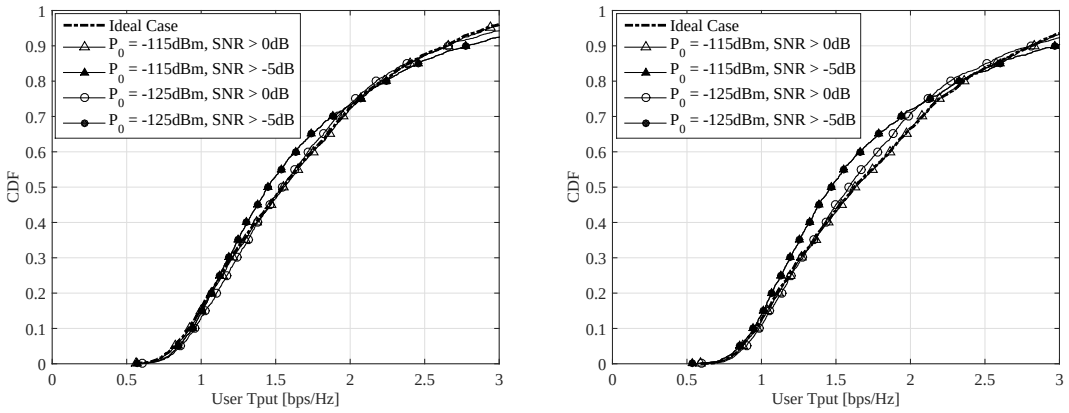

(a) User throughput with SHS CB algorithm **(b)** User throughput with LC-SHS CB algorithm

Figure 15. User throughput comparison with various power control configurations and pilot signal minimum detection threshold

pilot transmission power and pilot design to ensure high CE processing gain can reduce the performance losses incurred by partial and imperfect CSI knowledge.

3.5 Summary and Conclusions

This chapter has investigated multi-stream multi-user coordinated transmit beamforming for wireless networks with multiple transmit and receive antennas and developed low-complex iterative algorithms to compute coordinated beamforming matrices. The proposed algorithms can reach 95% of its convergence within an average of 5 iterations. The performance of the proposed algorithms significant improve upon the non-coordinating network and have 16% to 23% improvement for 5-th percentile user throughput compared with that of latest CB techniques while not degrading the average user throughput. The proposed algorithms are low-complex alternatives to the Max-Min-SINR CB algorithm that target the cell-edge users. The CB algorithms can be applied to more wider coordination area with many users as it only linearly scales with number of users and can be parallelized unlike the Max-Min-SINR CB algorithm, where the computational complexity scales in the cube of number of users. Research additionally shows that with proper uplink power control configurations in

Table 12. User throughput comparison with various CE processing gain and power control configurations

LC-SHS CB	P_0 = -115 dBm		P_0 = -125 dBm	
	5% User Tput [b/Hz/s]	User Avg. Tput [b/Hz/s]	5% User Tput [b/Hz/s]	User Avg. Tput [b/Hz/s]
Perfect CSI	0.87219	1.7695	0.90032	1.748
	+0.0%	+0.0%	+0.0%	+0.0%
4dB CE Gain	0.84888	1.7328	0.79309	1.5403
	2.67%	-2.07%	-11.91%	-11.88%
8dB CE Gain	0.86368	1.7559	0.84986	1.6526
	-0.97%	-0.76%	-5.60%	-5.45%
12dB CE Gain	0.86853	1.7654	0.87566	1.7068
	-0.41%	-0.22%	-2.73%	-2.35%

TDD systems, the performance loss due to partial and imperfect CSI knowledge is minimal for the propose CB algorithms.

CHAPTER IV

COORDINATED BEAMFORMING ALGORITHM WITH PER ANTENNA POWER CONSTRAINT IN OFDMA

4.1 Introduction

Greater number of transmit antennas for cellular systems enable higher throughput and efficiency through beamforming and spatial multiplexing gains. To reduce cost for large antenna arrays, each antenna element may be designed to output only a fraction of the total transmit power of the whole antenna array. This significantly reduces cost and design complexity of each antenna element. However, in order to send signals using such antenna arrays, transmit baseband signals must have *per-antenna power constraints* (PAPC). Therefore, development of *multiple input multiple output* (MIMO) techniques with PAPC is of a great importance.

Modern cellular systems, such as LTE, use of *orthogonal frequency division multiple access* (OFDMA) to multiplex multiple users and to obtain frequency selectivity gains through smart scheduling. The combination of OFDMA and high order MIMO imposes higher computational complexity of signal processing and scheduling performed by the *base station* (BS). The transmit power of an antenna in a multi-stream beamforming system is determined by the sum of transmit power of each subcarrier and each spatial stream. Therefore, even if transmit power of a given stream on a given subcarrier exceeds a certain power allowance, PAPC can be met as long as some other stream or subcarrier use less transmit power such that total transmit power constraint is met. Multi-carrier operations enable some flexibility of transmit power constraints on each subcarrier. However, designing a low complex beamforming techniques that fully utilize such flexibility while meeting PAPC as a whole will

be a challenge.

4.2 System Model

Consider a network with J BSs. Each link consists of a BS with N_t transmit antennas and users each with N_r receive antennas. They are all working at the same frequency and therefore may interfere with each other. Denote the $N_r \times N_t$ channel coefficient matrix from BS i to user k in BS j for subcarrier m to be $\mathbf{H}_{ij,m}^{(k)}$. Since BS j serves user k, channel coefficient matrix, $\mathbf{H}_{ij,m}^{(k)}$, with $i \neq j$, is the interference channel. Let K_j be the number of scheduled users in BS j, and users are randomly distributed in the network. Let M be the number of subcarriers in OFDMA system.

In *multi-user MIMO* (MU-MIMO), several users are scheduled in the same frequency band simultaneously with the help of spatial division. Let $L_j^{(k)}$ be the number spatial streams for user k in BS j. The received signal for user k in BS j of subcarrier m in a MU-MIMO system can be expressed as

$$\begin{aligned}\mathbf{y}_{j,m}^{(k)} &= \mathbf{H}_{jj,m}^{(k)}\mathbf{P}_{j,m}\mathbf{x}_{j,m} + \sum_{i=1,i\neq j}^{J} \mathbf{H}_{ij,m}\mathbf{P}_{i,m}\mathbf{x}_{i,m} + \mathbf{n}_{j,m}^{(k)}, \\ &= \mathbf{H}_{jj,m}^{(k)}\mathbf{P}_{j,m}^{(k)}\mathbf{x}_{j,m}^{(k)} + \sum_{l=1,l\neq k}^{K_j} \mathbf{H}_{jj,m}^{(k)}\mathbf{P}_{j,m}^{(l)}\mathbf{x}_{j,m}^{(l)} + \sum_{i=1,i\neq j}^{J}\sum_{l=1}^{K_i} \mathbf{H}_{ij,m}^{(k)}\mathbf{P}_{i,m}^{(l)}\mathbf{x}_{i,m}^{(l)} + \mathbf{n}_{j,m}^{(k)},\end{aligned} \tag{69}$$

where $\mathbf{P}_{j,m}$ and $\mathbf{x}_{j,m}$ is the overall precoding matrix and data signal of BS j and are given as $\mathbf{P}_{j,m} = [\mathbf{P}_{j,m}^{(1)}, \mathbf{P}_{j,m}^{(2)}, \cdots, \mathbf{P}_{j,m}^{(K_j)}]$ and $\mathbf{x}_{j,m} = [\mathbf{x}_{j,m}^{(1)T}, \mathbf{x}_{j,m}^{(2)T}, \cdots, \mathbf{x}_{j,m}^{(K_j)T}]^T$, respectively, where $(\cdot)^T$ is the matrix transpose operation, $\mathbf{P}_{j,m}^{(k)}$ and $\mathbf{x}_{j,m}^{(k)}$ are the $N_t \times L_j^{(k)}$ precoding matrix and the $L_j^{(k)} \times 1$ transmit-signal vector for user k from BS j, respectively, and $\mathbf{n}_j^{(k)}$ is the *additive white Gaussian noise* (AWGN) vector. The power of AWGN is σ_n^2.

The subcarrier index subscript, m, is omitted whenever the equation unambiguously represents description for a single subcarrier.

At each receiver, a $N_r \times L_j^{(k)}$ weight matrix, $\mathbf{W}_j^{(k)}$, is used to combine the received

signals from different antennas of user k. As a result,

$$\hat{\mathbf{x}}_j^{(k)} = \mathbf{W}_j^{(k)\dagger}\mathbf{y}_j^{(k)}, \tag{70}$$

and $\hat{\mathbf{x}}_j^{(k)}$ is the estimated desired signal.

From (69), the SINR of the r-th spatial stream of user k in BS j can be expressed as

$$\mathrm{SINR}_j^{(k,r)} = \frac{\left|[\mathbf{W}_j^{(k)}]_r^\dagger \mathbf{H}_{jj}^{(k)} [\mathbf{P}_j^{(k)}]_r\right|^2}{[\mathbf{W}_j^{(k)}]_r^\dagger \mathbf{Q}_j^{(k)} [\mathbf{W}_j^{(k)}]_r - \left|[\mathbf{W}_j^{(k)}]_r^\dagger \mathbf{H}_{jj}^{(k)} [\mathbf{P}_j^{(k)}]_r\right|^2}, \tag{71}$$

where $[\cdot]_r$ is the r-th column vector of the matrix, and $\mathbf{Q}_j^{(k)}$ is the total received signal covariance of user k in BS j and can be expressed as

$$\mathbf{Q}_j^{(k)} = \sum_{i=1}^{J}\sum_{l=1}^{K_i} \mathbf{H}_{ij}^{(k)} \mathbf{P}_i^{(l)} \mathbf{P}_i^{(l)\dagger} \mathbf{H}_{ij}^{(k)\dagger} + \sigma_n^2 \mathbf{I}. \tag{72}$$

The receive filter can be obtained by finding the column vectors of $\mathbf{W}_j^{(k)}$ that maximize SINR in (71), that is

$$\begin{aligned} [\hat{\mathbf{W}}_j^{(k)}]_r &= \arg \max_{[\mathbf{W}_j^{(k)}]_r} \mathrm{SINR}_j^{(k,r)} \\ &= \left(\mathbf{Q}_j^{(k)}\right)^{-1} \mathbf{H}_{jj}^{(k)} [\mathbf{P}_j^{(k)}]_r, \end{aligned} \tag{73}$$

which corresponds to *minimum mean-square error* (MMSE) receive filter.

4.3 CB Algorithms with PAPC

Some CB algorithms can be designed such that computed precoding matrices maximize *weighted sum-rate* (WSR), *minimize mean-squared error* (MSE), or maximize the *harmonic sum of SINRs* (HSS). The precoding matrix of these CB algorithms have a common structure, in the form of whitened matched filter, that enables efficient application of PAPC.

The optimization problem for mentioned CB algorithms can be described as

$$\text{maximize} \sum_{m=1}^{M} \mathcal{U}(\mathbf{P}_{1,m}, \mathbf{P}_{2,m}, \cdots, \mathbf{P}_{J,m}), \tag{74}$$

subject to

$$\mathbf{I} \circ \left(\sum_{m=1}^{M} \mathbf{P}_{j,m} \mathbf{P}_{j,m}^{\dagger} \right) \leq \mathbf{D}_j, \forall j, \tag{74a}$$

where $\circ$ denotes the entrywise product symbol (i.e. Hadamard product), $\mathcal{U}(\cdot)$ is the optimization objective, WSR, negative MSE, or HSS, and $\mathbf{D}_j$ is a diagonal matrix that contains power constraint values for each antenna in each diagonal element.

The utility metric, $\mathcal{U}(\mathbf{P})$, is partially convex over $\mathbf{P}$, and the optimal solution with respect to the precoding matrix can be found using the Lagrange multipliers method which can be expressed as

$$\mathcal{L}(\mathbf{P}, \Lambda) = \sum_{m=1}^{M} \mathcal{U}(\mathbf{P}_{1,m}, \cdots, \mathbf{P}_{J,m}) + \mathrm{Tr} \left(\sum_{j=1}^{J} \mathbf{\Lambda}_j \left(\mathbf{I} \circ \left(\sum_{m=1}^{M} \mathbf{P}_{j,m} \mathbf{P}_{j,m}^{\dagger} \right) - \mathbf{D}_j \right) \right), \tag{75}$$

where the diagonal matrix, $\mathbf{\Lambda}_j$, is dual variable of the PAPC. Using commutative property of Hadamard product, $\mathbf{I} \circ \mathbf{X} = \mathbf{X} \circ \mathbf{I}$, and matrix trace properties, $\mathrm{Tr}(\mathbf{I} \circ \mathbf{X}) = \mathrm{Tr}(\mathbf{X})$ and $\mathrm{Tr}(\mathbf{AB}) = \mathrm{Tr}(\mathbf{BA})$, the Lagrangian function can be further manipulated as

$$\begin{aligned} \mathcal{L}(\mathbf{P}, \Lambda) = & \sum_{m=1}^{M} \mathcal{U}(\mathbf{P}_{1,m}, \cdots, \mathbf{P}_{J,m}) \\ & + \sum_{j=1}^{J} \sum_{m=1}^{M} \sum_{k=1}^{K_j} \mathrm{Tr} \left(\mathbf{P}_{j,m}^{(k)\dagger} \mathbf{\Lambda}_j \mathbf{P}_{j,m}^{(k)} \right) - \sum_{j=1}^{J} \mathrm{Tr} \left(\mathbf{\Lambda}_j \mathbf{D}_j \right). \end{aligned} \tag{76}$$

Using complex matrix gradient result, $\nabla_{\mathbf{X}} \mathrm{Tr}(\mathbf{X}^{\dagger} \mathbf{A} \mathbf{X}) = 2\mathbf{A}\mathbf{X}$, in [68], the gradient of the Lagrangian function can be expressed as

$$\nabla_{\mathbf{P}_{j,m}^{(k)}} \mathcal{L}(\mathbf{P}, \mathbf{\Lambda}) = \nabla_{\mathbf{P}_{j,m}^{(k)}} \sum_{m=1}^{M} \mathcal{U}(\mathbf{P}_{1,m}, \mathbf{P}_{2,m}, \cdots, \mathbf{P}_{J,m}) + \sum_{j=1}^{J} \sum_{m=1}^{M} \sum_{k=1}^{K_j} 2\mathbf{\Lambda}_j \mathbf{P}_{j,m}^{(k)}. \tag{77}$$

For utility functions that are either convex or partially convex, we can derive an efficient algorithm based on alternating optimization, similar to the proposed CB algorithm in Chapter 2.3. Furthermore, if the critical solution to either maximizing or minimizing the utility functions result in whitened match filter like structure of the precoding matrix, low complex algorithm to compute the precoding matrix that achieves PAPC is possible.

4.3.1 WSR CB Algorithm with PAPC

WSR is useful metric when specific prioritization of users is known to the network. Configuration of weight parameters enable uses for various applications and deployment scenarios. Both use of convex programming [78, 77, 19] and Lagrangian multipliers [18] has been investigated to efficiently solve maximization of WSR metric. The following uses the latter approach to efficiency solve maximization of WSR, which enables development of less complex algorithms.

The WSR utility metric is expressed as

$$\begin{aligned}\mathcal{U}_{\text{WSR}}(\mathbf{P}) &= \sum_{j=1}^{J}\sum_{k=1}^{K_j}\sum_{m=1}^{M}\mu_j^{(k)}r_{j,m}^{(k)} \\ &= \sum_{j=1}^{J}\sum_{k=1}^{K_j}\sum_{m=1}^{M}\mu_j^{(k)}\log\left|\mathbf{I}+\mathbf{P}_{j,m}^{(k)\dagger}\mathbf{H}_{jj,m}^{(k)\dagger}(\tilde{\mathbf{Q}}_{j,m}^{(k)})^{-1}\mathbf{H}_{jj,m}^{(k)}\mathbf{P}_{j,m}^{(k)}\right|, \end{aligned} \tag{78}$$

where $|\cdot|$ is the matrix determinant, $\mu_j^{(k)}$ and $r_{j,m}^{(k)}$ are the the weight coefficient and the sum-rate of user k in BS j, respectively, and $\tilde{\mathbf{Q}}_{j,m}^{(k)}$ is the interference signal covariance of user k in BS j and can be expressed as

$$\tilde{\mathbf{Q}}_{j,m}^{(k)} = \mathbf{Q}_{j,m}^{(k)} - \mathbf{H}_{jj,m}^{(k)}\mathbf{P}_{j,m}^{(k)}\mathbf{P}_{j,m}^{(k)\dagger}\mathbf{H}_{jj,m}^{(k)\dagger} = \sum_{\substack{i=1\\(i,l)\neq(j,k)}}^{J}\sum_{l=1}^{K_i}\mathbf{H}_{ij}^{(k)}\mathbf{P}_i^{(l)}\mathbf{P}_i^{(l)\dagger}\mathbf{H}_{ij}^{(k)\dagger}+\sigma_n^2\mathbf{I}. \tag{79}$$

where $\mathbf{Q}_{j,m}^{(k)}$ is the total received signal covariance, (72).

WSR optimization problem can be solved as a *weighted minimum mean-square error* (WMMSE) problem with optimized weights [18]. The objective is convex with respect to the precoding matrix, $\mathbf{P}_j^{(k)}$, and receive filter, $\mathbf{W}_j^{(k)}$. However, it is not jointly convex. Therefore, alternating optimization method is used, where the precoding matrix and receive filter is updated iteratively. For partially-convex objectives, this method is known to converge. The CB precoding matrices are found using the Lagrange multipliers method. The gradient of the WSR Lagrangian function with

respect to the precoding matrix of user k in BS j can be expressed as

$$\nabla_{\mathbf{P}_{j,m}^{(k)}} \mathcal{L}(\mathbf{P}, \mathbf{\Lambda}) = 2\mathbf{H}_{jj,m}^{(k)\dagger} \mathbf{W}_{j,m}^{(k)} \mathbf{E}_{j,m}^{(k)} \mu_j^{(k)} - \left(\sum_{\substack{i=1 \\ (i,l)\neq(j,k)}}^{J} \sum_{l=1}^{K_i} 2\mu_i^{(l)} \mathbf{H}_{ji,m}^{(l)} \mathbf{W}_{i,m}^{(l)\dagger} \mathbf{E}_{i,m}^{(l)} \mathbf{W}_{i,m}^{(l)} \mathbf{H}_{ji,m}^{(l)\dagger} \right) \mathbf{P}_{j,m}^{(k)} - 2\mathbf{\Lambda}_j \mathbf{P}_{j,m}^{(k)}, \quad (80)$$

where $\mathbf{E}_j^{(k)}$ is the weight matrix and is expressed as

$$\mathbf{E}_{j,m}^{(k)} = \left(\mathbf{I} + \mathbf{P}_{j,m}^{(k)\dagger} \mathbf{H}_{jj,m}^{(k)\dagger} (\tilde{\mathbf{Q}}_{j,m}^{(k)})^{-1} \mathbf{H}_{jj,m}^{(k)} \mathbf{P}_{j,m}^{(k)\dagger} \right)^{-1}. \quad (81)$$

The derivation is shown in the Appendix C.1. The term, $\mathbf{\Lambda}_j \mathbf{P}_{j,m}^{(k)}$, stems directly from the gradient of the PAPC.

By setting the gradient of the WSR Lagrangian to be equal to zero, (80) can be manipulated into semi-closed form CB precoding matrix equation. Additionally, due to complementary slackness conditions, the dual variable, $\mathbf{\Lambda}_j$, must meet PAPC, (74a), with equality. The equation is semi-closed form because there is no close form solution for obtaining the dual variable, $\mathbf{\Lambda}_j$. The CB precoding matrix for maximizing WSR can be expressed as

$$\mathbf{P}_{j,m}^{(k)} = \left(\sum_{\substack{i=1 \\ (i,l)\neq(j,k)}}^{J} \sum_{l=1}^{K_i} \mathbf{H}_{ji,m}^{(l)} \mathbf{W}_{i,m}^{(l)\dagger} \mu_i^{(l)} \mathbf{E}_{i,m}^{(l)} \mathbf{W}_{i,m}^{(l)} \mathbf{H}_{ji,m}^{(l)\dagger} + \mathbf{\Lambda}_j \right)^{-1} \mathbf{H}_{jj,m}^{(k)\dagger} \mathbf{W}_{j,m}^{(k)} \mu_j^{(k)} \mathbf{E}_{j,m}^{(k)}, \quad (82)$$

which is the in the form of whitened matched filter equations.

The receive filter can be directly computed, as it is known that MMSE receive filter, (73), is sum-rate maximizing solution. The overall algorithm is shown in Table 13.

Table 13. WSR maximization CB algorithm

Algorithm WSR maximization CB algorithm

1: set $\mathbf{P}_{j,m}^{(k)}$ with initial values

2: **for** $t = 1 \cdots T_{\text{max-iteration}}$ **do**

3: compute $(\mathbf{W}_{j,m}^{(k)} | \mathbf{P}_{j,m}^{(k)}), \forall j, m, k$ using (73)

4: compute $(\mathbf{E}_{j}^{(k)} | \mathbf{P}_{j,m}^{(k)}), \forall j, m, k$ using (81)

5: compute $(\mathbf{P}_{j,m}^{(k)}, \mathbf{\Lambda}_j | \mathbf{W}_{j,m}^{(k)}), \forall j, m, k$ using (82)

6: break if converged

7: **end for**

4.3.2 MSE CB Algorithm with PAPC

Precoding matrix solution to minimizing MSE is partially derived during solving for CB that maximizes WSR. Furthermore, relationship between minimizing MSE and maximizing WSR is presented in [18].

Assuming that the signal power is one and the transmit power is controlled by the precoding matrix, the negative MSE metric can be expressed as

$$\begin{aligned} \mathcal{U}_{\text{MSE}}(\mathbf{P}) &= -\sum_{j=1}^{J} \sum_{k=1}^{K_j} E[\|\hat{x}_j^{(k)} - x_j^{(k)}\|_2^2] \\ &= -\sum_{j=1}^{J} \sum_{k=1}^{K_j} \text{Tr}\left(\mathbf{W}_{j,m}^{(k)} \mathbf{Q}_{j,m}^{(k)} \mathbf{W}_{j,m}^{(k)\dagger} - 2Re\left\{ \mathbf{P}_{j,m}^{(k)\dagger} \mathbf{H}_{jj,m}^{(k)\dagger} \mathbf{W}_{j,m}^{(k)} \right\} + \mathbf{I} \right). \end{aligned} \quad (83)$$

Similar to WSR CB algorithm, the MSE objective is partially convex over $\mathbf{P}$ and efficient algorithm can be obtained using the Lagrange multipliers method. The gradient of the MSE Lagrangian function with respect to the precoding matrix of

user k in BS j can be expressed as

$$\nabla_{\mathbf{P}_{j,m}^{(k)}} \mathcal{L}(\mathbf{P}, \Lambda) = 2\mathbf{H}_{jj,m}^{(k)\dagger} \mathbf{W}_{j,m}^{(k)} - 2\left(\sum_{i=1}^{J} \sum_{l=1}^{K_i} \mathbf{H}_{ji,m}^{(l)} \mathbf{W}_{i,m}^{(l)\dagger} \mathbf{W}_{i,m}^{(l)} \mathbf{H}_{ji,m}^{(l)\dagger} \right) \mathbf{P}_{j,m}^{(k)} - 2\mathbf{\Lambda}_j \mathbf{P}_{j,m}^{(k)}. \quad (84)$$

The derivation of the gradient of the Lagrangian is shown in Appendix C.2. The resulting MSE CB precoding matrix can be expressed as

$$\mathbf{P}_{j,m}^{(k)} = \left(\sum_{i=1}^{J} \sum_{l=1}^{K_i} \mathbf{H}_{ji,m}^{(l)} \mathbf{W}_{i,m}^{(l)\dagger} \mathbf{W}_{i,m}^{(l)} \mathbf{H}_{ji,m}^{(l)\dagger} + \mathbf{\Lambda}_j \right)^{-1} \mathbf{H}_{jj,m}^{(k)\dagger} \mathbf{W}_{j,m}^{(k)}, \quad (85)$$

which is also in the form of whitened match filter equations.

Since the objective is also partially convex over $\mathbf{W}$, the receive filter can computed using the Lagrange multipliers method. The gradient of the MSE with respect to the receive filter, $\mathbf{W}_j^{(k)}$, can be expressed as

$$\nabla_{\mathbf{W}_{j,m}^{(k)}} \mathcal{L}(\mathbf{W}, \Lambda) = 2\mathbf{H}_{jj,m}^{(k)} \mathbf{P}_{j,m}^{(k)} - 2\left(\sum_{i=1}^{J} \sum_{l=1}^{K_i} \mathbf{H}_{ji,m}^{(l)} \mathbf{P}_{i,m}^{(l)} \mathbf{P}_{i,m}^{(l)\dagger} \mathbf{H}_{ji,m}^{(l)\dagger} \right) \mathbf{W}_{j,m}^{(k)} - 2\sigma_n^2 \mathbf{W}_{j,m}^{(k)}. \quad (86)$$

By setting the gradient to be zero, a close form solution for the receive filter can be formulated, which can be expressed as

$$\mathbf{W}_{j,m}^{(k)} = \left(\sum_{i=1}^{J} \sum_{l=1}^{K_i} \mathbf{H}_{ij,m}^{(k)} \mathbf{P}_{i,m}^{(l)} \mathbf{P}_{i,m}^{(l)\dagger} \mathbf{H}_{ij,m}^{(k)\dagger} + \sigma_n^2 \mathbf{I} \right)^{-1} \mathbf{H}_{jj,m}^{(k)} \mathbf{P}_{j,m}^{(k)}. \quad (87)$$

The result is identical to the MMSE receive filter, (73). The overall algorithm is shown in Table 14.

Table 14. MSE minimization CB algorithm

Algorithm MSE minimization CB algorithm

1: set $\mathbf{P}_{j,m}^{(k)}$ with initial values

2: **for** $t = 1 \cdots T_{\text{max-iteration}}$ **do**

3: compute $(\mathbf{W}_{j,m}^{(k)} | \mathbf{P}_{j,m}^{(k)}), \forall j, m, k$ using (87)

4: compute $(\mathbf{P}_{j,m}^{(k)}, \mathbf{\Lambda}_j | \mathbf{W}_{j,m}^{(k)}), \forall j, m, k$ using (85)

5: break if converged

6: **end for**

4.3.3 HSS CB Algorithm with PAPC

Use of *harmonic sum of SINRs* (HSS) as a metric for solving beamforming problem is an old concept [8]. Although harmonic sum of SINRs for multi-user multi-stream MIMO beamforming is directly intractable, equivalent transformation of the harmonic sum of SINRs can be made such that Lagrangian multipliers method can be applied to directly solve beamforming solutions [49]. It can be shown that maximizing the harmonic sum of SINR metric also yield similar precoding matrix structure as precoding matrix of maximizing WSR or minimizing MSE.

The harmonic sum of SINR metric is expressed as

$$\mathcal{U}_{\text{HSS}}(\mathbf{P}) = \frac{1}{\sum_{j=1}^{J} \sum_{k=1}^{K_j} \sum_{r=1}^{L_j^{(k)}} \frac{1}{\text{SINR}_j^{(k,r)}}}. \tag{88}$$

Solving maximizing HSS is equivalent to minimizing inverse of HSS. Inverse of HSS metric is expressed as

$$\begin{aligned} \mathcal{U}_{\text{inv-HSS}}(\mathbf{P}) &= \sum_{j=1}^{J} \sum_{k=1}^{K_j} \sum_{r=1}^{L_j^{(k)}} \frac{1}{\text{SINR}_j^{(k,r)}} \\ &= \sum_{j=1}^{J} \sum_{k=1}^{K_j} \sum_{r=1}^{L_j^{(k)}} \frac{[\mathbf{W}_j^{(k)}]_r^{\dagger} \mathbf{Q}_{j,m}^{(k)} [\mathbf{W}_{j,m}^{(k)}]_r - \left| [\mathbf{W}_{j,m}^{(k)}]_r^{\dagger} \mathbf{H}_{jj,m}^{(k)} [\mathbf{P}_{j,m}^{(k)}]_r \right|^2}{\left| [\mathbf{W}_{j,m}^{(k)}]_r^{\dagger} \mathbf{H}_{jj,m}^{(k)} [\mathbf{P}_{j,m}^{(k)}]_r \right|^2}. \end{aligned} \tag{89}$$

The inverse HSS objective can be manipulated into a partially convex form with addition of an equality constraint. (add description on how this is done) The equivalent form of the HSS optimization can be expressed as

$$\text{minimize} \quad \sum_{m=1}^{M}\sum_{j=1}^{J}\sum_{k=1}^{K_j} \text{Tr}(\mathbf{W}_{j,m}^{(k)\dagger}\mathbf{Q}_{j,m}^{(k)}\mathbf{W}_{j,m}^{(k)} - \mathbf{I}), \tag{90}$$

subject to (74a) and

$$\mathbf{I} \circ \left(\mathbf{W}_{j,m}^{(k)\dagger}\mathbf{H}_{jj,m}^{(k)}\mathbf{P}_{j,m}^{(k)}\right) = \mathbf{I}. \tag{90a}$$

The Lagrangian function of the equivalent form of HSS objective with PAPC can be expressed as

$$\begin{aligned}\mathcal{L}(\mathbf{P}, \boldsymbol{\Psi}, \boldsymbol{\Lambda}) = &\sum_{j=1}^{J}\sum_{k=1}^{K_j} \text{Tr}\left(\mathbf{W}_{j,m}^{(k)\dagger}\mathbf{Q}_{j,m}^{(k)}\mathbf{W}_{j,m}^{(k)} - \mathbf{I}\right) \\ &+ \sum_{j=1}^{J}\sum_{k=1}^{K_j} \text{Tr}\left(\boldsymbol{\Psi}_j^{(k)}\left(\mathbf{I} - \mathbf{W}_{j,m}^{(k)\dagger}\mathbf{H}_{jj,m}^{(k)}\mathbf{P}_{j,m}^{(k)}\right)\right) \\ &+ \sum_{j=1}^{J}\sum_{k=1}^{K_j} \text{Tr}\left(\mathbf{P}_{j,m}^{(k)\dagger}\boldsymbol{\Lambda}_j\mathbf{P}_{j,m}^{(k)} - \boldsymbol{\Lambda}_j\mathbf{D}_j\right),\end{aligned} \tag{91}$$

where $\boldsymbol{\Psi}_j^{(k)}$ is the dual variable associated with the equality constraint, (90a). Therefore, the gradient of the Lagrangian function can be expressed as

$$\begin{aligned}\nabla_{\mathbf{P}_{j,m}^{(k)}}\mathcal{L}(\mathbf{P}, \boldsymbol{\Psi}, \boldsymbol{\Lambda}) = &-2\mathbf{H}_{jj,m}^{(k)\dagger}\mathbf{W}_{j,m}^{(k)}\boldsymbol{\Psi}_{j,m}^{(k)\dagger} \\ &+ 2\left(\sum_{i=1}^{J}\sum_{l=1}^{K_i}\mathbf{H}_{ji,m}^{(l)}\mathbf{W}_{i,m}^{(l)\dagger}\mathbf{W}_{i,m}^{(l)}\mathbf{H}_{ji,m}^{(l)\dagger}\right)\mathbf{P}_{j,m}^{(k)} + 2\boldsymbol{\Lambda}_j\mathbf{P}_{j,m}^{(k)},\end{aligned} \tag{92}$$

where $\boldsymbol{\Psi}_j^{(k)}$ is the dual variable associated with equality condition, (90a), and it is a diagonal matrix. The derivation of the gradient of the Lagrangian is shown in Appendix C.2. It has a semi closed-form expression and can be expressed as

$$\boldsymbol{\Psi}_{j,m}^{(k)} = \left(\mathbf{I} \circ \left(\mathbf{W}_{j,m}^{(k)\dagger}\mathbf{H}_{jj,m}^{(k)}\left(\sum_{i=1}^{J}\sum_{l=1}^{K_i}\mathbf{H}_{ji,m}^{(l)}\mathbf{W}_{i,m}^{(l)\dagger}\mathbf{W}_{i,m}^{(l)}\mathbf{H}_{ji,m}^{(l)\dagger} + \boldsymbol{\Lambda}_j\right)^{-1}\mathbf{H}_{jj,m}^{(k)\dagger}\mathbf{W}_{j,m}^{(k)}\right)\right)^{-1}. \tag{93}$$

As a result of finding the zero gradient, the HSS CB precoding matrix can be expressed as

$$\mathbf{P}_{j,m}^{(k)} = \left(\sum_{i=1}^{J} \sum_{l=1}^{K_i} \mathbf{H}_{ji,m}^{(l)} \mathbf{W}_{i,m}^{(l)\dagger} \mathbf{W}_{i,m}^{(l)} \mathbf{H}_{ji,m}^{(l)\dagger} + \mathbf{\Lambda}_j \right)^{-1} \mathbf{H}_{jj,m}^{(k)\dagger} \mathbf{W}_{j,m}^{(k)} \mathbf{\Psi}_{j,m}^{(k)}. \tag{94}$$

The equivalent HSS objective, (90), is partially convex over the receive filter, $\mathbf{W}_{j,m}^{(k)}$. Therefore, the receive filter can derived by finding the zero gradient of the Lagrangian. The gradient of the Lagrangian with respect to the receive filter, $\mathbf{W}_{j,m}^{(k)}$, can be expressed as

$$\begin{aligned} \nabla_{\mathbf{W}_{j,m}^{(k)}} \mathcal{L}(\mathbf{W}, \mathbf{\Psi}, \mathbf{\Lambda}) = & -2\mathbf{H}_{jj,m}^{(k)} \mathbf{P}_{j,m}^{(k)} \hat{\mathbf{\Psi}}_{j,m}^{(k)} \\ & + 2 \left(\sum_{i=1}^{J} \sum_{l=1}^{K_i} \mathbf{H}_{ij,m}^{(k)} \mathbf{P}_{i,m}^{(l)} \mathbf{P}_{i,m}^{(l)\dagger} \mathbf{H}_{ij,m}^{(k)\dagger} \right) \mathbf{W}_{j,m}^{(k)} + 2\sigma_n^2 \mathbf{W}_{j,m}^{(k)}, \end{aligned} \tag{95}$$

By setting the gradient to be zero, a close form solution for the receive filter can be formulated, which can be expressed as

$$\mathbf{W}_{j,m}^{(k)} = \left(\sum_{i=1}^{J} \sum_{l=1}^{K_i} \mathbf{H}_{ij,m}^{(k)} \mathbf{P}_{i,m}^{(l)} \mathbf{P}_{i,m}^{(l)\dagger} \mathbf{H}_{ij,m}^{(k)\dagger} + \sigma_n^2 \mathbf{I} \right)^{-1} \mathbf{H}_{jj,m}^{(k)} \mathbf{P}_{j,m}^{(k)} \hat{\mathbf{\Psi}}_{j,m}^{(k)}, \tag{96}$$

where $\hat{\mathbf{\Psi}}_{j,m}^{(k)}$ is the dual variable associated with equality condition, (90a), and an be expressed as

$$\hat{\mathbf{\Psi}}_{j,m}^{(k)} = \left(\mathbf{I} \circ \left(\mathbf{P}_{j,m}^{(k)\dagger} \mathbf{H}_{jj,m}^{(k)\dagger} \left(\sum_{i=1}^{J} \sum_{l=1}^{K_i} \mathbf{H}_{ij,m}^{(k)} \mathbf{P}_{i,m}^{(l)} \mathbf{P}_{i,m}^{(l)\dagger} \mathbf{H}_{ij,m}^{(k)\dagger} + \sigma_n^2 \mathbf{I} \right)^{-1} \mathbf{H}_{jj,m}^{(k)} \mathbf{P}_{j,m}^{(k)} \right) \right)^{-1}. \tag{97}$$

It should be noted that the computation of $\hat{\mathbf{\Psi}}_{j,m}^{(k)}$, (97) is different from that of $\mathbf{\Psi}_{j,m}^{(k)}$, (93).

The overall algorithm is shown in Table 15.

Table 15. HSS maximization CB algorithm

Algorithm HSS maximization CB algorithm

1: set $\mathbf{P}_{j,m}^{(k)}$ with initial values

2: **for** $t = 1 \cdots T_{\text{max-iteration}}$ **do**

3: compute $(\mathbf{W}_{j,m}^{(k)} | \mathbf{P}_{j,m}^{(k)}), \forall j, m, k$ using (96)

4: compute $(\mathbf{P}_{j,m}^{(k)}, \mathbf{\Lambda}_j | \mathbf{W}_{j,m}^{(k)}), \forall j, m, k$ using (94)

5: break if converged

6: **end for**

4.3.4 Low Complexity Computation of $\mathbf{\Lambda}_j$

From the CB algorithms precoding matrix equations, (82), (85), and (94), $\mathbf{\Lambda}_j$ is the regulating variable that controls power constraints of the precoding matrix. For PBPC cases, the diagonal matrix simply becomes a scaled identity matrix as derived in [18, 73, 75]. Computing the correct $\mathbf{\Lambda}_j$ is no small feat. There are no closed-form solutions to computing $\mathbf{\Lambda}_j$. Furthermore, $\mathbf{\Lambda}_j$ is common diagonal matrix for all subcarriers and all scheduled users in OFDM transmission for a given cell, which creates issues in computing a unique solution that satisfies the power constraints taking into account he precoding matrix of all users in all subcarriers.

For most straightforward method of computing the correct $\mathbf{\Lambda}_j$ is to use *second-order cone programing* (SOCP) techniques, such as interior point methods. However, the dimension of the SOCP problem quickly becomes intractable in OFDM systems with many subcarriers and large bandwidths. Estimated computational complexity of SOCP is $\mathcal{O}(M^2 \cdot K^3 \cdot N_t^3 \cdot L^3)$ calculations per iteration of the interior point method [57]. Given that the number of users, K, and number of subcarriers, M, is expected to be huge, this method is infeasible in practice.

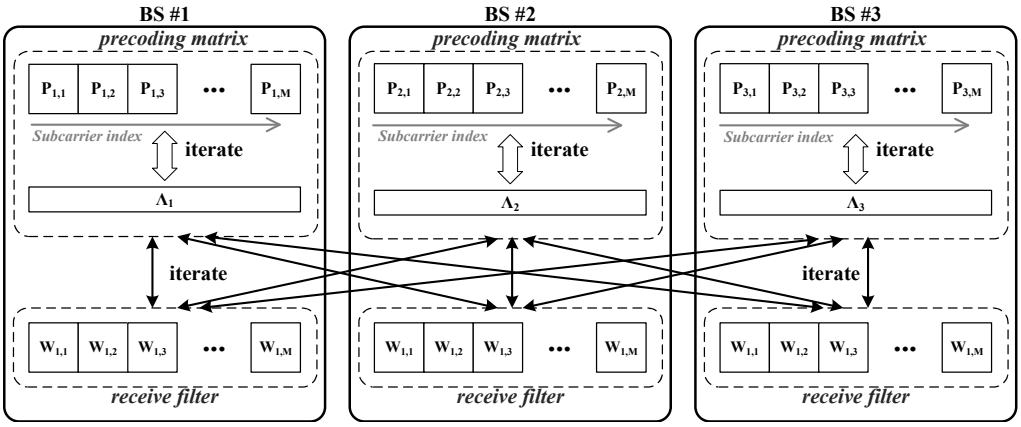

Figure 16. Conceptual diagram of proposed CB algorithm

There has been some research on developing low complexity algorithms for precoding matrix with PAPC [69, 46]. These algorithms compute the row vectors of the precoding matrix successively and iteratively. A heuristic algorithm with even lower complexity and requiring even less computational iterations is proposed. The proposed algorithm updates the all precoding matrices of all subcarriers with a common dual variable, $\mathbf{\Lambda}_j$, and scales very well for multi-carrier systems.

Let $\hat{\mathbf{D}}_j$ be the estimate of the transmit power of each antenna of BS j, and can be expressed as

$$\hat{\mathbf{D}}_j = \mathbf{I} \circ \left(\sum_{m=1}^{M} \sum_{k=1}^{K_j} \mathbf{P}_{j,m}^{(k)} \mathbf{P}_{j,m}^{(k)\dagger} \right). \tag{98}$$

The bi-section method essentially increases $\mathbf{\Lambda}_j$ if $\hat{\mathbf{D}}_j$ is too large and decreases $\mathbf{\Lambda}_j$ if $\hat{\mathbf{D}}_j$ is too small. Based on the principles of the bi-section method, the following heuristic update algorithm performs the following update,

$$\mathbf{\Lambda}_{j,(n+1)} = \mathbf{\Lambda}_{j,(n)} \cdot \left(\hat{\mathbf{D}}_j \cdot \mathbf{D}_j^{-1} \right)^{\frac{1}{2}}, \tag{99}$$

where $\mathbf{D}_j$ is the PAPC for BS j.

A conceptual diagram of the proposed algorithm is shown in Figure 16. The idea is to scale the r-th element of the diagonal matrix, $[\mathbf{\Lambda}_j]_{r,r}$, such that it grows when $[\hat{\mathbf{D}}_j]_{r,r}$ is large, and to shrink when it is small. Finally, if $\hat{\mathbf{D}}_j = \mathbf{D}_j$, $\mathbf{\Lambda}_j$ is not updated further and PAPC is met with equality.

The low-complexity alternating optimization algorithm is shown in Table 16. Although, the convergence of the low-complexity algorithm is not confirmed analytically, it has been demonstrated to converge numerically. More importantly, it provides better cell-edge user performance when the total number of iterations of the algorithm is very small, such as 4.

Table 16. Low Complex PAPC CB algorithm

Algorithm Low Complex PAPC CB algorithm

1: set $\mathbf{\Lambda}_{j,(0)}$ with initial values

2: **for** $n = 1 \cdots T_{\text{max-iteration}}$ **do**

3: compute $(\mathbf{P}_{j,m}^{(k)} | \mathbf{W}_{j,m}^{(k)}, \mathbf{\Lambda}_j), \forall j, m, k$ using (82), (85), or (94)

4: update $\mathbf{\Lambda}_{j,(n)}$ using (99)

5: break if converged

6: **end for**

4.4 Simulation Evaluation

In this section, numerical results of the proposed algorithm are presented. All simulation results are based on 3GPP simulation methodology [1]. The simulated network consists of 57 sectorized BSs with directional antennas as in Figure 10. Each BS site has 3 sectors and they are located in a hexagonal grid with geographical wrap around to mimic an infinitely large network. The distance between any two BS sites is 500 m. The maximum transmit power for a 10 MHz channel is 43 dBm, and the noise power density is -174 dBm/Hz. The directional antennas have a half-power beam-width of 70° and 17 dBi antenna gain with 20 dB front-to-back ratio. The channel is spatially uncorrelated and with flat fading, generated by complex Gaussian random variable. Pathloss model is $128.1+37.6 \log_{10}(d/1000)$, where d is the distance between the transmitter and the receiver. Users are uniformly and randomly distributed over the entire

network. The received SINR has been mapped to throughput using $\log_2(1 + \text{SINR})$. Simulation is with 2 scheduled users per BS, 2 spatial streams per user, and 4 receive antennas at each user, unless specified otherwise. The network is assumed to have full CSI of links between users and BS, which is obtained through channel reciprocity in the TDD systems, and all 57 cells are cooperating in the CB. Additionally, the maximum transmit power limit of each transmit antenna is inversely proportional to total number of transmit antennas. For example, if 8 transmit antennas is used at BS and maximum transmit power is configured to 43 dBm (i.e. 20 W), the maximum transmit power of each antenna is limited to 34 dBm (i.e 2.5 W).

4.4.1 Antenna Power Efficiency Comparison

Generally, precoding matrix for downlink signals are not computed for each subcarrier of OFDMA transmission. Applying different precoding matrix on different subcarriers changes the channel phase continuity and creates issues during channel estimation from sparsely positioned pilots within the resources allocated. Because of this, a single precoding matrix is computed and applied to a group of subcarriers, denoted as a subband. In LTE systems, precoding matrix grouping operation is known as physical resource block bundling [4]. In 10 MHz LTE system, there are 50 resource blocks and each subband is defined as three resource blocks, which results in 17 subbands. In 20 MHz LTE system, there are 100 resource blocks and each subband is defined as two resource blocks, which results in 50 subbands.

If the OFDMA systems has large number of subbands, the BS will have more flexibility in terms of adjusting the transmit power for each subband and antenna. Therefore, the BS will able to operate CB with high power efficiency. Power efficiency is defined as ratio of the power utilization of each transmit antenna with respect to maximum transmit power limit of each transmit antenna. For example, an antenna using 0.5 W of power out of 1 W will have power efficiency of 50% and antenna that

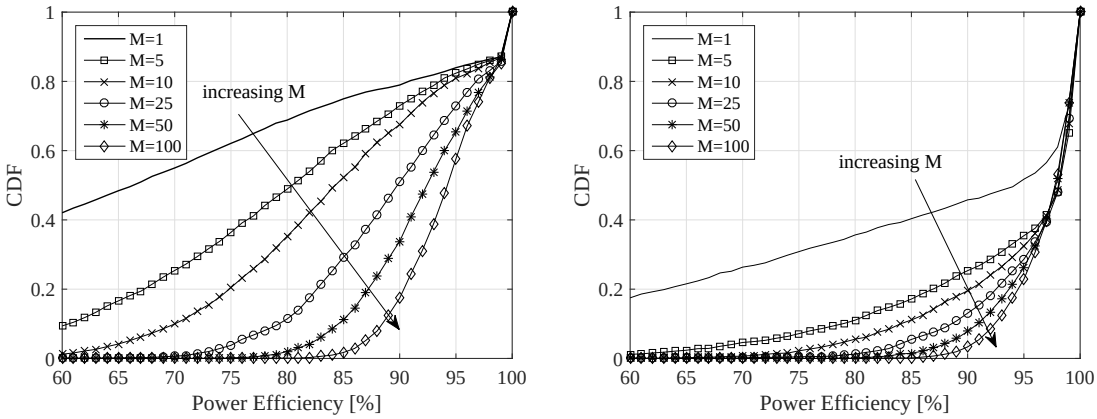

(a) CB with PBPC **(b)** CB with PAPC

Figure 17. Comparison of power efficiency vs. number of subbands between CB algorithms with PBPC and PAPC

meets PAPC with equality will have antenna power efficiency of 100 %. This can be easily verified by simulations as shown in Figure 17. Simulation for Figure 17 was conducted with 8 transmit antennas at the BS and using maximizing HSS CB algorithm algorithm with PBPC and PAPC. It shows the cumulative distribution of measured power efficiency of the transmit antenna for different number of subbands, M. Power efficiency of the the BSs increase as number of subbands increase for the proposed CB algorithm with PAPC. Power efficiency of CB algorithm that only take into account PBPC is also improved with increase in number of subbands. However, this is mainly due to the averaging of the random transmit power usage of each subband.

Opposite trend is observed when number of transmit antennas is increased. Figure 18 shows the cumulative power efficiency of CB algorithms with PBPC and PAPC for different number of transmit antennas. The number of subbands was fixed to 15. The power efficiency of CB algorithm that only consider PBPC drops significantly as number of transmit antenna increases. This is because the maximum transmit power limit for each antenna decreases for large number of antennas. For the proposed CB algorithm with PAPC, this is not the case. In fact, power efficiency is significantly

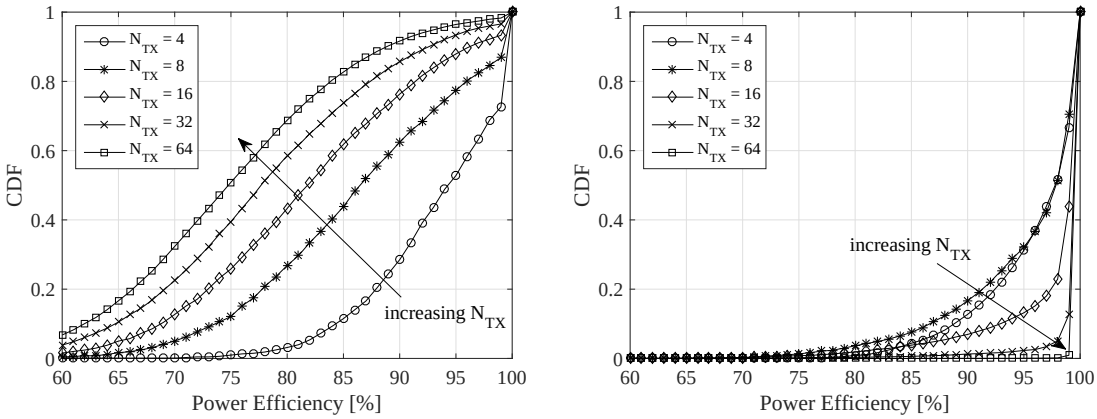

(a) CB with PBPC **(b)** CB with PAPC

Figure 18. Comparison of power efficiency vs. number transmit antennas between CB algorithms with PBPC and PAPC

improved with larger antenna arrays. As number of transmit antennas increase, more degrees of freedom for beamforming is obtained. Therefore, the proposed CB algorithm with PAPC is able to find precoding matrices that improve signal strength for intended users, decrease interference for non-intended users in other BS, and achieve higher power efficiency (i.e. higher chance of meeting PAPC with equality) with more ease.

4.4.2 User Throughput Performance Comparison

Figure 19 shows the cumulative distribution of user throughput based on proposed CB algorithms in Section 4.3. The reference throughput curves, denoted as MU BF in the figure, is multi-user MIMO beamforming algorithm without any cooperation among BSs. The simulated CB algorithm used 20 iterative computation of $\mathbf{P}_{j,m}^{(k)}$ and $\mathbf{W}_{j,m}^{(k)}$. The proposed CB algorithm improve user throughput significantly by effectively mitigating ICI. The performance improvement is greater for larger number of transmit antennas, due to larger degrees of freedom at the BS to null out interference to users. The throughput trend among proposed CB algorithm are shown to be similar.

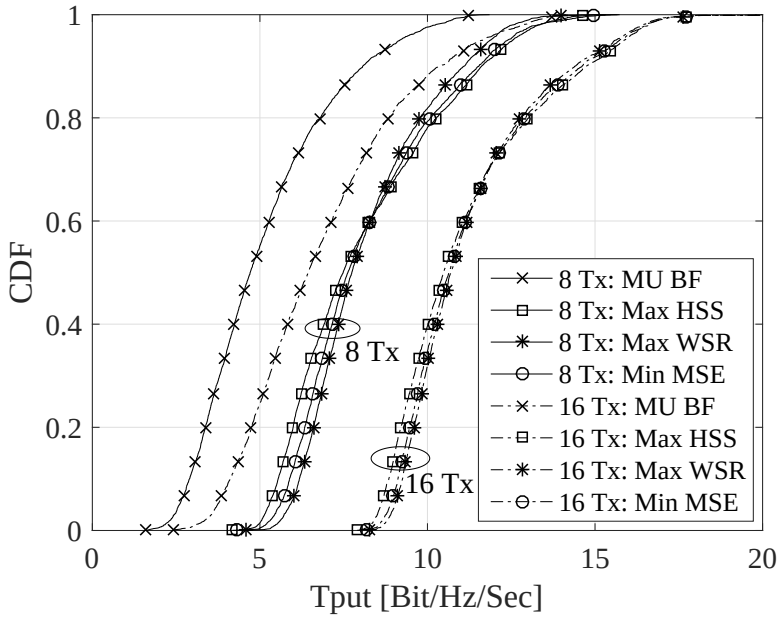

Figure 19. User throughput for the proposed CB algorithm with PAPC

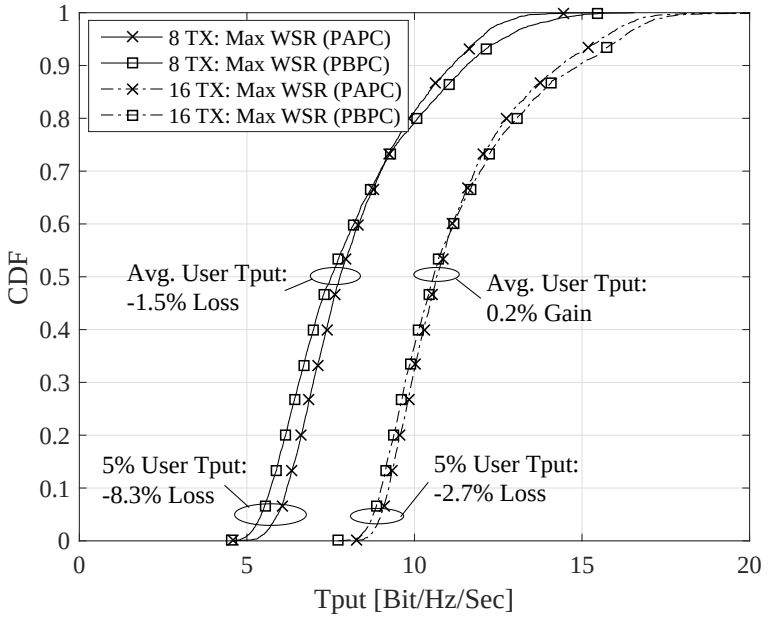

Figure 20. User throughput for the proposed CB algorithm with PAPC

Further comparison of the proposed CB algorithm against CB algorithm that only considers PBPC is shown in Figure 20. Same transmit per-antenna power limit was applied to both CB algorithm that consider PAPC and PBPC. Not considering per-antenna power limit, denoted as PBPC in Figure 20, resulted in -8.3% loss in cell-edge

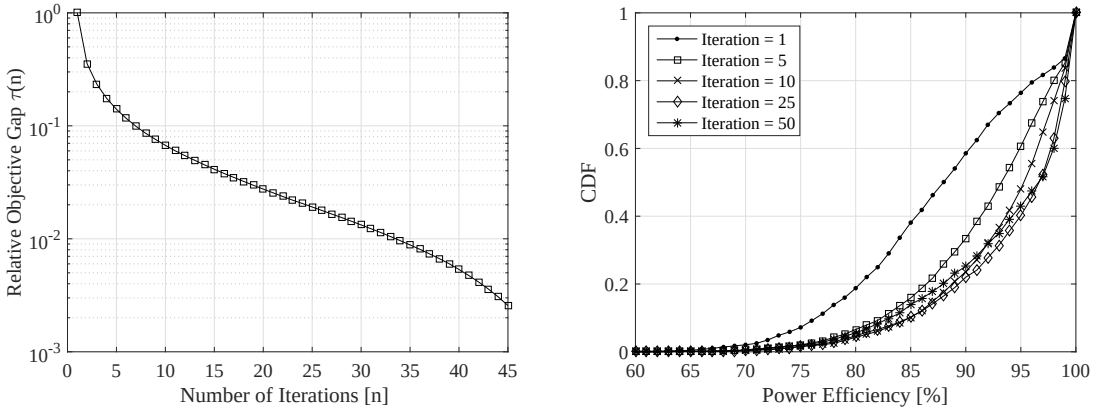

(a) Utility metric convergence **(b)** Power efficiency convergence

Figure 21. Convergence of utility metric and power efficiency with 8 Tx antennas

user throughput (i.e. 5th percentile user throughput) and -1.5% loss in average user throughput for 8 transmit antenna BS. In case of 16 transmit antenna BS, cell-edge user throughput loss was only -2.7% and average user throughput had 0.2% gain. The performance trend for other proposed CB algorithms, maximize HSS CB algorithm and minimize MSE CB algorithm, are similar to maximize WSR CB algorithm.

4.4.3 Convergence Analysis of the Proposed CB Algorithm

As shown in Figure 16, the proposed CB algorithms that take into account PAPC are dual-iterative algorithms. Precoding matrix, $\mathbf{P}_{j,m}^{(k)}$, and hypothetical receive filter, $\mathbf{W}_{j,m}^{(k)}$, are updated in the outer iteration, and per-antenna power regulating dual variable, $\mathbf{\Lambda}_j$, is iteratively updated during computation of the precoding matrix, $\mathbf{P}_{j,m}^{(k)}$. If the algorithm is slowly converging and taking many iterations to achieve appropriate performance and antenna power efficiency, it will not be practical. Therefore, convergence of the proposed algorithms are investigated.

Figure 21 and 22 shows the convergence of the utility metric and the power efficiency for maximizing HSS CB algorithm with 8 and 32 transmit antennas at the BS, respectively. The relative convergence gap, $\tau(n)$, shown in Figure 21a and 22a is

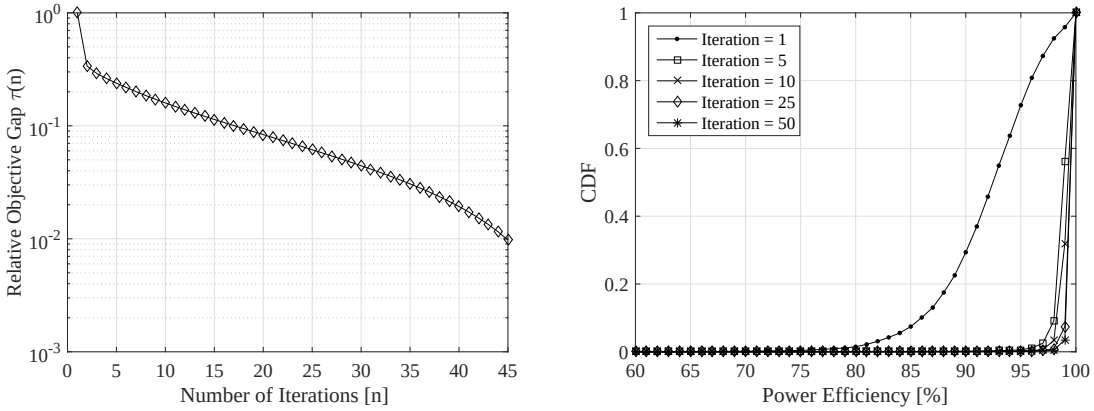

(a) Utility metric convergence **(b)** Power efficiency convergence

Figure 22. Convergence of utility metric and power efficiency with 32 Tx antennas

defined as

$$\tau(n) = \frac{f(\infty) - f(n)}{f(\infty) - f(1)}, \tag{100}$$

where $f(n)$ is the value of the utility metric at outer iteration n and $f(100)$ was used to approximate $f(\infty)$. The proposed CB algorithm converge quickly and achieves utility metric convergence with 10% of the final value in 7 and 17 iterations for 8 Tx and 32 Tx antenna cases, respectively. Power efficiency convergence is achieved even faster and only about 5 iterations is needed to get good power efficiency.

4.5 Summary and Conclusion

In this chapter, multi-carrier coordinated beamforming for wireless networks with per-antenna power constraints is investigated. Low complex iterative algorithm to enable per-antenna power constraint to CB algorithm with whitened match filter like precoding matrix structure is proposed. The main idea is to update a common antenna power regulating diagonal matrix, which is part of the precoding matrix equation, in each iteration. The algorithm can be scaled to any number of subcarriers because it only updates a common diagonal matrix for all subbands. Simulations show that proposed algorithm enables excellent antenna power efficiency with low number of iterations and converges quickly. Additionally, it can significantly mitigate ICI and

improve performance over non-coordinating system.

APPENDIX A

APPENDIX FOR CHAPTER 2

A.1 SINR Approximation for SFR Users

The approximation of the average SINR for SFR users is derived by taking the expectation of the interference plus noise power of the SINR as

$$\begin{aligned}\hat{P}_{\text{in}} &= E\left[P_{\text{in}}\right] \\ &= E\left[\sum_{i\in\mathcal{F},i\neq l}\left(\tau_{k,i}\gamma_i + (1-\tau_{k,i})\beta_i\right)P_{j,i}^{(l)} + \frac{\sigma_n^2}{N}\right].\end{aligned} \tag{101}$$

If the system is interference limited, the noise power in the SINR formulation can be ignored and the SINR expectation can be computed as

$$\hat{P}_{\text{in}} = \sum_{\substack{\forall\bar{\tau}_k \\ \tau_{k,i}\in 0,1 \\ i=1,\ldots,|\mathcal{F}|}} \sum_{i\in\mathcal{F},i\neq l}\left(\tau_{k,i}\gamma_i + (1-\tau_{k,i})\beta_i\right)P_{j,i}^{(l)} p_\tau(\bar{\tau}_k), \tag{102}$$

where $\bar{\tau}_k = (\bar{\tau}_{k,1},\ldots,\bar{\tau}_{k,|F|})$, the CEB indicator $\tau_{k,i}$ is *independent identically distributed* (i.i.d.) binary random variable with probability of $p_\tau(1) = 1/N$ and $p_\tau(0) = (N-1)/N$. (102) can be explicitly computed by using the relationship between γ_i

and β_i. The derivation is as follows;

$$\begin{aligned}
\hat{P}_{\text{in}} &= \sum_{i\in\mathcal{F},i\neq l} \sum_{\substack{\forall \bar{\tau}_k,\tau_{k,i}\in 0,1 \\ i=1,\ldots,|\mathcal{F}|}} \left(\tau_{k,i}\gamma_i + (1-\tau_{k,i})\beta_i\right) P_{j,i}^{(l)} p_\tau(\bar{\tau}_k) \\
&= \sum_{i\in\mathcal{F},i\neq l} \gamma_i P_{j,i}^{(l)} \sum_{\substack{\forall \bar{\tau}_k,\tau_{k,i}\in 0,1 \\ i=1,\ldots,|\mathcal{F}|}} \tau_{k,i} p_\tau(\bar{\tau}_k) + \sum_{i\in\mathcal{F},i\neq l} \beta_i P_{j,i}^{(l)} \sum_{\substack{\forall \bar{\tau}_k,\tau_{k,i}\in 0,1 \\ i=1,\ldots,|\mathcal{F}|}} (1-\tau_{k,i}) p_\tau(\bar{\tau}_k) \\
&= \sum_{i\in\mathcal{F},i\neq l} \left(\gamma_i P_{j,i}^{(l)} \frac{1}{N} + \beta_i P_{j,i}^{(l)} \frac{N-1}{N}\right) \\
&= \sum_{i\in\mathcal{F},i\neq l} \frac{1}{N}(\gamma_i + \beta_i(N-1)) P_{j,i}^{(l)} \\
&= \sum_{i\in\mathcal{F},i\neq l} P_{j,i}^{(l)}. \qquad (103)
\end{aligned}$$

Therefore, the SINR approximation using the approximated interference and noise power, $\hat{P}_{\text{in}}$, in the SINR formulation is expressed as

$$\begin{aligned}
\widehat{\text{SINR}'}_{k,j}^{(l)} &= \frac{\left(\delta_j\gamma_l + (1-\delta_j)\beta_l\right) P_{j,l}^{(l)}}{\hat{P}_{\text{in}}} \\
&= \frac{\left(\delta_j\gamma_l + (1-\delta_j)\beta_l\right) P_{j,l}^{(l)}}{\sum_{i\in\mathcal{F},i\neq l} P_{j,i}^{(l)}}.
\end{aligned}$$

In actual deployments, the distribution of the CEB indicator, $\bar{\tau}_k$, will not be i.i.d. binary random variable but will be configured similarly to the simulation assumption in (43). To verify the usefulness of the derived average interference power under non-i.i.d. random variable assumption, the received interference power is compuated from simulation assuming that $\bar{\tau}_k$ is configured as in (43) and configured randomly. Figure 23 shows the cumulative distribution of the interference power estimate error, where the interference power estimate error is defined as the actual interference power minus the average interference power computed by (103) and can be expressed as

$$e_{in} = \left(\sum_{i\in\mathcal{F},i\neq l} \left(\tau_{k,i}\gamma_i + (1-\tau_{k,i})\beta_i\right) P_{j,i}^{(l)} + \frac{\sigma_n^2}{N}\right) - \hat{P}_{\text{in}}. \qquad (104)$$

The dotted lines correspond to the distribution of e_{in} in dB scale when $\bar{\tau}_k$ is i.i.d random binary variable with $1/N$ probability of being 1. The solid lines correspond

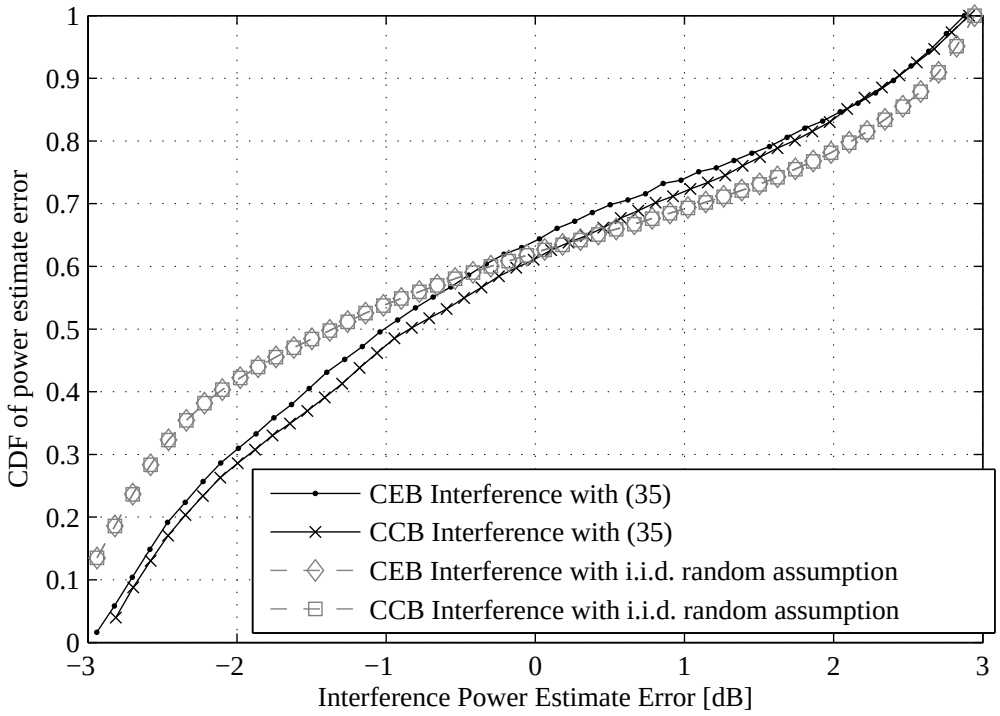

Figure 23. Cumulative distribution of interference power estimate error

to the distribution of e_{in} when $\bar{\tau}_k$ is configured as in (43). Both distributions are quite similar and have a mean of 0 dB. Therefore, the average interference power estimate derived in (103) can be used to represent the average interference power under non-i.i.d. random distribution of $\bar{\tau}_k$.

The SINR for the worst case is derived by computing the lower and upper interference bound. The lower bound corresponding to the most naive case can be derived by

$$\sum_{i\in\mathcal{F},i\neq l}\left(\tau_{k,i}\gamma_i+(1-\tau_{k,i})\beta_i\right)P_{j,i}^{(l)}\geq\sum_{i\in\mathcal{F},i\neq l}\beta_i P_{j,i}^{(l)}\geq\beta^{\min}\sum_{i\in\mathcal{F},i\neq l}P_{j,i}^{(l)}. \tag{105}$$

The upper interference bound corresponding to the most worst case can be expressed by

$$\sum_{i\in\mathcal{F},i\neq l}\left(\tau_{k,i}\gamma_i+(1-\tau_{k,i})\beta_i\right)P_{j,i}^{(l)}\leq\sum_{i\in\mathcal{F},i\neq l}\gamma_i P_{j,i}^{(l)}\leq\gamma^{\max}\sum_{i\in\mathcal{F},i\neq l}P_{j,i}^{(l)}. \tag{106}$$

This results in the lower and upper throughput bounds of the UEs in ICIC systems as

$$\begin{aligned}\widehat{\mathrm{SINR}'}_{k,j}^{\text{min-}(l)} &= \frac{\left(\delta_j\gamma_l + (1-\delta_j)\beta_l\right) P_{j,l}^{(l)}}{\gamma^{\max}\sum_{i\in\mathcal{F},i\neq l} P_{j,i}^{(l)}} \\ &= \frac{1}{\gamma^{\max}}\widehat{\mathrm{SINR}'}_{k,j}^{(l)},\end{aligned} \tag{107}$$

and

$$\begin{aligned}\widehat{\mathrm{SINR}'}_{k,j}^{\text{max-}(l)} &= \frac{\left(\delta_j\gamma_l + (1-\delta_j)\beta_l\right) P_{j,l}^{(l)}}{\beta^{\min}\sum_{i\in\mathcal{F},i\neq l} P_{j,i}^{(l)}} \\ &= \frac{1}{\beta^{\min}}\widehat{\mathrm{SINR}'}_{k,j}^{(l)},\end{aligned} \tag{108}$$

respectively.

A.2 Equivalent Transformation of Harmonic Sum Optimization Problem

Let a convex program with the harmonic sum objective function be defined as

$$\text{maximize} \quad \frac{1}{\displaystyle\sum_{j=1}^{\mathcal{J}} \frac{1}{A_j\delta_j + B_j(1-\delta_j)}}, \tag{109}$$

where A_j and B_j are constants, $\mathcal{J}$ is the number of optimization variables, and δ_j is the optimization variable confined to be defined in [0,1]. The optimization problem (109) can be rewritten by transforming it into a epigraph form. The epigraph form is expressed as

$$\text{minimize} \sum_{j\in\mathcal{J}} t_j$$

subject to

$$\frac{1}{A_j\delta_j + B_j(1-\delta_j)} \leq t_j, \tag{110a}$$

$$-t_j \leq 0 \tag{110b}$$

The constraint in (110a) is changed into a quadratic form and then into a second order conic form. Let, $z_j = A_j\delta_j + B_j(1-\delta_j)$ and $z_j \geq 0$, then the derivation is as follows:

$$\begin{aligned} 1 &\leq z_j t_j, \\ 4 &\leq 4 z_j t_j, \\ 4 + z_j^2 - 2 z_j t_j + t_j^2 &\leq z_j^2 + 2 z_j t_j + t_j^2, \\ \left\| \begin{bmatrix} 2 \\ z_j - t_j \end{bmatrix} \right\|_2 &\leq (z_j + t_j). \end{aligned}$$

Finally, the optimization program is expressed as

$$\text{minimize} \sum_{j \in \mathcal{J}} t_j,$$

subject to constraint in (110b) and

$$\left\| \begin{bmatrix} 2 \\ A_j\delta_j + B_j(1-\delta_j) - t_j \end{bmatrix} \right\|_2 \leq (A_j\delta_j + B_j(1-\delta_j) + t_j).$$

APPENDIX B

APPENDIX FOR CHAPTER 3

B.1 Solving for Optimal CB Precoding Matrices and Receive Filters

First, the Lagrangian in (58) is convex over $\mathbf{P}$ with fixed $\mathbf{W}$ and it's vice versa is shown. From $\mathbf{P}$ perspective, the Lagrangian is a quadratic function of $\mathbf{P}$ and therefore a convex function of $\mathbf{P}$. Similarly, the Lagrangian is also quadratic function of $\mathbf{W}$ and therefore a convex function of $\mathbf{W}$. It should be noted that the Lagrangian is not jointly convex over both $\mathbf{P}$ and $\mathbf{W}$.

There is only single minimum value of a convex function and it occur when partial derivative of the function is zero. As a result,

$$\frac{\partial}{\partial \mathbf{P}_j^{(k)}} L(\mathbf{P}, \mathbf{W}, \lambda, \Psi) = 0,$$

$$2\left(\sum_{i=1}^{J}\sum_{l=1}^{K_i} \mathbf{H}_{ji}^{(l)\dagger}\mathbf{W}_i^{(l)}\mathbf{W}_i^{(l)\dagger}\mathbf{H}_{ji}^{(l)}\right)\mathbf{P}_j^{(k)} + 2\lambda_j\mathbf{P}_j^{(k)} - \mathbf{H}_{jj}^{(k)\dagger}\mathbf{W}_j^{(k)}\mathbf{\Psi}_j^{(k)\dagger} = 0. \tag{112}$$

Therefore, optimal precoding matrix, $\hat{\mathbf{P}}_j^{(k)}$, is expressed as

$$\hat{\mathbf{P}}_j^{(k)} = \frac{1}{2}\left(\mathbf{R}_j^{(k)}\right)^{-1}\mathbf{H}_{jj}^{(k)\dagger}\mathbf{W}_j^{(k)}\mathbf{\Psi}_j^{(k)\dagger}, \tag{113}$$

where $\mathbf{R}_j^{(k)}$ is the uplink interference-plus-noise covariance and given as (61). The dual variables, $\mathbf{\Psi}_j^{(k)}$ and λ_j, should be configured so that it the optimal precoding matrix satisfies constraint $\sum_{k=1}^{K_j}\|\hat{\mathbf{P}}_j^{(k)}\|_F^2 \leq 1$ and $[\mathbf{W}_j^{(k)}]_r^\dagger\mathbf{H}_{jj}^{(k)}[\hat{\mathbf{P}}_j^{(k)}]_r = 1$. The optimal values of the dual variable, $\mathbf{\Psi}_j^{(k)}$, is obtained by inserting the optimal precoding matrix, $\hat{\mathbf{P}}_j^{(k)}$, into the equality constraint, which is given as

$$\mathbf{\Psi}_j^k = \left(\mathbf{I} \circ \left(\frac{1}{2}\mathbf{W}_j^{(k)\dagger}\mathbf{H}_{jj}^{(k)}(\mathbf{R}_j^{(k)})^{-1}\mathbf{H}_{jj}^{(k)\dagger}\mathbf{W}_j^{(k)}\right)\right)^{-1}. \tag{114}$$

From complementary slackness conditions, it is sufficient to find a non-zero λ_j that can satisfy $\|\hat{\mathbf{P}}_j^{(k)}\|_F^2 = 1$, which can be done using the bi-section method.

The conditions for $\mathbf{W}$ can be derived similarly and as follows:

$$\hat{\mathbf{W}}_j^{(k)} = \frac{1}{2}\left(\mathbf{Q}_j^{(k)}\right)^{-1}\mathbf{H}_{jj}^{(k)}\mathbf{P}_j^{(k)}\mathbf{\Psi}_j^{(k)\dagger}, \tag{115}$$

where $\mathbf{Q}_j^{(k)}$ is downlink interference covariance and given as (47). The dual variable, $\mathbf{\Psi}_j^{(k)}$, is given as

$$\mathbf{\Psi}_j^k = \left(\mathbf{I} \circ \left(\frac{1}{2}\mathbf{P}_j^{(k)\dagger}\mathbf{H}_{jj}^{(k)\dagger}(\mathbf{Q}_j^{(k)})^{-1}\mathbf{H}_{jj}^{(k)}\mathbf{P}_j^{(k)}\right)\right)^{-1}. \tag{116}$$

B.2 Proof of Convergence of Alternating Optimization Algorithm

Let $f(\mathbf{P}, \mathbf{W})$ be the optimization objective (57). Then for any feasible value of $\mathbf{P}$ and $\mathbf{W}$ (i.e. constraints are satisfied), the Lagrangian, $L(\mathbf{P}, \mathbf{W}, \lambda, \Psi)$, in (58) is equal to $f(\mathbf{P}, \mathbf{W})$.

Since $L(\mathbf{P}, \mathbf{W}, \lambda, \Psi)$ is convex for $\mathbf{P}$ when all other variables are fixed, a feasible optimal precoding matrix, $\mathbf{P}_{(n)}^*$, will be the minimum of the objective with respect to a given receive filter, $\mathbf{W}_{(n)}$. That is

$$L(\mathbf{P}_{(n)}^*, \mathbf{W}_{(n)}, \lambda, \Psi) = \min_{\mathbf{P}} L(\mathbf{P}, \mathbf{W}_{(n)}, \lambda, \Psi) \tag{117}$$

The same observation can be made for the receive filter, $\mathbf{W}_j^{(k)}$. That is

$$L(\mathbf{P}_{(n)}, \mathbf{W}_{(n+1)}^*, \lambda, \Psi) = \min_{\mathbf{W}} L(\mathbf{P}_{(n)}, \mathbf{W}, \lambda, \Psi). \tag{118}$$

Combining observations made in (117) and (118), the following inequality statement is made:

$$L(\mathbf{P}_{(n+1)}^*, \mathbf{W}_{(n+1)}^*, \lambda, \Psi) \leq L(\mathbf{P}_{(n)}^*, \mathbf{W}_{(n+1)}^*, \lambda, \Psi) \leq L(\mathbf{P}_{(n)}^*, \mathbf{W}_{(n)}, \lambda, \Psi). \tag{119}$$

The iteration between computing optimal precoding matrix and receive filter guarantees that the Lagrangian is always updated with equal or smaller value by (119).

The Lagrangian with any feasible value of $\mathbf{P}$ and $\mathbf{W}$ is lower bounded by zero and therefore the algorithm guarantees that the objective to converges to some limit value.

B.3 Proof of Monotonicity of $\|\mathbf{P}_j^{(k)\dagger}\|_F^2$ with Respect to λ_j

In order to prove that $\|\mathbf{P}_j^{(k)}\|_F^2 = \mathrm{Tr}(\mathbf{P}_j^{(k)\dagger}\mathbf{P}_j^{(k)})$ is monotonically decreasing as λ_j increases, the following basics are defined.

Lemma 1: Let, f_1, f_2, and g be positive valued function of λ. If f_1/g and f_2/g are monotonically decreasing function of λ, then $(f_1 + f_2)/g$ is also a monotonically decreasing function.

Proof of lemma 1 is straight forward. Summation of monotonically decreasing function is also monotonically decreasing and $\frac{f_1+f_2}{g} = \frac{f_1}{g} + \frac{f_2}{g}$.

Lemma 2: Let, f, g_1, and g_2 be positive valued function of λ. If f/g_1 and f/g_2 are monotonically decreasing function of λ, then $f/(g_1 + g_2)$ is also a monotonically decreasing function.

Proof of lemma 2 can be derived through the derivatives. Monotonically decreasing function has a strictly negative derivative. So if f/g_k is a monotonically decreasing function, then

$$\left(\frac{f}{g_k}\right)' = \frac{f'g_k - fg_k'}{g_k^2} < 0,$$

where $(\cdot)'$ is the first order derivative of the function. Since g_k^2 is always positive, $f'g_k - fg_k' < 0$. The derivative of $f/(g_1 + g_2)$ is given as

$$\begin{aligned}\left(\frac{f}{g_1+g_2}\right)' &= \frac{f'(g_1+g_2) - f(g_1' + g_2')}{(g_1+g_2)^2}, \\ &= \frac{f'g_1 - fg_1'}{(g_1+g_2)^2} + \frac{f'g_2 - fg_2'}{(g_1+g_2)^2}.\end{aligned}$$

Summation is negative functions is negative thus $\left(\frac{f}{g_1+g_2}\right)'$ is negative and $f/(g_1 + g_2)$ is a monotonically decreasing function.

Lemma 3: If f_i and g_j are positive valued functions for $i = 1 \cdots N$ and $j = 1 \cdots M$, respectively, and f_i/g_j is a monotonically decreasing function for all i and j,

then

$$\frac{\sum_{i=1}^{N} f_i}{\sum_{j=1}^{M} g_j}$$

is also a monotonically decreasing function. Proof of this can be derived from the combination of lemma 1 and 2.

Let, a_k and s_k be N non-negative values for $k = 1 \cdots N$, then

$$\frac{(s_j + \lambda)}{a_j(s_k + \lambda)} \tag{120}$$

is monotonically decreasing function of λ for $\lambda \geq 0$. This can be easily seen from the derivative of (120). (120) is manipulated into

$$\frac{(s_j + \lambda)}{a_j(s_k + \lambda)} = \frac{a_k \frac{1}{s_k+\lambda}}{a_k a_j \frac{1}{s_j+\lambda}} = \frac{a_k \frac{1}{(s_k+\lambda)^2}}{a_k a_j \frac{1}{s_j+\lambda}\frac{1}{s_k+\lambda}}.$$

Based on lemma 3, the following function is monotonically decreasing.

$$\begin{aligned} &\frac{\sum_{k=1}^{N} a_k \left(\frac{1}{s_k+\lambda}\right)^2}{\sum_{k=1}^{N}\sum_{j=1}^{N} a_k a_j \frac{1}{s_j+\lambda}\frac{1}{s_k+\lambda}}, \\ &= \frac{\sum_{k=1}^{N} a_k \frac{1}{(s_k+\lambda)^2}}{\left(\sum_{k=1}^{N} a_k \frac{1}{s_k+\lambda}\right)^2} \end{aligned} \tag{121}$$

Next, $\mathrm{Tr}(\mathbf{P}_j^{(k)\dagger}\mathbf{P}_j^{(k)})$, which is equal to square Frobenius norm of precoding matrix, $\mathbf{P}_j^{(k)}$, is shown to be equivalent to a function form of (121). Since, interference-plus-noise covariance is summation of semi-positive definite matrices, it is semi-positive definite. Therefore the uplink interference-plus-noise covariance, $\mathbf{R}_j^{(k)}$, can be decomposed into

$$\begin{aligned} \mathbf{R}_j^{(k)} &= \sum_{i=1}^{J}\sum_{l=1}^{K_i} \mathbf{H}_{ji}^{(l)\dagger}\mathbf{W}_i^{(l)}\mathbf{W}_i^{(l)\dagger}\mathbf{H}_{ji}^{(l)} + \lambda_j\mathbf{I} \\ &= \mathbf{U}(\mathbf{S} + \lambda_j\mathbf{I})\mathbf{U}^\dagger, \end{aligned} \tag{122}$$

where $\mathbf{U}$ is an unitary matrix and $\mathbf{S}$ is a diagonal matrix. The derivation can be

shown using the decomposition from above, and expressed as

$$\begin{aligned}
&\mathbf{W}_j^{(k)\dagger}\mathbf{H}_{jj}^{(k)}(\mathbf{U}(\mathbf{S}+\lambda_j\mathbf{I})\mathbf{U}^\dagger)^{-2}\mathbf{H}_{ij}^{(k)\dagger}\mathbf{W}_j^{(k)},\\
&=\mathbf{W}_j^{(k)\dagger}\mathbf{H}_{ij}^{(k)}\mathbf{U}(\mathbf{S}+\lambda_j\mathbf{I})^{-2}\mathbf{U}^\dagger\mathbf{H}_{ij}^{(k)\dagger}\mathbf{W}_j^{(k)},\\
&=\mathbf{T}^\dagger(\mathbf{S}+\lambda_j^k\mathbf{I})^{-2}\mathbf{T},
\end{aligned}$$

where n is any arbitrary integer and $\mathbf{T}=\mathbf{U}^\dagger\mathbf{H}_{ij}^{(k)\dagger}\mathbf{W}_j^{(k)}$.

With the result above, the Frobenius norm of the precoding matrix can be expressed as

$$\begin{aligned}
&\mathrm{Tr}(\hat{\mathbf{P}}_j^{(k)\dagger}\hat{\mathbf{P}}_j^{(k)})\\
&=\frac{1}{4}\mathrm{Tr}\left(\mathbf{\Psi}_j^{(k)}\mathbf{W}_j^{(k)\dagger}\mathbf{H}_{jj}^{(k)}(\mathbf{R}_j^{(k)})^{-2}\mathbf{H}_{jj}^{(k)\dagger}\mathbf{W}_j^{(k)}\mathbf{\Psi}_j^{k\dagger}\right),\\
&=\frac{1}{4}\mathrm{Tr}\left((\mathbf{\Psi}_j^{(k)})^2\mathbf{T}^\dagger(\mathbf{S}+\lambda_j\mathbf{I})^{-2}\mathbf{T}\right),\\
&=\frac{1}{4}\sum_{r=1}^{L_j^{(k)}}\psi_{jkr}^2[\mathbf{T}]_r^\dagger(\mathbf{S}+\lambda_j\mathbf{I})^{-2}[\mathbf{T}]_r,\\
&=\frac{1}{4}\sum_{r=1}^{L_j^{(k)}}\psi_{jkr}^2\sum_{m=1}^{M}|t_{rm}|^2\frac{1}{(s_m+\lambda_j^k)^2},
\end{aligned}$$

where $\mathrm{Tr}(\cdot)$ is the trace of the matrix, t_{rm} is the m-th element of the vector $[\mathbf{T}]_r$, s_m is the m-th diagonal elements of $\mathbf{S}$, and ψ_{jkr}^2 is the r-th diagonal element of $(\mathbf{\Psi}_j^{(k)})^2$, which can be expressed as

$$\begin{aligned}
(\mathbf{\Psi}_j^{(k)})^2&=\left(\mathbf{I}\circ\left(\frac{1}{2}\mathbf{W}_j^{(k)\dagger}\mathbf{H}_{ij}^{(k)}(\mathbf{R}_j^{(k)})^{-1}\mathbf{H}_{ij}^{(k)\dagger}\mathbf{W}_j^{(k)}\right)\right)^{-2},\\
&=\left(\mathbf{I}\circ\left(\frac{1}{2}\mathbf{T}^\dagger(\mathbf{S}+\lambda_j\mathbf{I})^{-1}\mathbf{T}\right)\right)^{-2}.
\end{aligned}$$

Therefore, $\psi_{jkr}=2([\mathbf{T}]_r^\dagger(\mathbf{S}+\lambda_j\mathbf{I})^{-1}[\mathbf{T}]_r)^{-1}$ and $\mathrm{Tr}(\hat{\mathbf{P}}_j^{(k)\dagger}\hat{\mathbf{P}}_j^{(k)})$ can be shown as

$$\mathrm{Tr}(\hat{\mathbf{P}}_j^{(k)\dagger}\hat{\mathbf{P}}_j^{(k)})=\sum_{r=1}^{L_j^{(k)}}\frac{\sum_{m=1}^{M}|t_{rm}|^2\frac{1}{(s_m+\lambda_j)^2}}{\left(\sum_{m=1}^{M}|t_{rm}|^2\frac{1}{(s_m+\lambda_j)}\right)^2}. \tag{123}$$

$\|\hat{\mathbf{P}}_j^{(k)}\|_F^2$ is proven to be a monotonically decreasing function of λ_j because (123) is summation of monotonically decreasing functions, (121).

APPENDIX C

APPENDIX FOR CHAPTER 4

C.1 Derivation of the Gradient of WSR metric

The derivation of the gradient of the WSR metric can be found based on the results in [18]. Using the determinant gradient properties, $\nabla_{\mathbf{X}} \log|\mathbf{X}| = \mathrm{Tr}(\mathbf{X}^{-1}\nabla_{\mathbf{X}}\mathbf{X})$, the gradient of the sum-rate, $r_{j,m}^{(k)}$, with respect to the (u,v) element of the precoding matrix, $[\mathbf{P}_{j,m}^{(k)}]_{u,v}$, can be expressed as

$$\begin{aligned}
\nabla_{[\mathbf{P}_{j,m}^{(k)}]_{u,v}} \log\left|(\mathbf{E}_{j,m}^{(k)})^{-1}\right| &= \mathrm{Tr}\left(\mathbf{E}_{j,m}^{(k)}\nabla_{[\mathbf{P}_{j,m}^{(k)}]_{u,v}}(\mathbf{E}_{j,m}^{(k)})^{-1}\right) \\
&= 2\mathrm{Tr}\left(\mathbf{E}_{j,m}^{(k)}\mathbf{J}_{u,v}\mathbf{H}_{jj,m}^{(k)\dagger}(\tilde{\mathbf{Q}}_{j,m}^{(k)})^{-1}\mathbf{H}_{jj,m}^{(k)}\mathbf{P}_{j,m}^{(k)}\right), \\
&= 2\mathrm{Tr}\left(\mathbf{J}_{u,v}\mathbf{H}_{jj,m}^{(k)\dagger}(\tilde{\mathbf{Q}}_{j,m}^{(k)})^{-1}\mathbf{H}_{jj,m}^{(k)}\mathbf{P}_{j,m}^{(k)}\mathbf{E}_{j,m}^{(k)}\right), \\
&= 2\left[\mathbf{H}_{jj,m}^{(k)\dagger}(\tilde{\mathbf{Q}}_{j,m}^{(k)})^{-1}\mathbf{H}_{jj,m}^{(k)}\mathbf{P}_{j,m}^{(k)}\mathbf{E}_{j,m}^{(k)}\right]_{u,v}, \qquad (124)
\end{aligned}$$

where $\mathbf{J}_{u,v}$ is a single-entry matrix with one at element in (u,v) and zero elsewhere. Therefore, gradient of the sum-rate with respect to the precoding matrix can be expressed as

$$\nabla_{\mathbf{P}_{j,m}^{(k)}} \log\left|(\mathbf{E}_{j,m}^{(k)})^{-1}\right| = 2\mathbf{H}_{jj,m}^{(k)\dagger}(\tilde{\mathbf{Q}}_{j,m}^{(k)})^{-1}\mathbf{H}_{jj,m}^{(k)}\mathbf{P}_{j,m}^{(k)}\mathbf{E}_{j,m}^{(k)}. \qquad (125)$$

It should be noted that $(\tilde{\mathbf{Q}}_{j,m}^{(k)})^{-1}\mathbf{H}_{jj,m}^{(k)}\mathbf{P}_{j,m}^{(k)}$ is equal to the MMSE receive filter, $\mathbf{W}_{j,m}^{(k)}$. Therefore, the expression can be further simplified and the gradient of the rate for user k in BS j with respect to the precoding matrix, $\mathbf{P}_{j,m}^{(k)}$ can be expressed as

$$\nabla_{\mathbf{P}_{j,m}^{(k)}} \log\left|(\mathbf{E}_{j,m}^{(k)})^{-1}\right| = 2\mathbf{H}_{jj,m}^{(k)\dagger}\mathbf{W}_{j,m}^{(k)}\mathbf{E}_{j,m}^{(k)}. \qquad (126)$$

The gradient of the rate for user l in BS i, $r_{i,m}^{(l)}$, with respect to the (u,v) element

of the precoding matrix, $[\mathbf{P}_{j,m}^{(k)}]_{u,v}$, can be expressed as

$$\begin{aligned}
&\nabla_{[\mathbf{P}_{j,m}^{(k)}]_{u,v}} \log \left|(\mathbf{E}_{i,m}^{(l)})^{-1}\right| \\
&= \mathrm{Tr}\left(\mathbf{E}_{i,m}^{(l)} \nabla_{[\mathbf{P}_{j,m}^{(k)}]_{u,v}} (\mathbf{E}_{i,m}^{(l)})^{-1}\right) \\
&= \mathrm{Tr}\left(\mathbf{E}_{j,m}^{(k)} \nabla_{[\mathbf{P}_{j,m}^{(k)}]_{u,v}} \left(\mathbf{I} + \mathbf{P}_{i,m}^{(l)\dagger} \mathbf{H}_{ii,m}^{(l)\dagger} (\tilde{\mathbf{Q}}_{i,m}^{(l)})^{-1} \mathbf{H}_{ii,m}^{(l)} \mathbf{P}_{i,m}^{(l)}\right)\right).
\end{aligned} \tag{127}$$

The gradient of $\mathbf{P}_{i,m}^{(l)\dagger} \mathbf{H}_{ii,m}^{(l)\dagger} (\tilde{\mathbf{Q}}_{i,m}^{(l)})^{-1} \mathbf{H}_{ii,m}^{(l)} \mathbf{P}_{i,m}^{(l)}$ can be obtained using the matrix inverse gradient property, $\nabla_x \mathbf{Y}^{-1} = -\mathbf{Y}^{-1} \cdot \nabla_x \mathbf{Y} \cdot \mathbf{Y}^{-1}$, in [68], and the gradient of the sum-rate can be further simplified as

$$\begin{aligned}
&\nabla_{[\mathbf{P}_{j,m}^{(k)}]_{u,v}} \log \left|(\mathbf{E}_{i,m}^{(l)})^{-1}\right| \\
&= \mathrm{Tr}\left(\mathbf{E}_{j,m}^{(k)} \nabla_{[\mathbf{P}_{j,m}^{(k)}]_{u,v}} \left(\mathbf{I} + \mathbf{P}_{i,m}^{(l)\dagger} \mathbf{H}_{ii,m}^{(l)\dagger} (\tilde{\mathbf{Q}}_{i,m}^{(l)})^{-1} \mathbf{H}_{ii,m}^{(l)} \mathbf{P}_{i,m}^{(l)}\right)\right) \\
&= -\mathrm{Tr}\left(\mathbf{E}_{i,m}^{(l)} \mathbf{P}_{i,m}^{(l)\dagger} \mathbf{H}_{ii,m}^{(l)\dagger} (\tilde{\mathbf{Q}}_{i,m}^{(l)})^{-1} \left(\nabla_{[\mathbf{P}_{j,m}^{(k)}]_{u,v}} (\tilde{\mathbf{Q}}_{i,m}^{(l)})\right) (\tilde{\mathbf{Q}}_{i,m}^{(l)})^{-1} \mathbf{H}_{ii,m}^{(l)} \mathbf{P}_{i,m}^{(l)}\right) \\
&= -2\mathrm{Tr}\left(\mathbf{E}_{i,m}^{(l)} \mathbf{P}_{i,m}^{(l)\dagger} \mathbf{H}_{ii,m}^{(l)\dagger} (\tilde{\mathbf{Q}}_{i,m}^{(l)})^{-1} \left(\mathbf{H}_{ji,m}^{(l)} \mathbf{P}_{j,m}^{(k)} \mathbf{J}_{u,v} \mathbf{H}_{ji,m}^{(l)\dagger}\right) (\tilde{\mathbf{Q}}_{i,m}^{(l)})^{-1} \mathbf{H}_{ii,m}^{(l)} \mathbf{P}_{i,m}^{(l)}\right) \\
&= -2\mathrm{Tr}\left(\mathbf{J}_{u,v} \mathbf{H}_{ji,m}^{(l)\dagger} (\tilde{\mathbf{Q}}_{i,m}^{(l)})^{-1} \mathbf{H}_{ii,m}^{(l)} \mathbf{P}_{i,m}^{(l)} \mathbf{E}_{i,m}^{(l)} \mathbf{P}_{i,m}^{(l)\dagger} \mathbf{H}_{ii,m}^{(l)\dagger} (\tilde{\mathbf{Q}}_{i,m}^{(l)})^{-1} \mathbf{H}_{ji,m}^{(l)} \mathbf{P}_{j,m}^{(k)}\right) \\
&= -2\left[\mathbf{H}_{ji,m}^{(l)\dagger} (\tilde{\mathbf{Q}}_{i,m}^{(l)})^{-1} \mathbf{H}_{ii,m}^{(l)} \mathbf{P}_{i,m}^{(l)} \mathbf{E}_{j,m}^{(k)} \mathbf{P}_{i,m}^{(l)\dagger} \mathbf{H}_{ii,m}^{(l)\dagger} (\tilde{\mathbf{Q}}_{i,m}^{(l)})^{-1} \mathbf{H}_{ji,m}^{(l)} \mathbf{P}_{j,m}^{(k)}\right]_{u,v} \\
&= -2\left[\mathbf{H}_{ji,m}^{(l)\dagger} \mathbf{W}_{i,m}^{(l)} \mathbf{E}_{i,m}^{(l)} \mathbf{W}_{i,m}^{(l)\dagger} \mathbf{H}_{ji,m}^{(l)} \mathbf{P}_{j,m}^{(k)}\right]_{u,v}.
\end{aligned} \tag{128}$$

Therefore, gradient of the rate for user l in BS i with respect to the precoding matrix, $\mathbf{P}_{j,m}^{(k)}$ can be expressed as

$$\nabla_{\mathbf{P}_{j,m}^{(k)}} \log \left|(\mathbf{E}_{i,m}^{(l)})^{-1}\right| = -2\mathbf{H}_{ji,m}^{(l)\dagger} \mathbf{W}_{i,m}^{(l)} \mathbf{E}_{i,m}^{(l)} \mathbf{W}_{i,m}^{(l)\dagger} \mathbf{H}_{ji,m}^{(l)} \mathbf{P}_{j,m}^{(k)}. \tag{129}$$

Putting together the results in (126) and (129), the gradient of the weighted sum-rate

Lagrangian is expressed as

$$\begin{aligned}
&\nabla_{\mathbf{P}_{j,m}^{(k)}} \mathcal{L}(\mathbf{P}, \mathbf{\Lambda}) \\
&= \nabla_{\mathbf{P}_{j,m}^{(k)}} \sum_{j=1}^{J} \sum_{k=1}^{K_j} \sum_{m=1}^{M} \mu_j^{(k)} \log \left| (\mathbf{E}_{j,m}^{(k)})^{-1} \right| + \mathrm{Tr}\left(\mathbf{\Lambda}_j \mathbf{D}_j - \mathbf{P}_{j,m}^{(k)\dagger} \mathbf{\Lambda}_j \mathbf{P}_{j,m}^{(k)} \right) \\
&= 2\mathbf{H}_{jj,m}^{(k)\dagger} \mathbf{W}_{j,m}^{(k)} \mathbf{E}_{j,m}^{(k)} \mu_j^{(k)} - 2 \sum_{\substack{i=1 \\ (i,l) \neq (j,k)}}^{J} \sum_{l=1}^{K_i} \mu_i^{(l)} \mathbf{H}_{ji,m}^{(l)} \mathbf{W}_{i,m}^{(l)\dagger} \mathbf{E}_{i,m}^{(l)} \mathbf{W}_{i,m}^{(l)} \mathbf{H}_{ji,m}^{(l)\dagger} \mathbf{P}_{j,m}^{(k)} \\
&- 2\mathbf{\Lambda}_j \mathbf{P}_{j,m}^{(k)}.
\end{aligned} \tag{130}$$

C.2 Derivation of the Gradient of MSE and HSS metric

The gradient of the MSE and HSS metric can be found by using the gradient trace property, $\nabla \mathrm{Tr}(\mathbf{X}^\dagger \mathbf{A} \mathbf{X}) = 2\mathbf{A}\mathbf{X}$. The gradient of the total received covariance can be expressed as

$$\begin{aligned}
&\nabla_{\mathbf{P}_{j,m}^{(k)}} \sum_{j=1}^{J} \sum_{k=1}^{K_j} \mathrm{Tr}\left(\mathbf{W}_{j,m}^{(k)} \mathbf{Q}_{j,m}^{(k)} \mathbf{W}_{j,m}^{(k)\dagger} \right) \\
&= \nabla_{\mathbf{P}_{j,m}^{(k)}} \sum_{j=1}^{J} \sum_{k=1}^{K_j} \sum_{i=1}^{J} \sum_{l=1}^{K_i} \mathrm{Tr}\left(\mathbf{W}_{j,m}^{(k)} \mathbf{H}_{ij,m}^{(k)} \mathbf{P}_{i,m}^{(l)} \mathbf{P}_{i,m}^{(l)\dagger} \mathbf{H}_{ij,m}^{(k)} \mathbf{W}_{j,m}^{(k)\dagger} \right) \\
&+ \nabla_{\mathbf{P}_{j,m}^{(k)}} \sum_{j=1}^{J} \sum_{k=1}^{K_j} \mathrm{Tr}\left(\sigma_n^2 \mathbf{W}_{j,m}^{(k)} \mathbf{W}_{j,m}^{(k)\dagger} \right) \\
&= \nabla_{\mathbf{P}_{j,m}^{(k)}} \sum_{j=1}^{J} \sum_{k=1}^{K_j} \sum_{i=1}^{J} \sum_{l=1}^{K_i} \mathrm{Tr}\left(\mathbf{P}_{i,m}^{(l)\dagger} \mathbf{H}_{ij,m}^{(k)} \mathbf{W}_{j,m}^{(k)\dagger} \mathbf{W}_{j,m}^{(k)} \mathbf{H}_{ij,m}^{(k)} \mathbf{P}_{i,m}^{(l)} \right) \\
&= \nabla_{\mathbf{P}_{j,m}^{(k)}} \sum_{i=1}^{J} \sum_{l=1}^{K_i} \sum_{j=1}^{J} \sum_{k=1}^{K_j} \mathrm{Tr}\left(\mathbf{P}_{j,m}^{(k)\dagger} \mathbf{H}_{ji,m}^{(l)} \mathbf{W}_{i,m}^{(l)\dagger} \mathbf{W}_{i,m}^{(l)} \mathbf{H}_{ji,m}^{(l)} \mathbf{P}_{j,m}^{(k)} \right) \\
&= 2 \sum_{i=1}^{J} \sum_{l=1}^{K_i} \mathbf{H}_{ji,m}^{(l)} \mathbf{W}_{i,m}^{(l)\dagger} \mathbf{W}_{i,m}^{(l)} \mathbf{H}_{ji,m}^{(l)} \mathbf{P}_{j,m}^{(k)}
\end{aligned} \tag{131}$$

Based on the results in (131), the gradient of the MSE Lagrangian is expressed as

$$\begin{aligned}
&\nabla_{\mathbf{P}_{j,m}^{(k)}} \mathcal{L}(\mathbf{P}, \Lambda) \\
&= -\nabla_{\mathbf{P}_{j,m}^{(k)}} \sum_{j=1}^{J} \sum_{k=1}^{K_j} \mathrm{Tr}\left(\mathbf{W}_{j,m}^{(k)} \mathbf{Q}_{j,m}^{(k)} \mathbf{W}_{j,m}^{(k)\dagger}\right) + 2\nabla_{\mathbf{P}_{j,m}^{(k)}} Re\left\{\mathbf{P}_{j,m}^{(k)\dagger} \mathbf{H}_{jj,m}^{(k)\dagger} \mathbf{W}_{j,m}^{(k)}\right\} \\
&- \nabla_{\mathbf{P}_{j,m}^{(k)}} \mathrm{Tr}\left(\mathbf{P}_{j,m}^{(k)\dagger} \mathbf{\Lambda}_j \mathbf{P}_{j,m}^{(k)} - \mathbf{\Lambda}_j \mathbf{D}_j\right) \\
&= -2 \sum_{i=1}^{J} \sum_{l=1}^{K_i} \mathbf{H}_{ji,m}^{(l)} \mathbf{W}_{i,m}^{(l)\dagger} \mathbf{W}_{i,m}^{(l)} \mathbf{H}_{ji,m}^{(l)} \mathbf{P}_{j,m}^{(k)} + 2\mathbf{H}_{jj,m}^{(k)\dagger} \mathbf{W}_{j,m}^{(k)} - 2\mathbf{\Lambda}_j \mathbf{P}_{j,m}^{(k)}, \qquad (132)
\end{aligned}$$

and the gradient of HSS Lagrangian as

$$\begin{aligned}
&\nabla_{\mathbf{P}_{j,m}^{(k)}} \mathcal{L}(\mathbf{P}, \mathbf{\Psi}, \mathbf{\Lambda}) \\
&= \nabla_{\mathbf{P}_{j,m}^{(k)}} \sum_{j=1}^{J} \sum_{k=1}^{K_j} \mathrm{Tr}\left(\mathbf{W}_{j,m}^{(k)} \mathbf{Q}_{j,m}^{(k)} \mathbf{W}_{j,m}^{(k)\dagger} - \mathbf{I}\right) \\
&- 2\nabla_{\mathbf{P}_{j,m}^{(k)}} \mathrm{Tr}\left(\mathbf{\Psi}_j^{(k)} - \mathbf{\Psi}_j^{(k)} \mathbf{W}_{j,m}^{(k)\dagger} \mathbf{H}_{jj,m}^{(k)} \mathbf{P}_{j,m}^{(k)}\right) + \nabla_{\mathbf{P}_{j,m}^{(k)}} \mathrm{Tr}\left(\mathbf{P}_{j,m}^{(k)\dagger} \mathbf{\Lambda}_j \mathbf{P}_{j,m}^{(k)} - \mathbf{\Lambda}_j \mathbf{D}_j\right) \\
&= 2 \sum_{i=1}^{J} \sum_{l=1}^{K_i} \mathbf{H}_{ji,m}^{(l)} \mathbf{W}_{i,m}^{(l)\dagger} \mathbf{W}_{i,m}^{(l)} \mathbf{H}_{ji,m}^{(l)} \mathbf{P}_{j,m}^{(k)} - 2\mathbf{H}_{jj,m}^{(k)\dagger} \mathbf{W}_{j,m}^{(k)} \mathbf{\Psi}_j^{(k)\dagger} + 2\mathbf{\Lambda}_j \mathbf{P}_{j,m}^{(k)}. \qquad (133)
\end{aligned}$$

REFERENCES

[1] 3GPP, "TR25.814 Physical layer aspects for evolved Universal Terrestrial Radio Access (UTRA)," v 7.1.0, 3GPP, Sophia Antipolis, France, Sept. 2006.

[2] 3GPP, "TS36.331 evolved universal terrestrial radio access (E-UTRA); radio resource control (RRC)," v 8.6.0, Sophia Antipolis, France, June 2009.

[3] 3GPP, "TS36.214 Evolved Universal Terrestrial Radio Access (E-UTRA); Physical layer; Measurements," v 10.1.0, Sophia Antipolis, France, Mar. 2011.

[4] 3GPP, "TS36.213 Evolved Universal Terrestrial Radio Access (E-UTRA); Physical layer procedures," v 12.3.0, 3GPP, Sophia Antipolis, France, Sept. 2014.

[5] Ali, S. H. and Leung, V. C. M., "Dynamic frequency allocation in fractional frequency reused OFDMA networks," *IEEE Trans. Wireless Commun.*, vol. 8, pp. 4286–4295, Aug. 2009.

[6] Assaad, M., "Optimal fractional frequency reuse (FFR) in multicellular OFDMA system," in *Veh. Tech. Conf. (VTC), IEEE 68th*, pp. 1–5, Sept. 2008.

[7] Avidor, D., Mukherjee, S., Ling, J., and Papadias, C., "On some properties of the proportional fair scheduling policy," in *Personal, Indoor and Mobile Radio Commun., (PIMRC), IEEE 15th Int. Symp. on*, vol. 2, pp. 853–858, 2004.

[8] Bengtsson, M. and Ottersten, B., "Optimal and suboptimal transmit beamforming," in *Handbook of Antennas in Wireless Communications* (Godar, L. C., ed.), Roca Ranton, Florida: CRC Press, 2001.

[9] Bjornson, E., Kountouris, M., Bengtsson, M., and Ottersten, B., "Receive combining vs. multi-stream multiplexing in downlink systems with multi-antenna users," *IEEE Trans. Signal Process.*, vol. 61, p. 34313446, July 2013.

[10] Boccardi, F. and Huang, H., "Zero-Forcing Precoding for the MIMO Broadcast Channel under Per-Antenna Power Constraints," in *Signal Process. Advances in Wireless Commun., IEEE 7th Workshop on*, pp. 1–5, July 2006.

[11] Bogale, T. E. and Vandendorpe, L., "Weighted sum rate optimization for downlink multiuser MIMO systems with per antenna power constraint: Downlink-uplink duality approach," in *Acoustics, Speech and Signal Processing (ICASSP), IEEE Int. conf. on*, pp. 3245–3248, Mar. 2012.

[12] Bohge, M., Gross, J., and Wolisz, A., "Optimal power masking in soft frequency reuse based OFDMA networks," in *European Wireless Conf.*, pp. 162–166, 2009.

[13] Boyd, S. and Vandenberghe, L., *Convex Optimization*. Cambridge University Press, 2004.

[14] Cai, D. W. H., Quek, T. Q. S., Tan, C. W., and Low, S. H., "Max-min SINR coordinated multipoint downlink transmissionduality and algorithms," *IEEE Trans. Signal Process.*, vol. 60, pp. 5384–5395, Oct. 2012.

[15] Chang, R. Y., Tao, Z., Zhang, J., and Kuo, C.-C. J., "Multicell OFDMA downlink resource allocation using a graphic framework," *IEEE Trans. Veh. Technol.*, vol. 58, pp. 3494–3507, Sept. 2009.

[16] Chen, L. and Yuan, D., "Soft frequency reuse in large networks with irregular cell pattern: How much gain to expect?," in *20th IEEE International Symp. on Personal, Indoor and Mobile Radio Commun.*, pp. 1467–1471, 2009.

[17] Cheng, P., Tao, M., and Zhang, W., "A new SLNR-based linear precoding for downlink multi-user multi-stream MIMO systems," *IEEE Commun. Lett.*, vol. 14, pp. 1008–1010, Nov. 2010.

[18] Christensen, S., Agarwal, R., Carvalho, E., and Cioffi, J., "Weighted sum-rate maximization using weighted MMSE for MIMO-BC beamforming design," *IEEE Trans. Wireless Commun.*, vol. 7, pp. 4792–4799, Dec. 2008.

[19] Codreanu, M., Tolli, A., Juntti, M., and Latva-aho, M., "Mimo downlink weighted sum rate maximization with power constraints per antenna groups," in *Vehicular Technology Conference, 2007. VTC2007-Spring. IEEE 65th*, pp. 2048–2052, April 2007.

[20] Daewon Lee; Li, G. S. T., "Intercell interference coordination for LTE systems," *IEEE Trans. Veh. Commun.*, vol. 62, pp. 4408–4420, Nov. 2013.

[21] Dahrouj, H. and Yu, W., "Coordinated beamforming for the multicell multi-antenna wireless system," *IEEE Trans. Wireless Commun.*, vol. 9, pp. 1748–1759, May 2010.

[22] Ding, M., Zhang, M., Luo, H., and Chen, W., "Leakage-Based Robust Beamforming for Multi-Antenna Broadcast System with Per-Antenna Power Constraints and Quantized CDI," *IEEE Trans. Signal Process.*, vol. 61, pp. 5181–5192, Nov. 2013.

[23] Escudero Garzas, J. J., Hong, M., Garcia, A., and Garcia-Armada, A., "Interference Pricing Mechanism for Downlink Multicell Coordinated Beamforming," *IEEE Trans. Commun.*, vol. 62, pp. 1871–1883, June 2014.

[24] F. Rashid-Farrokhi, L. T. and Liu, K., "Joint optimal power control and beamforming in wireless networks using antenna arrays," *IEEE Trans. Commun.*, vol. 46, pp. 1313–13240, Oct. 1998.

[25] Fan, J., Yin, Q., Li, G. Y., Peng, B., and Zhu, X., "MCS Selection for Throughput Improvement in Downlink LTE Systems," in *Proc. of 20th International Conf. on Comp. Commun. and Networks*, pp. 1–5, 2011.

[26] Fehske, A. J., Richter, F., and Fettweis, G. P., "SINR Balancing for the Multi-User Downlink under General Power Constraints," in *Global Telecommun. Conf. (GLOBECOM), IEEE*, pp. 1–6, IEEE, 2008.

[27] Feng, S., Wang, M. M., Yaxi, W., Haiqiang, F., and Jinhui, L., "An efficient power allocation scheme for leakage-based precoding in multi-cell multiuser MIMO downlink," *IEEE Commun. Lett.*, vol. 15, pp. 1053–1055, Oct. 2011.

[28] Foschini, G., Chizhik, D., Gans, M., Papadias, C., and Valenzuela, R., "Analysis and performance of some basic space-time architectures," *IEEE J. Sel. Areas Commun.*, vol. 21, pp. 303–320, Apr. 2003.

[29] Giuliano, R., Monti, C., and Loreti, P., "WiMAX fractional frequency reuse for rural environments," *IEEE Trans. Wireless Commun.*, vol. 15, pp. 60–65, June 2008.

[30] He, J. and Salehi, M., "Low-Complexity Coordinated Interference-Aware Beamforming for MIMO Broadcast Channels," in *Veh. Technol. Conf. (VTC), IEEE 66th*, pp. 685–689, Sept. 2007.

[31] He, S., Huang, Y., Yang, L., Nallanathan, A., and Liu, P., "A multi-cell beamforming design by uplink-downlink max-min SINR duality," *IEEE Trans. Wireless Commun.*, vol. 11, pp. 2858–2867, Aug. 2012.

[32] Himayat, N., Talwar, S., Rao, A., and Soni, R., "Interference management for 4G cellular standards," *IEEE Commun. Mag.*, vol. 48, pp. 86–92, Aug. 010.

[33] Holtzman, J. M., "Asymptotic analysis of proportional fair algorithm," in *Int. Symp. on Personal, Indoor and Mobile Radio Commun., 12th IEEE*, pp. F33–F37, 2001.

[34] Huang, Q., Ghogho, M., Li, Y., Ma, D., and Wei, J., "Transmit Beamforming for MISO Frequency-Selective Channels with Per-Antenna Power Constraint and Limited-Rate Feedback," *IEEE Trans. Veh. Technol.*, vol. 60, pp. 3726–3735, Oct. 2011.

[35] Huang, Y., Zheng, G., Bengtsson, M., Wong, K.-K., Yang, L., and Ottersten, B., "Distributed multicell beamforming design approaching pareto boundary with max-min fairness," *IEEE Trans. Wireless Commun.*, vol. 11, pp. 2921–2933, Aug. 2012.

[36] Huawei, "Soft frequency reuse scheme for UTRAN LTE," R1- 050507, 3GPP TSG RAN WG1 #41, May 2005.

[37] International Telecommunication Union, "Guidelines for evaluation of radio interface technologies for IMT-Advanced," Report M.2135-1, ITU-R, 2010.

[38] Jeon, Y.-s., Kim, Y.-j., Min, M., and Im, G.-h., "Distributed Block Diagonalization with Selective Zero Forcing for Multicell MU-MIMO Systems," *IEEE Signal Process. Lett.*, vol. 21, pp. 605–609, May 2014.

[39] Karakayali, K., Yates, R., Foschini, G., and Valenzuela, R., "Optimum Zero-forcing Beamforming with Per-antenna Power Constraints," in *Information Theory, IEEE Int. Symp.*, pp. 101–105, June 2007.

[40] Kaviani, S. and Krzymień, W. A., "Optimal Multiuser Zero Forcing with Per-Antenna Power Constraints for Network MIMO Coordination," *EURASIP J. on Wireless Commun. and Net.*, vol. 2011, no. 1, p. 190461, 2011.

[41] Kaviani, S., Simeone, O., Krzymien, W. A., and Shamai, S., "Linear Precoding and Equalization for Network MIMO with Partial Cooperation," *IEEE Trans. Veh. Technol.*, vol. 61, no. 5, pp. 2083–2096, 2012.

[42] Kelly, F., Maulloo, A., and Tan, D., "Rate control for communication networks: shadow prices, proportional fairness and stability," *J. of the Operational Research Society*, vol. 49, pp. 237–252, Mar. 1998.

[43] Kim, J., Lee, H.-w., and Chong, S., "Virtual Cell Beamforming in Cooperative Networks," *IEEE J. Sel. Areas Commun.*, vol. 32, pp. 1126–1138, June 2014.

[44] Kim, K.-H., Lee, J.-H., Lee, C.-H., Jeon, N.-R., and Kim, S.-C., "Coordinated Beamforming with Limited BS Cooperation for Multicell Multiuser MIMO Broadcast Channel," in *Veh. Technol. Conf. (VTC), IEEE 69th*, pp. 1–5, Apr. 2009.

[45] Kim, T. M., Sun, F., and Paulraj, A., "Low-complexity MMSE precoding for coordinated multipoint with per-antenna power constraint," *IEEE Signal Process. Lett.*, vol. 20, pp. 395–398, Apr. 2013.

[46] Kim, T. M., Sun, F., and Paulraj, A. J., "Low-Complexity MMSE Precoding for Coordinated Multipoint with Per-Antenna Power Constraint," *IEEE Signal Process. Lett.*, vol. 20, pp. 395–398, Apr. 2013.

[47] Komulainen, P., Tolli, A., and Juntti, M., "Effective CSI signaling and decentralized beam coordination in TDD multi-cell MIMO systems," *IEEE Trans. Signal Process.*, vol. 61, pp. 2204–2218, May 2013.

[48] Lan, T. L. T. and Yu, W. Y. W., "Input optimization for multi-antenna broadcast channels with per-antenna power constraints," in *Global Telecommun. Conf. (GLOBECOM), IEEE*, vol. 1, pp. 420–424, 2004.

[49] Lee, D., Li, G., Zhu, X., and Fu, Y., "Multi-stream multi-user coordinated beamforming for cellular networks with multiple receive antennas," *IEEE Transactions on Vehicular Technology*, vol. PP, pp. 1–1, June 2015.

[50] Lee, D.-W., Seo, H., Clerckx, B., Hardouin, E., Mazzarese, D., Nagata, S., and Sayana, K., "Coordinated multipoint transmission and reception in LTE-Advanced: Deployment scenarios and operational challenges," *IEEE Commun. Mag.*, vol. 50, pp. 148–155, Feb. 2012.

[51] Lee, D., Li, G. Y., , and Tang, S., "Inter-cell interference coordination for LTE systems," in *Global Telecommun. Conf. (GLOBECOM), IEEE*, pp. 4828–4833, 2012.

[52] Lee, D., Li, G. Y., Zhu, X., and Fu, Y., "Coordinated beamforming for users with multi-receive antennas in cellular networks," in *Personal Indoor and Mobile Radio Commun. (PIMRC), IEEE 24th Int. Symp. on*, pp. 564–569, Sept. 2013.

[53] Lei, H., Zhang, L., Zhang, X., and Yang, D., "A novel multi-cell OFDMA system structure using fractional frequency reuse," in *Personal Indoor and Mobile Radio Commun. (PIMRC), IEEE 18th Int. Symp. on*, pp. 1–5, 2007.

[54] Liu, T., Lu, S., and Zheng, M., "Beamforming for Per-Antenna Power Constrained Downlink SINR Optimization," in *Veh. Technol. Conf. (VTC), IEEE 71st*, pp. 1–5, 2010.

[55] Liu, Y.-F., Dai, Y.-H., and Luo, Z.-Q., "Coordinated beamforming for MISO interference channel: Complexity analysis and efficient algorithms," *IEEE Trans. Signal Process.*, vol. 59, pp. 1142–1157, Mar. 2011.

[56] Liu, Y.-F., Dai, Y.-H., and Luo, Z.-Q., "Max-min fairness linear transceiver design for a multi-user MIMO interference channel," *IEEE Trans. Signal Process.*, vol. 61, pp. 2413–2423, May 2013.

[57] Lobo, M. S., Vandenberghe, L., Boyd, S., and Lebret, H., "Linear algebra and its applications," *Journal of Computational and Applied Mathematics*, vol. 284, pp. 193–228, Nov. 1998.

[58] Mohammed, S. K. and Larsson, E. G., "Per-Antenna Constant Envelope Precoding for Large Multi-User MIMO Systems," *IEEE Trans. Commun.*, vol. 61, pp. 1059–1071, Mar. 2013.

[59] Next Generation Mobile Networks Alliance, "*NGMN Optimised Backhaul Requirements*." `http://www.ngmn.org/nc/downloads/techdownloads/browse/2.html`, Aug. 2008.

[60] Nguyen, D. H. N. and Le-Ngoc, T., "Multiuser Downlink Beamforming in Multicell Wireless Systems: A Game Theoretical Approach," *IEEE Trans. Signal Process.*, vol. 59, pp. 3326–3338, July 2011.

[61] Nortel Networks, "Reference simulation methodology for the performance evaluation of OFDM/WCDMA in UTRAN," R1- 030785, 3GPP TSG RAN WG1 #33, Aug. 2003.

[62] Novlan, T., Andrews, J. G., Sohn, I., Ganti, R. K., and Ghosh, A., "Comparison of Fractional Frequency Reuse Approaches in the OFDMA Cellular Downlink," in *IEEE Global Telecommun. Conf.*, pp. 1–5, 2010.

[63] Novlan, T. D., Ganti, R. K., Ghosh, A., and Andrews, J. G., "Analytical evaluation of fractional frequency reuse for OFDMA cellular networks," *IEEE Trans. Wireless Commun.*, vol. 10, pp. 4294–4305, Dec. 2011.

[64] Novlan, T. D., Ganti, R. K., Ghosh, A., and Andrews, J. G., "Analytical evaluation of fractional frequency reuse for heterogeneous cellular networks," *IEEE Trans. Commun.*, vol. 60, pp. 2029–2039, July 2012.

[65] Park, J., Lee, G., Sung, Y., and Yukawa, M., "Coordinated Beamforming with Relaxed Zero Forcing: The Sequential Orthogonal Projection Combining Method and Rate Control," *IEEE Trans. Signal Process.*, vol. 61, pp. 3100–3112, June 2013.

[66] Park, S.-H., Park, H., Kong, H., and Lee, I., "New Beamforming Techniques Based on Virtual SINR Maximization for Coordinated Multi-Cell Transmission," *IEEE Trans. Wireless Commun.*, vol. 11, pp. 1034–1044, Mar. 2012.

[67] Peng, J., Wei, G., and Zhu, J., "Power Allocation Method for OFDM System with both Total and Per-Antenna Power Constraints," *IEEE Commun. Lett.*, vol. 12, pp. 621–623, Sept. 2008.

[68] Petersen, K. B. and Pedersen, M. S., "*The Matrix Cookbook.*" `http://www2.imm.dtu.dk/pubdb/p.php?3274`, Nov. 2012.

[69] Pi, Z., "Optimal MIMO transmission with per-antenna power constraints," in *Global Commun. Conf. (GLOBECOM), IEEE*, pp. 2493–2498, Dec. 2012.

[70] Pi, Z., "Optimal transmitter beamforming with per-antenna power constraints," in *Int. Conf. on Commun. (ICC), IEEE*, pp. 3779–3784, June 2012.

[71] Quek, T., Lei, Z., and Sun, S., "Adaptive interference coordination in multi-cell OFDMA systems," in *Personal Indoor and Mobile Radio Commun. (PIMRC), IEEE 20th Int. Symp. on*, pp. 2380–2384, 2009.

[72] Sadek, M., Tarighat, A., and Sayed, A. H., "A leakage-based precoding scheme for downlink mulit-user MIMO channels," *IEEE Trans. Wireless Commun.*, vol. 6, pp. 1711–1721, May 2007.

[73] Schmidt, D., Shi, C., Berry, R., Honig, M., and Utschick, W., "Comparison of distributed beamforming algorithms for mimo interference networks," *IEEE Trans. Signal Process.*, vol. 61, pp. 3476–3489, July 2013.

[74] Sharma, V. and Lambotharan, S., "Robust Multiuser Downlink Beamforming with Per Antenna Power Constraints using Worst-Case Performance Optimization," in *Commun. and Inf. Technol., Int. Symp. on*, pp. 5–8, Oct. 2008.

[75] Shen, H., Li, B., Tao, M., and Wang, X., "MSE-Based Transceiver Designs for the MIMO Interference Channel," *IEEE Trans. Wireless Commun.*, vol. 9, pp. 3480–3489, Nov. 2010.

[76] Shi, Q., Razaviyayn, M., Luo, Z.-Q., and He, C., "An iteratively weighted MMSE approach to distributed sum-utility maximization for a MIMO interfering broadcast channel," *IEEE Trans. Signal Process.*, vol. 59, pp. 4331–4340, Sept. 2011.

[77] Shi, S., Schubert, M., and Boche, H., "Rate optimization for multiuser mimo systems with linear processing," *IEEE Transactions on Signal Processing*, vol. 56, pp. 4020–4030, Aug 2008.

[78] Shi, S., Schubert, M., and Boche, H., "Per-antenna power constrained rate optimization for multiuser MIMO systems," in *Smart Antennas, Int. ITG Workshop on*, pp. 270–277, Feb. 2008.

[79] Srinivasan, R., Zhuang, J., Jalloul, L., Novak, R., and Park, J., "IEEE 802.16m Evaluation Methodology Document (EMD)," IEEE 802.16m- 08/004r2, 3GPP TSG RAN WG1 #41, July 2008.

[80] Starr, J., El Ayach, O., and Heath, R. W., "Interference alignment with per-antenna power constraints," in *Inf. Theory Proc., IEEE Int. Symp. on*, pp. 2746–2750, July 2011.

[81] Stiakogiannakis, I. N., Athanasiadou, G. E., Tsoulos, G. V., and Kaklamani, D. I., "Performance analysis of fractional frequency reuse for multi-cell WiMAX networks based on site-specific propagation modeling [wireless corner]," *IEEE Antennas Propag. Mag.*, vol. 54, pp. 214–226, Feb. 2012.

[82] Sun, F. and De Carvalho, E., "A leakage-based MMSE beamforming design for a MIMO interference channelaints," *IEEE Signal Process. Lett.*, vol. 19, pp. 368–371, June 2012.

[83] Tiwana, M. I., Sayrac, B., and Altman, Z., "Statistical learning in automated troubleshooting: Application to LTE interference mitigation," *IEEE Trans. Veh. Technol.*, vol. 59, pp. 3651–3656, Sept. 2010.

[84] Tolli, A., Codreanu, M., and Juntti, M., "Linear Multiuser MIMO Transmission with Quality of Service and Per Antenna Power Constraints," in *Global Telecommun. Conf. (Globecom), IEEE*, pp. 3285–3289, IEEE, Nov. 2007.

[85] Tutuncu, R., Toh, K., and Todd, M., "Solving semidefinite-quadratic-linear programs using sdpt3," *Mathematical Programming Ser. B*, vol. 95, pp. 189–217, 2003.

[86] Venturino, L., Prasad, N., and Wang, X., "Coordinated linear beamforming in downlink multi-cell wireless networks," *IEEE Trans. Wireless Commun.*, vol. 9, pp. 1451–1461, Apr. 2010.

[87] Vu, M., "MISO Capacity with Per-Antenna Power Constraint," *IEEE Trans. Commun.*, vol. 59, pp. 1268–1274, May 2011.

[88] Weng, C.-C. and Vaidyanathan, P. P., "Per-antenna power constrained MIMO transceivers optimized for BER," in *Asilomar Conf. on Signals, Systems and Computers, 42nd*, pp. 1300–1304, Oct. 2008.

[89] Wengerter, C., Ohlhorst, J., and von Elbwart, A. G. E., "Fairness and throughput analysis for generalized proportional fair frequency scheduling in OFDMA," in *Veh. Technol. Conf. (VTC), IEEE 61st*, vol. 3, pp. 1903–1907, June 2005.

[90] Wiesel, A., Eldar, Y. C., and Shamai, S., "Linear precoding via conic optimization for fixed mimo receivers," *IEEE Trans. Signal Process.*, vol. 54, pp. 161–176, Jan. 2006.

[91] Yazarel, Y. K. and Aktas, D., "Downlink Beamforming Under Individual SINR and Per Antenna Power Constraints," in *Pacific Rim Conf. on Commun., Computers and Signal Process., IEEE*, pp. 422–425, IEEE, Aug. 2007.

[92] Yu, W., Kwon, T., and Shin, C., "Multicell Coordination via Joint Scheduling, Beamforming, and Power Spectrum Adaptation," *IEEE Trans. Wireless Commun.*, vol. 12, pp. 1–14, July 2013.

[93] Yu, W. and Lan, T., "Downlink beamforming with per-antenna power constraints," in *Signal Process. Advances in Wireless Commun., IEEE 6th Workshop on*, vol. 2005, pp. 1058–1062, 2005.

[94] Yu, W. and Lan, T., "Transmitter Optimization for the Multi-Antenna Downlink with Per-Antenna Power Constraints," *IEEE Trans. Signal Process.*, vol. 55, pp. 2646–2660, June 2007.

[95] Zhang, H., Venturino, L., Prasad, N., Li, P., Rangarajan, S., and Wang, X., "Weighted sum-rate maximization in multi-cell networks via coordinated scheduling and discrete power control," *IEEE J. Sel. Areas Commun.*, vol. 29, pp. 1214 – 1224, June 2011.

[96] Zheng, S., Tian, H., Hu, Z., Chen, L., and Zhu, J., "QoS-Guaranteed Radio Resource Allocation with Distributed Inter-Cell Interference Coordination for Multi-Cell OFDMA Systems," in *71st IEEE Veh. Technol. Conf.*, pp. 1–5, 2010.